THE UNIVERSITY OF MICHIGAN

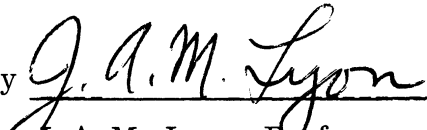7140-1-F

AFAL-TR-66-101

STUDY AND INVESTIGATION OF UHF-VHF ANTENNAS

Final Engineering Report
February 1965 through February 1966

April 1966

J.A.M. Lyon, N.G. Alexopoulos, C-C Chen,
A.M. Kazi, G.G. Rassweiler, D.L. Smith
and P.R. Wu

Approved by *[signature]*

J.A.M. Lyon, Professor
Electrical Engineering

FOREWORD

This report was prepared by the University of Michigan, under the direction of Professors Ralph Hiatt and J. A. M. Lyon on Air Force Contract AF 33(615)-2102 under Task Nr 627801 of Project 6278. The work was administered under the direction of the Research and Technology Division, Air Force Avionics Laboratory, Electronic Warfare Division, Wright-Patterson AFB Ohio. The Task Engineer was Mr. Olin E. Horton; the Project Engineer was Mr. James F. Rippin, Jr.

The studies presented herein began 1 February 1965 and were concluded 31 January 1966.

This report was submitted 16 February 1966.

This technical report has been reviewed and is approved.
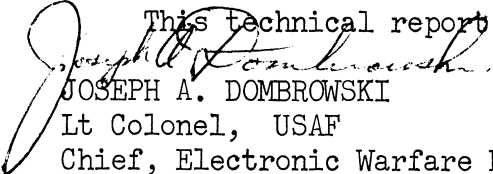
JOSEPH A. DOMBROWSKI
Lt Colonel, USAF
Chief, Electronic Warfare Division

TABLE OF CONTENTS

TABLE OF CONTENTS
(continued)

LIST OF FIGURES

LIST OF FIGURES
(continued)

LIST OF FIGURES
(continued)

LIST OF FIGURES
(continued)

ABSTRACT

This report indicates some of the advantages of using ferrite loading in a number of types of traveling wave antennas. Studies have been made on ferrite loaded helices and ferrite loaded log conical antennas. For a given frequency of operation it has been found possible to reduce the diameter of each of these types of antennas by a factor of approximately 55 - 70 per cent. Some variation in performance as a function of the amount of loading or thickness of the ferrite layer was observed. Near field probing techniques were used to show that ferrite loading changes the position of the active region on the log conical spiral. Likewise, near field probing shows that a particular region is active at a lower frequency when ferrite loading is applied to a helix. The effects of ferrite loading on the log zigzag type are also indicated. Relatively high efficiencies have been obtained for the ferrite loading of helices and log conical spirals. The power limitation occasioned by the use of ferrite loading for the rectangular slot antenna has been examined. For rectangular slots loaded with powdered EAF-2 ferrite designed to operate at 300 MHz it is estimated that the cw power limit is less than 50 watts.

I

INTRODUCTION

The research and development effort described in this report is concerned with a number of topics related to the ferrite loading of UHF-VHF antennas. A substantial part of the time has been spent on the loading of the log conical spiral and the helical antenna. The understanding of the helical antenna in the loaded condition appears basic to the understanding of the loaded log conical spiral antenna. In general, backward-fire traveling wave antennas of these two types were used rather than forward-fire or bidirectional traveling wave antennas. In this way the influence of any backing reflector or cavity was eliminated.

The analytical effort was devoted largely to the helical antenna. This antenna with ferrite loading was studied using a sheath helix model. With this model the appropriate boundary conditions were represented and the determinantal equation obtained. This equation was then used in conjunction with a Brillouin diagram in designating the radiation region of the ferrite loaded helix. The n = -1 mode corresponding to circular polarization of a helix was emphasized. Extensions of analysis to the tape helix with ferrite loading have been started. Computer studies are involved in the analyses.

In previous work the ferrite loaded rectangular slot antenna was appraised. In this contract the ferrite loaded rectangular slot was incorporated in a simple linear slot array. A preliminary examination has been made but this report does not presume to present any final analysis of the array. Efforts in this direction will continue under a subsequent contract.

Further studies were made on ferrite filled slot antennas utilizing ridges and irises. This work involved experiments where the ferrite filled slot took a different shape other than rectangular due to the use of a ridge. Also, some of the

ferrite elements were replaced by balsa wood, thereby effectively changing the shape of the aperture. This later arrangement would correspond to a slot antenna with an iris. Some changes in radiation pattern and efficiency were observed with these various arrangements.

Some basic studies were made concerning the manner of energy transfer from a helix to a ferrite slab. In this way the end of the ferrite slab was an excited aperture and its radiation characteristics were observed. However, the experiments and the analysis did not progress to the point where one could evaluate the efficiency of energy transfer or its efficiency of radiation as an antenna.

In the study of loaded antennas, it has been necessary to make some refinements in the methods used to determine their efficiencies. Although the problem of measuring efficiency is generally circumvented in much antenna work, the necessity for such a determination is very apparent when loading is considered for the efficiency of radiation tends to deterioriate with loading. Any resultant reduction in the size of an antenna must be considered in comparison with a reduction in the efficiency of radiation. Thus, the efficiency of radiation is one of the most important criteria. Very acceptable levels of efficiency (on the order of 50 per cent) have been obtained in the case of ferrite loaded helices and ferrite loaded log conical spiral antennas.

A loaded log zigzag antenna was designed and tested. The advantage of ferrite loading in this type of antenna was marginal due to a breakup of the near field pattern and excitation of the forward wave region. This effect has also been noticed with the loading of log pyramidal antennas. Further investiagtion of the causes and methods for alleviating the near field breakup will be necessary.

For the first time substantial attention has been given to the power limitations of ferrite loaded antennas. However, due to limitations of equipment, information is still lacking on their ultimate power handling capability. It was found possible

to test a ferrite loaded rectangular slot with 9 watts power input. Steady state temperatures within the ferrite loading of a rectangular slot were obtained for various positions for three levels of power input. The previously determined efficiency for such an antenna would indicate that approximately one-third of the input power goes into heat in the ferrite material. Power tests up to 100 watts input at 300 MHz are planned for the future effort.

This report gives additional information on available ferrite materials useful for the loading of antennas. The materials considered in some detail are the EAF-2 ferrite and the type Q-3 ferrite. The latter material has been obtained from the Indiana General Corporation and is useful for loading for frequencies below 200 MHz. In the work covered by this report, the type Q-3 ferrite was used for the preliminary measurements on the slot array antenna.

II

LOADED CONICAL, PYRAMIDAL AND HELICAL ANTENNAS

It is very desirable to solve for the effect of loading material on the conical log-spiral antenna. The log-spiral antenna is inherently broadband; thus the decrease of bandwidth noticeable in some loaded antennas may not be a major problem in loaded spirals. The helix and conical antennas are discussed together because, as has been shown in the literature, the bifilar helix antenna at its best radiating frequency behaves very much as the active zone of a conical-helix antenna of equal diameter. The helix has the advantage that it may be solved theoretically for some material loadings since it is a periodic cylindrical structure.

2.1 Loaded Helical Antennas

Solutions for the propagation velocities and attenuations of the currents on the helix are possible for a loading of concentric cylinders with a material of arbitrary μ and ϵ, the permeability and permittivity. A theoretical discussion of the loaded bifilar helical antenna appears in Appendix B, where it is shown that a possible rough approximation to the antenna diameter reduction with full core or thick-layer material loading is given by the formula,

$$\text{Reduction} = \sqrt{\frac{\dfrac{1}{\mu} + 1}{\epsilon + 1}}$$

where ϵ, μ = relative dielectric and magnetic constants, respectively. This calculation assumed an approximate sheath analysis and only a small $\epsilon (< 10)$. Calculations using a tape model (Shestopalov, 1961) show the same dependence on ϵ, using the same small ϵ assumption. All the theory to date is for the slow wave region, extrapolated into the radiation region. It should also be noted that this reduction is in diameter. No theoretical estimation of length of the active zone

has been made yet, since the entire radiation process has not yet been solved. The diameter reduction is due to the phase velocity and wavelength reduction of the current traveling around the wire, which causes a smaller circumference to be phased properly for radiation when the structure is loaded with a material.

2.1.1 Construction of Antennas

The experimental portion of the helix antenna investigation consisted of making a number of monofilar and bifilar helix antennas wound on fiberglass shells and loaded with powders of various μ and ϵ. Table II-1 describes the helix-type antennas used in the past year of work. Figure 2-1 shows a picture of a bifilar helix with a balsa wood core. This balsa wood, which has been found experimentally to have little electrical effect on the antenna, is used as an inside retainer to the loading powder so that a layer of loading powder may be inserted next to the bifilar helix windings as shown in Fig. 2-2. Figure 2-3 shows a sample fiberglass epoxy tube, made in this laboratory, as a form for winding the helix antennas. Figure 2-4 shows the effects of the building materials on antenna patterns; the effect of these materials is small at the frequencies (> 300 MHz) used in most of the experiments. The fiberglass does seem to affect the patterns at 300 MHz, possibly due to a loading effect since fiberglass has an ϵ = 4 and a thickness of .04", comparable to our thinnest shell loading; however, this frequency is much too low for good operation with a loading of this thin shell of fiberglass, according to present theory and experience.

2.1.2 Measured Far Field Patterns

Figures 2-5 through 2-12 show the normalized antenna patterns ($E_\phi{}^2$) for various loadings of bifilar helical antennas. The loading materials used were the EAF-2 ferrite powder (ϵ = 3.8, μ = 2.2), described in Section VI and a dielectric powder (Eccoflo Hi K 10, ϵ = 10) obtained from Emerson and Cuming, Inc. Thus, powders with two different values of μ and ϵ were available as a partial

TABLE II-1:

SPECIFICATIONS OF HELIX TEST ANTENNAS

Dimension	I.D. Number					
	213	214	215	217	218	231
Type	Bifilar	Monofilar	Monofilar	Bifilar	Bifilar	Bifilar
Diameter	4.15"	4.13"	3.85"	4.65"	2.1"	1.1"
Length	10"	10"	14.5"	16"	15"	8"
Conductor	58-U	$\frac{1}{8}$" cu. tube	*	58-U	174-U	174-U
Turns	6.5	7.0	5	9.5	20	20
Pitch	6.6° (1.5")	.7"	13° 3"	7° (1.8")	6.5° (.75")	6.6° (.4")

* 7-strand, 14 gauge copper antenna wire.

Note: All antennas above, except No. 218, are constructed on three-layer fiberglass epoxy tubes, .04" thick and fed by infinite baluns. No. 218 used a paper phenolic tube. Conductor was commercial coaxial stripped of the outer insulation, and is specified without the RG prefix.
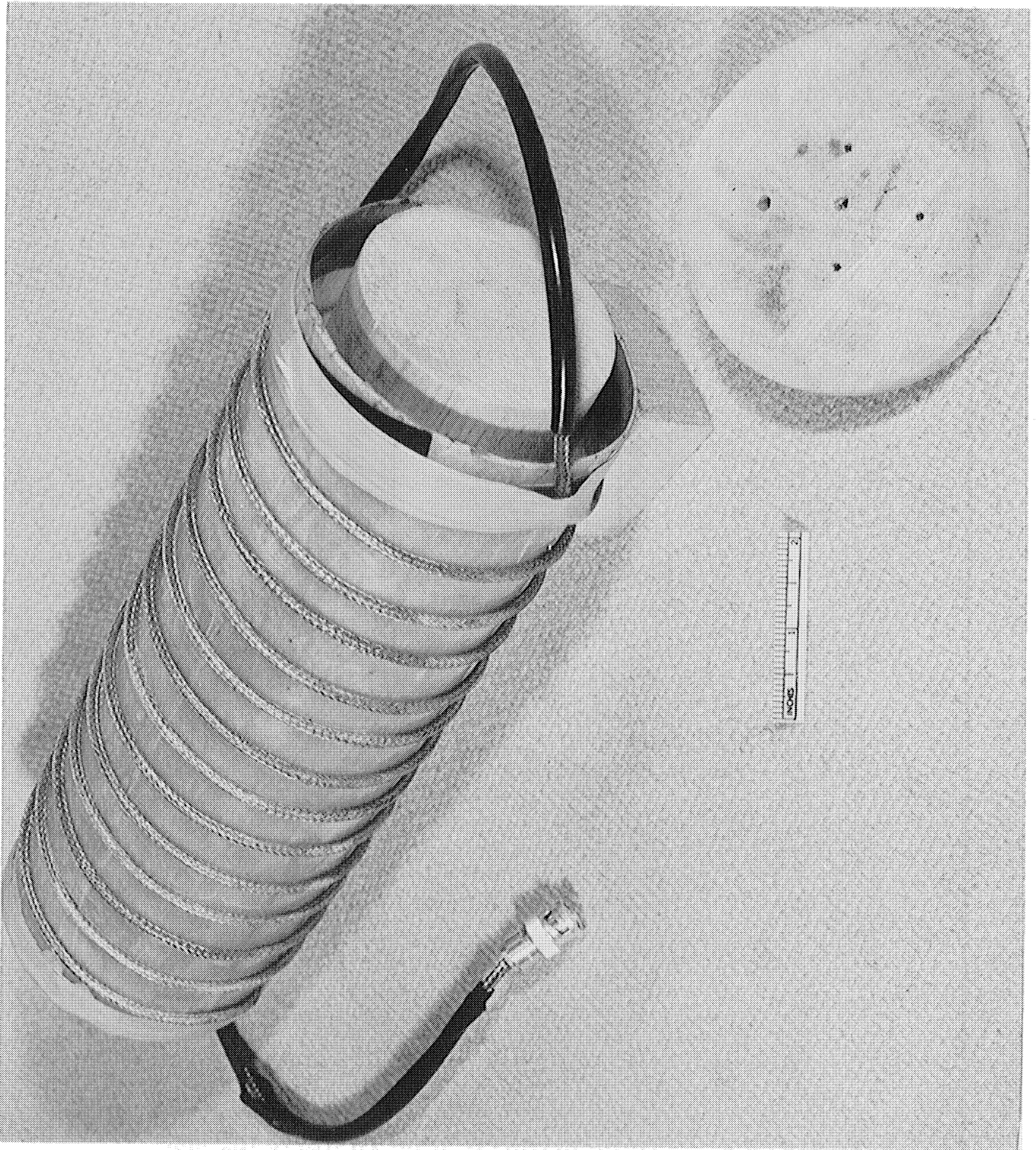
FIG. 2-1: BIFILAR 4" DIA. HELIX WITH BALSA WOOD CORE AND CAP.

4" Dia. Fiberglass Tube, 11 3/8" Long.

1/2" Layer
Ferrite Powder

3" dia
Balsa Wood
Core

1/2" Balsa
Wood Plugs

Side View

1/2" layer
Ferrite Powder

Balsa Wood Core

End View
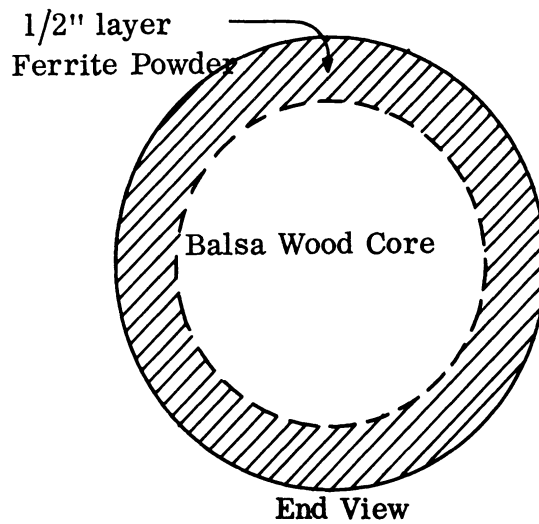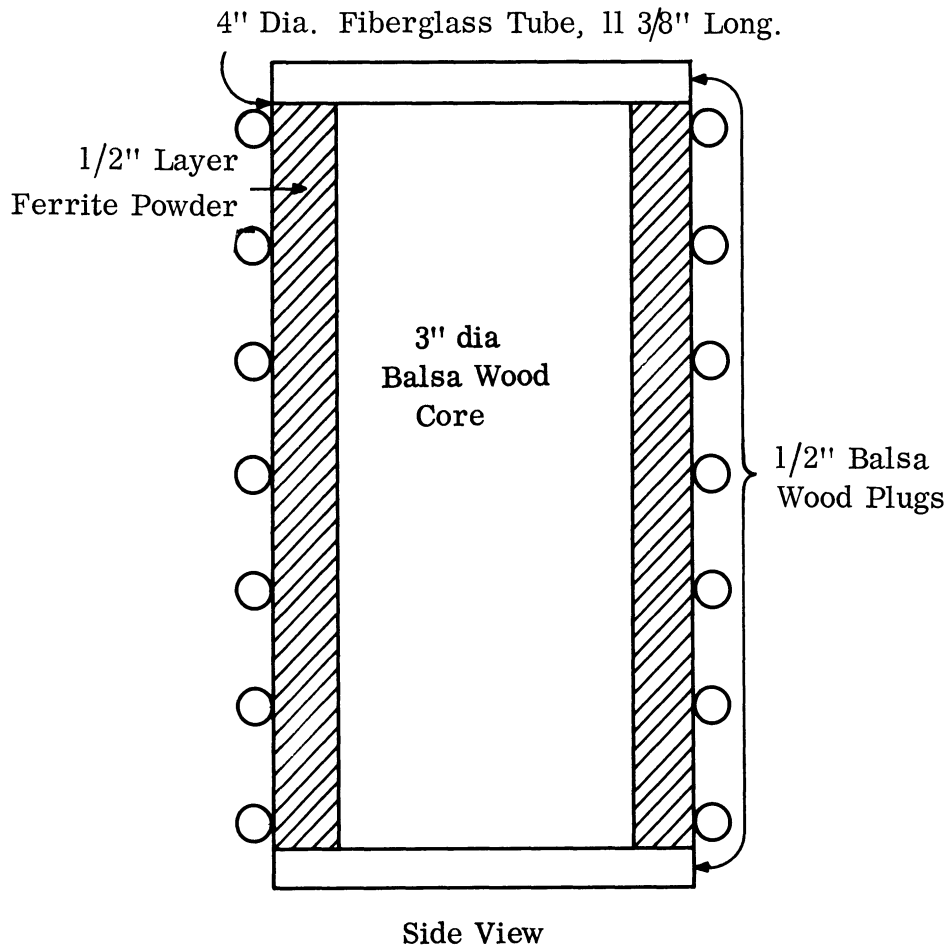
FIG. 2-2: LOADING DIAGRAM: BIFILAR HELIX (No. 213)
LAYER LOADING.
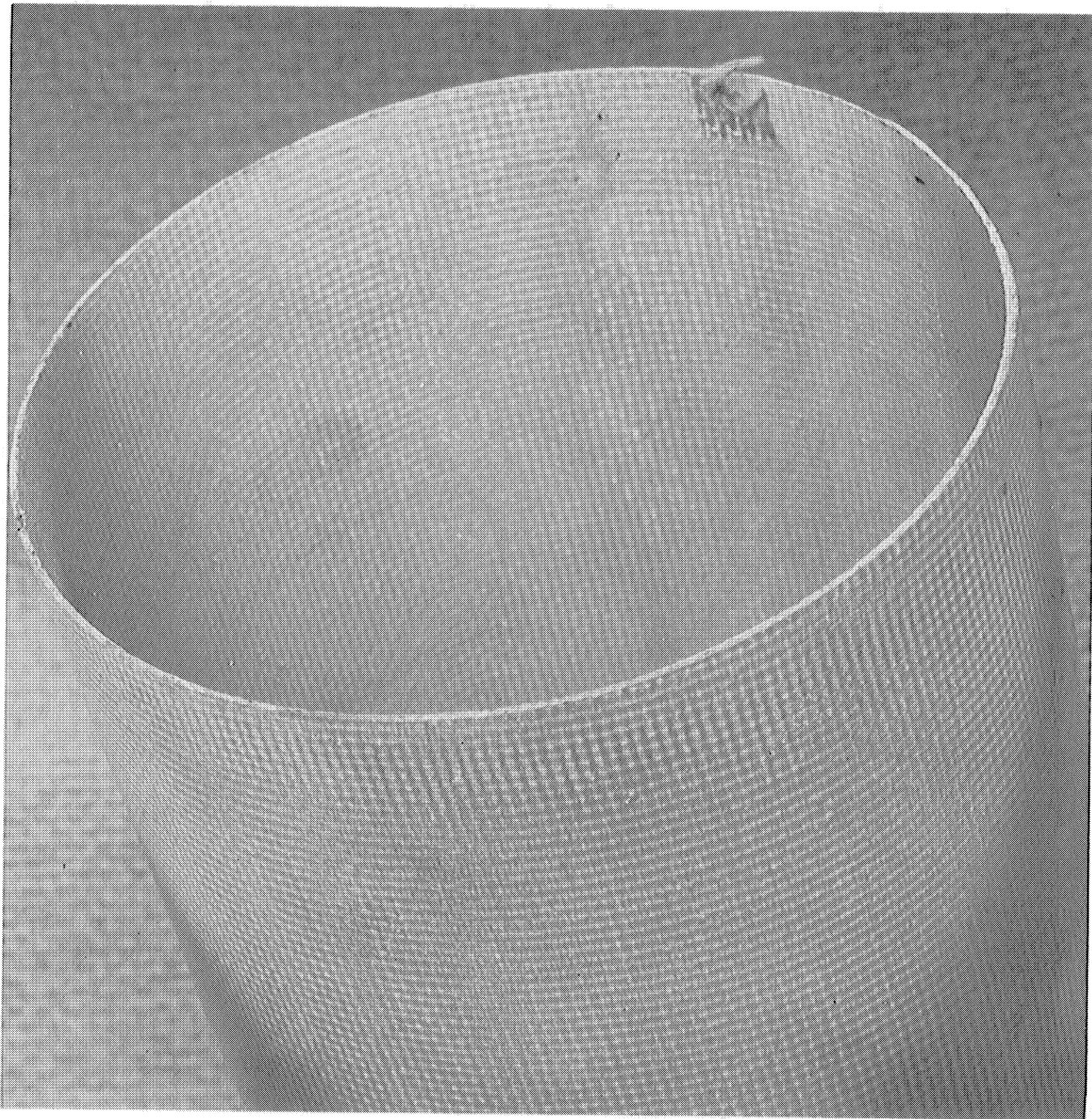
FIG. 2-3: FIBERGLASS-EPOXY TUBE FORM FOR HELICES.

900 MHz

710 MHz

600 MHz

500 MHz

400 MHz

——— Unloaded Helix

– – – – Balsa Wood Core

— — Fiberglass Tube Inside
Against Helix.

300 MHz
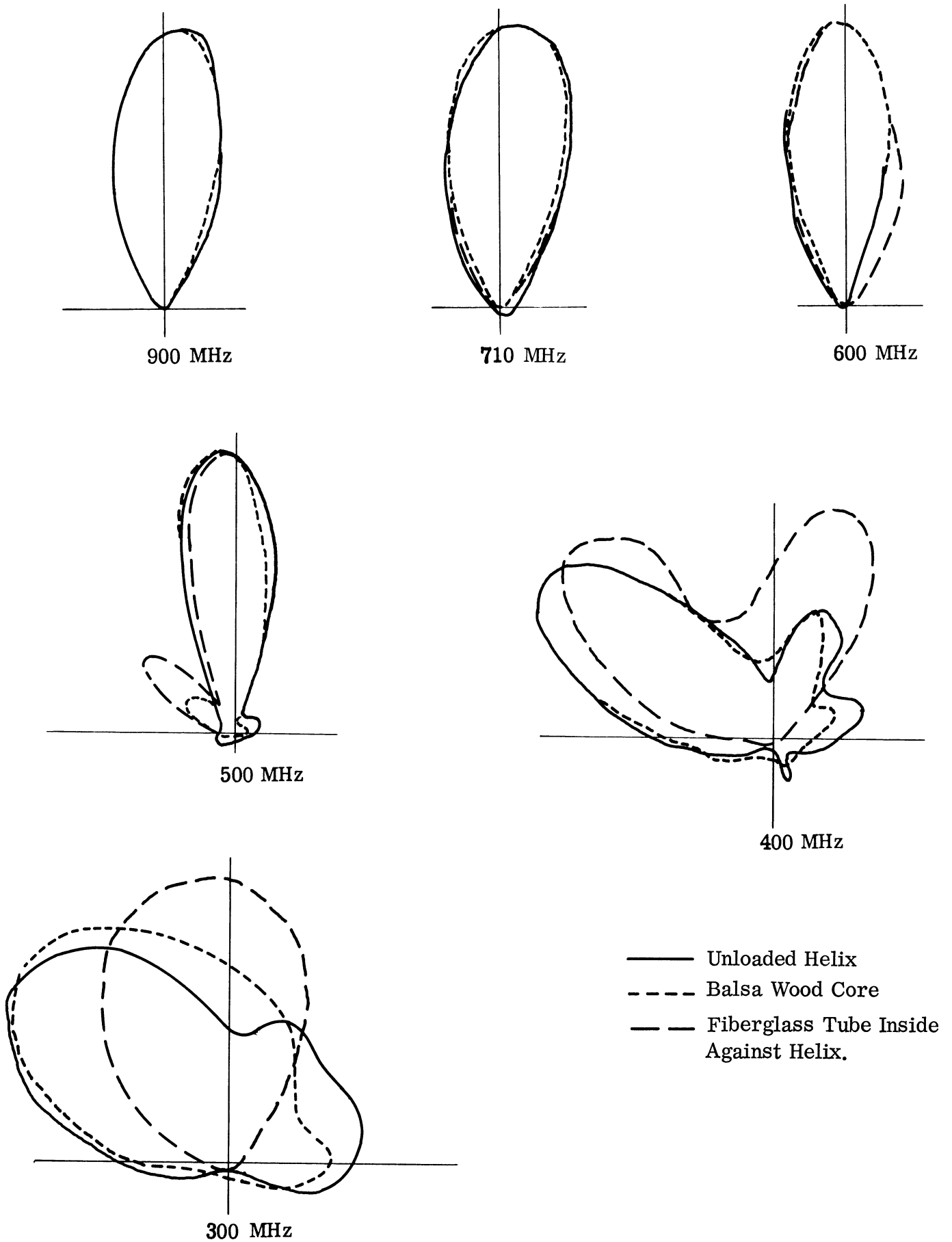
FIG. 2-4: EFFECTS OF BALSA WOOD AND EPOXY-FIBERGLASS
ON HELIX ANTENNA

10
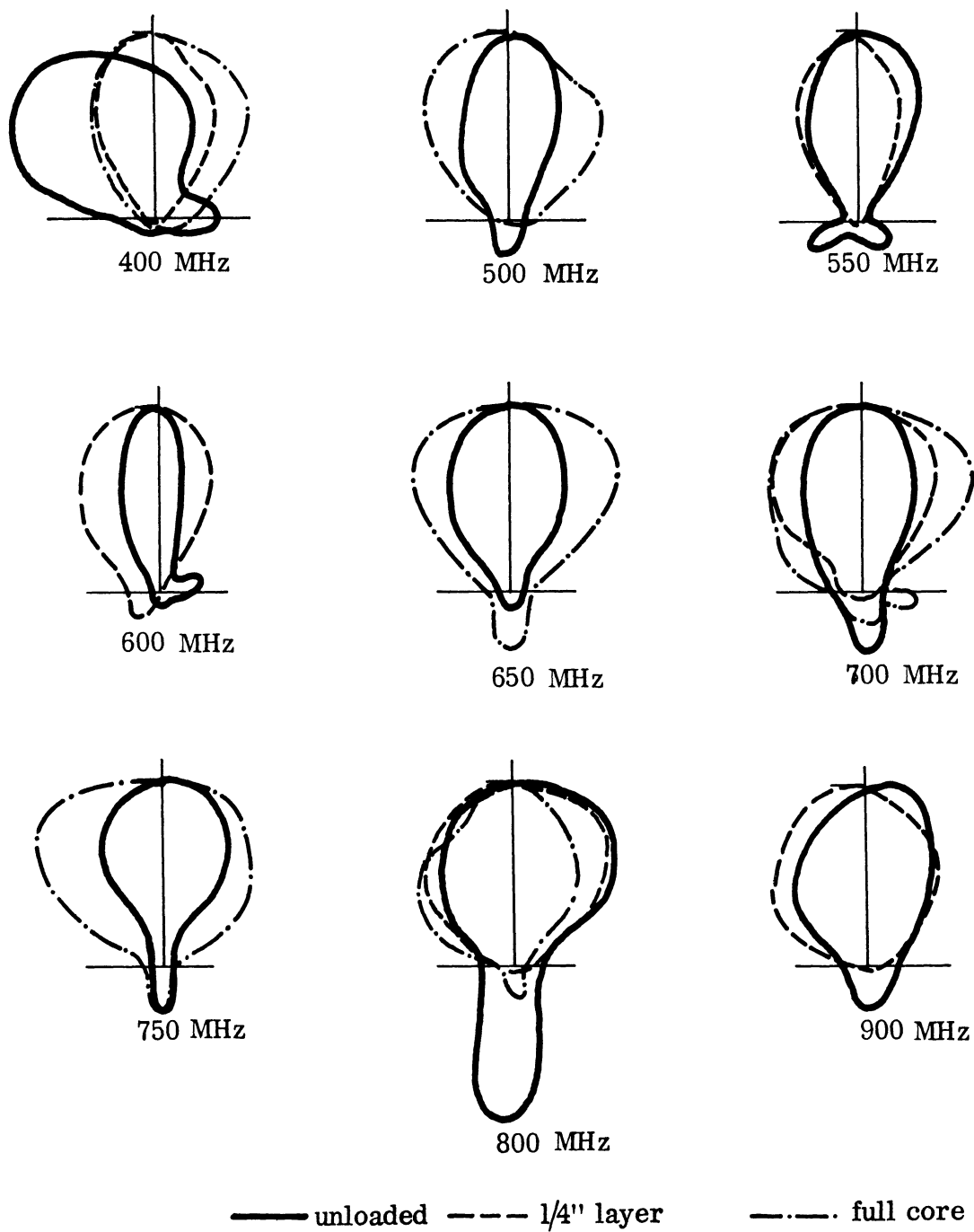
FIG. 2-5: HELIX WITH THICK LAYER FERRITE LOADING
Linear plots of E_ϕ^2. Ferrite μ=2.2, ϵ=3.8, Helix
Diameter = 4.5".

400 MHz

500 MHz

550 MHz

600 MHz

650 MHz

700 MHz

750 MHz

900 MHz

800 MHz

——— unloaded   — — — 1/16" layer   —·—·— 1/8" layer.

FIG. 2-6 : HELIX WITH THIN LAYER FERRITE LOADING
Linear plots of E_ϕ^2, Ferrite $\mu = 2.2$, $\epsilon = 3.8$, Helix
Diameter = 4. 5" .

400 MHz   500 MHz   550 MHz

600 MHz   620 MHz   700 MHz

750 MHz   800 MHz

900 MHz

——— unloaded   — — — .5" interior layer   —·— full core load
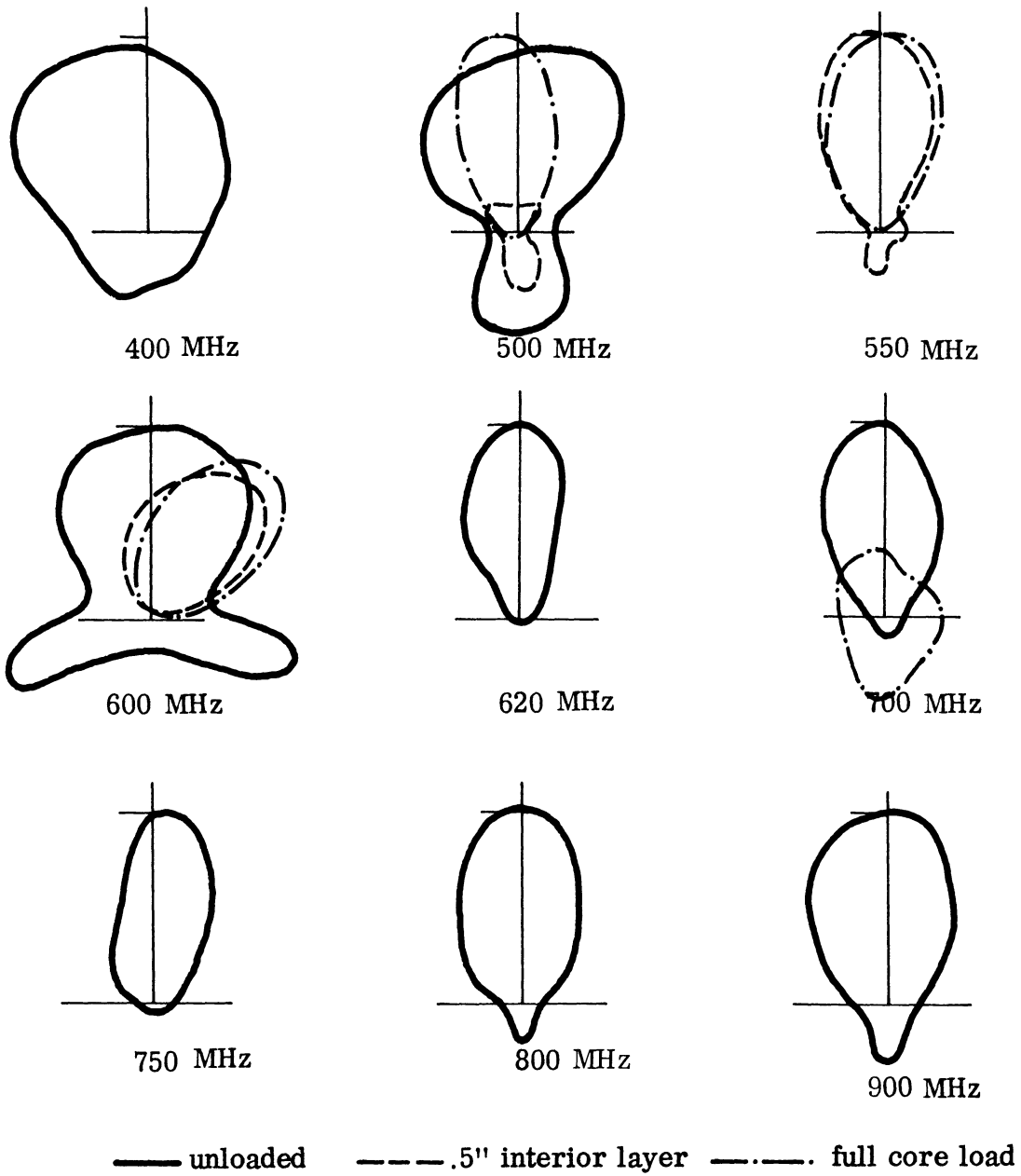
FIG. 2-7: HELIX WITH THICK LAYER FERRITE LOADING

Plot of E_ϕ^2, Ferrite μ =2.2, ϵ = 3.8, Helix Diameter = 4" .

400 MHz

500 MHz

550 MHz

600 MHz

650 MHz

700 MHz

750 MHz

800 MHz

900 MHz

—— unloaded   — — — 1/8" layer   —·——·— 1/4" layer
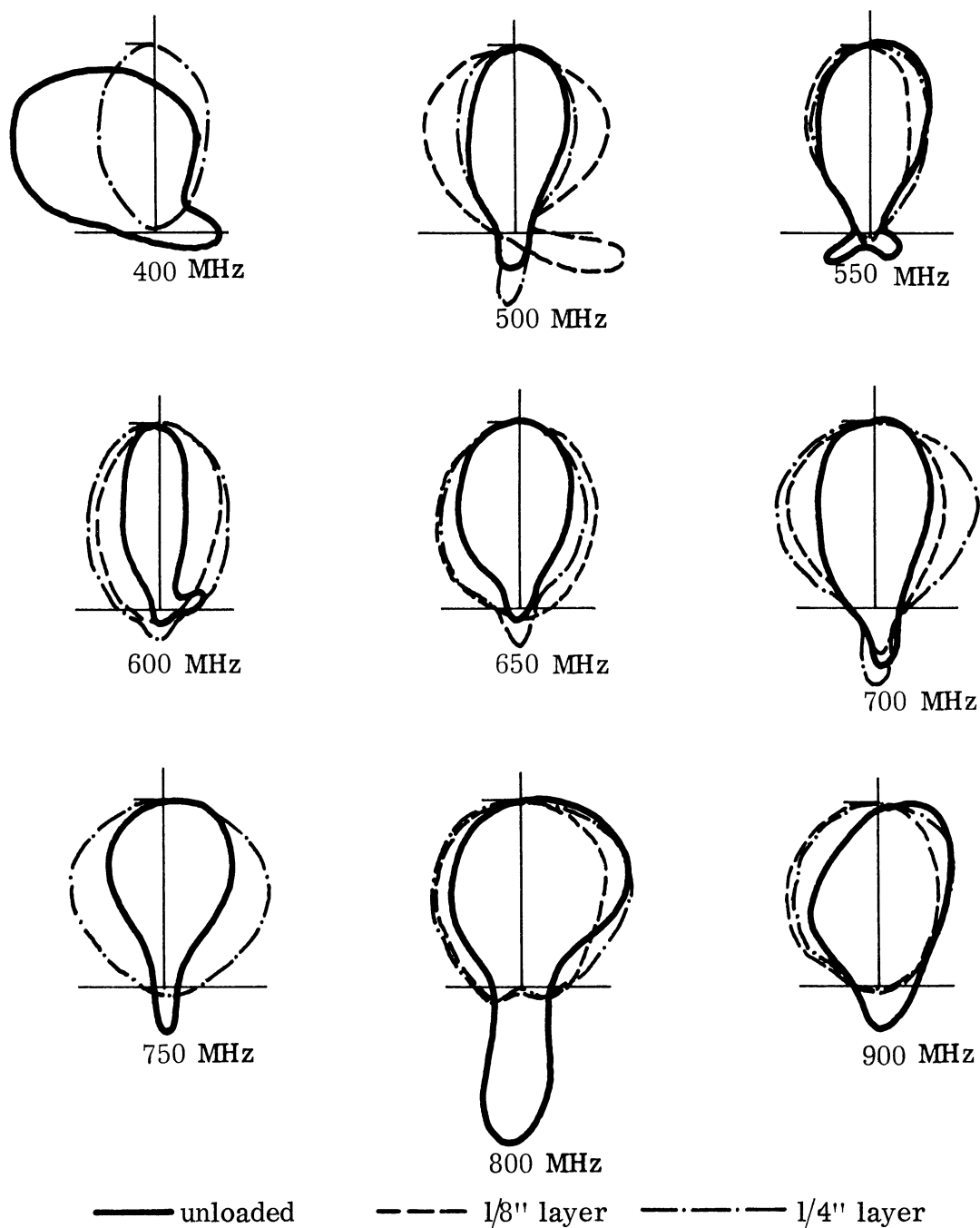
FIG. 2-8: HELIX WITH DIELECTRIC LOADING Plots of E_ϕ^2,
Dielectric $\epsilon=10$. Helix Diameter = 4.5".
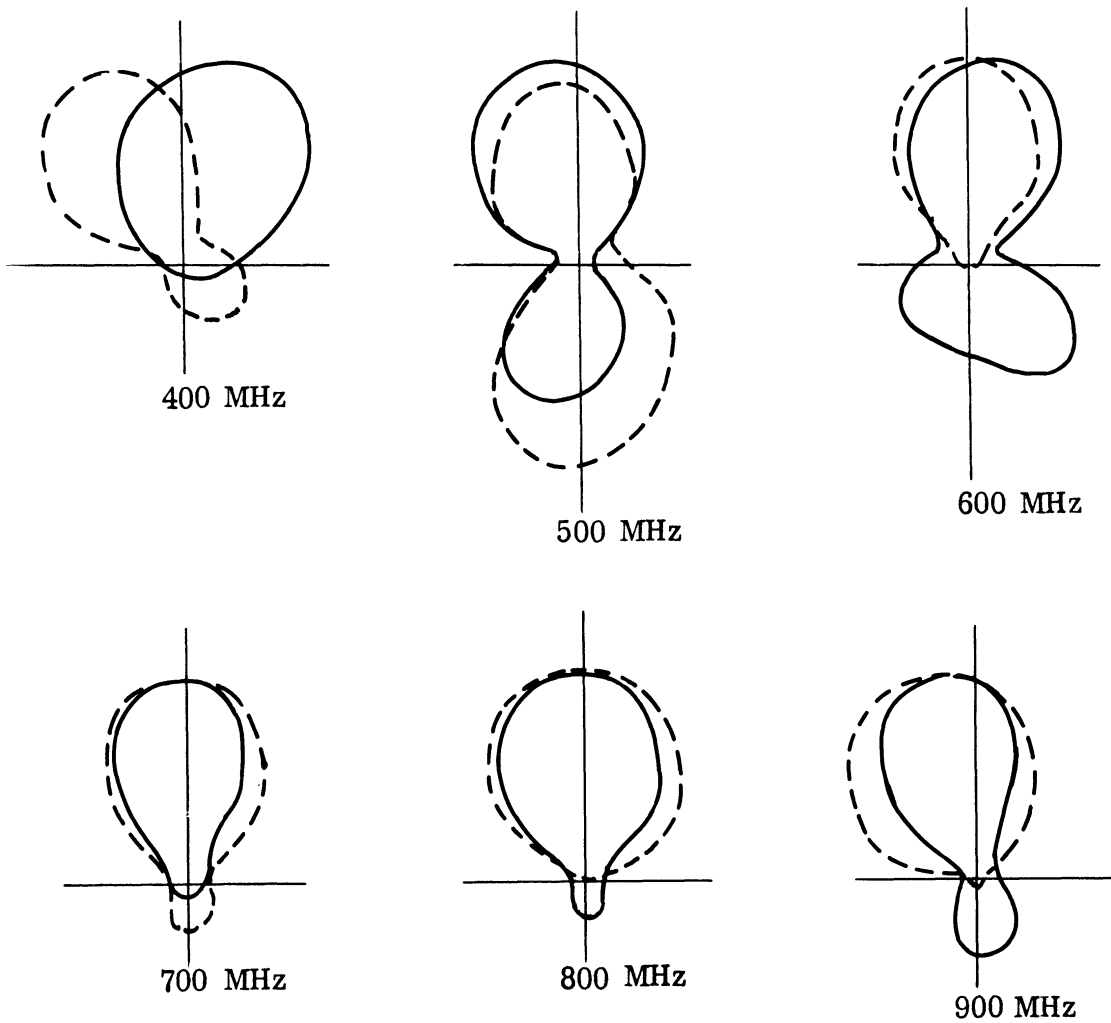
FIG. 2-9: EAF-2 FERRITE LOADED HELIX (NO. 213) —— AIR LOADED,
- - - - 1/2" INSIDE LAYER FERRITE. 400 - 900 MHz.

400 MHz

500 MHz

600 MHz

700 MHz
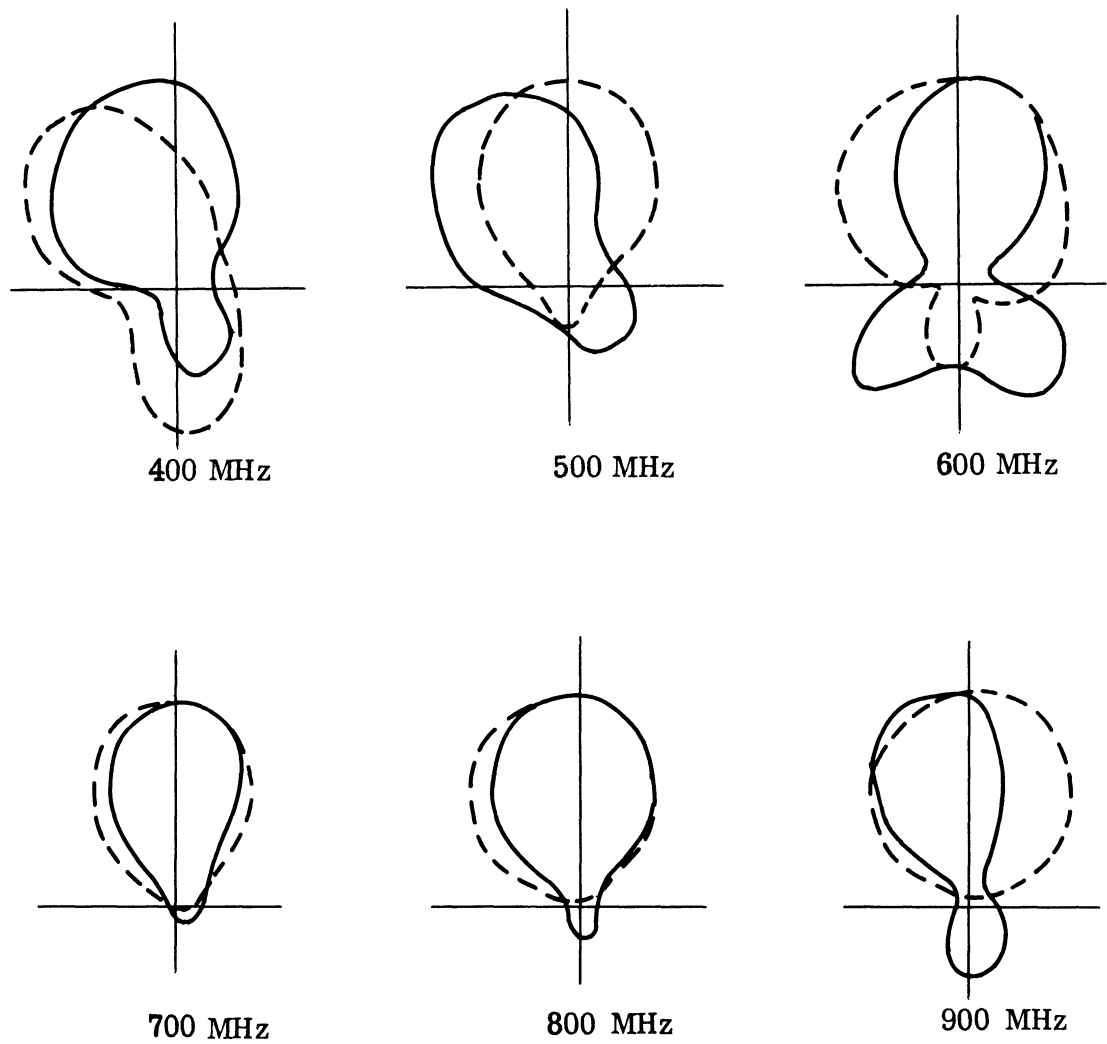
800 MHz

900 MHz

FIG. 2-10: EAF-2 FERRITE LOADED HELIX (NO. 213) —— AIR LOADED,
--- FERRITE LOADED 1/2" LAYER OUTSIDE, 400 - 900 MHz.
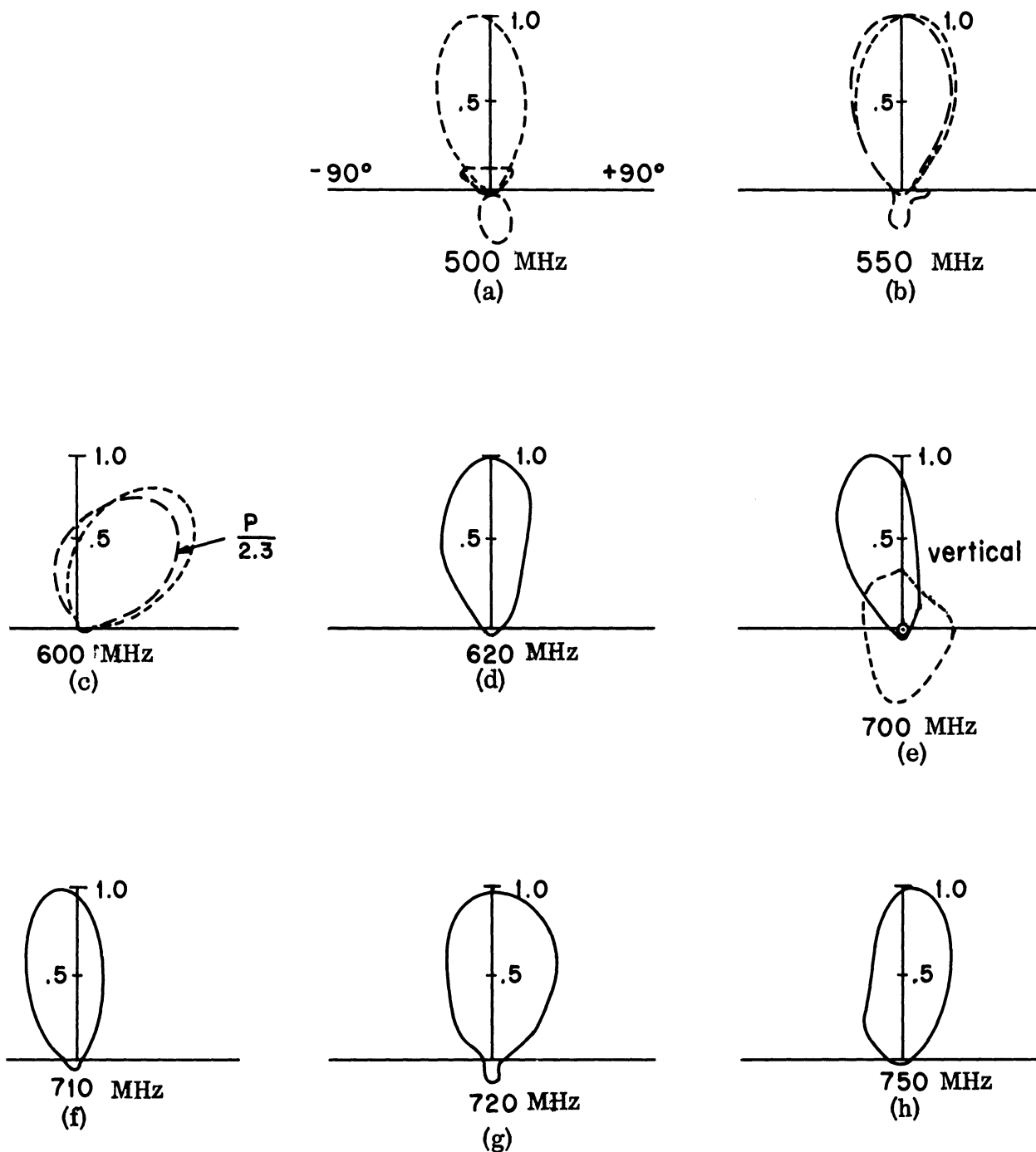
FIG. 2-11: BIFILAR HELIX (No. 213) ANTENNA PATTERNS. UNLOADED VS LOADED
E_ϕ^2 = LINEAR POWER, θ = POLAR ANGLE, P = POWER RECEIVED,
—— AIR LOADED, ---- FULL CORE FERRITE POWDER LOADED,
— — — .5" INTERIOR LAYER FERRITE POWDER LOADED
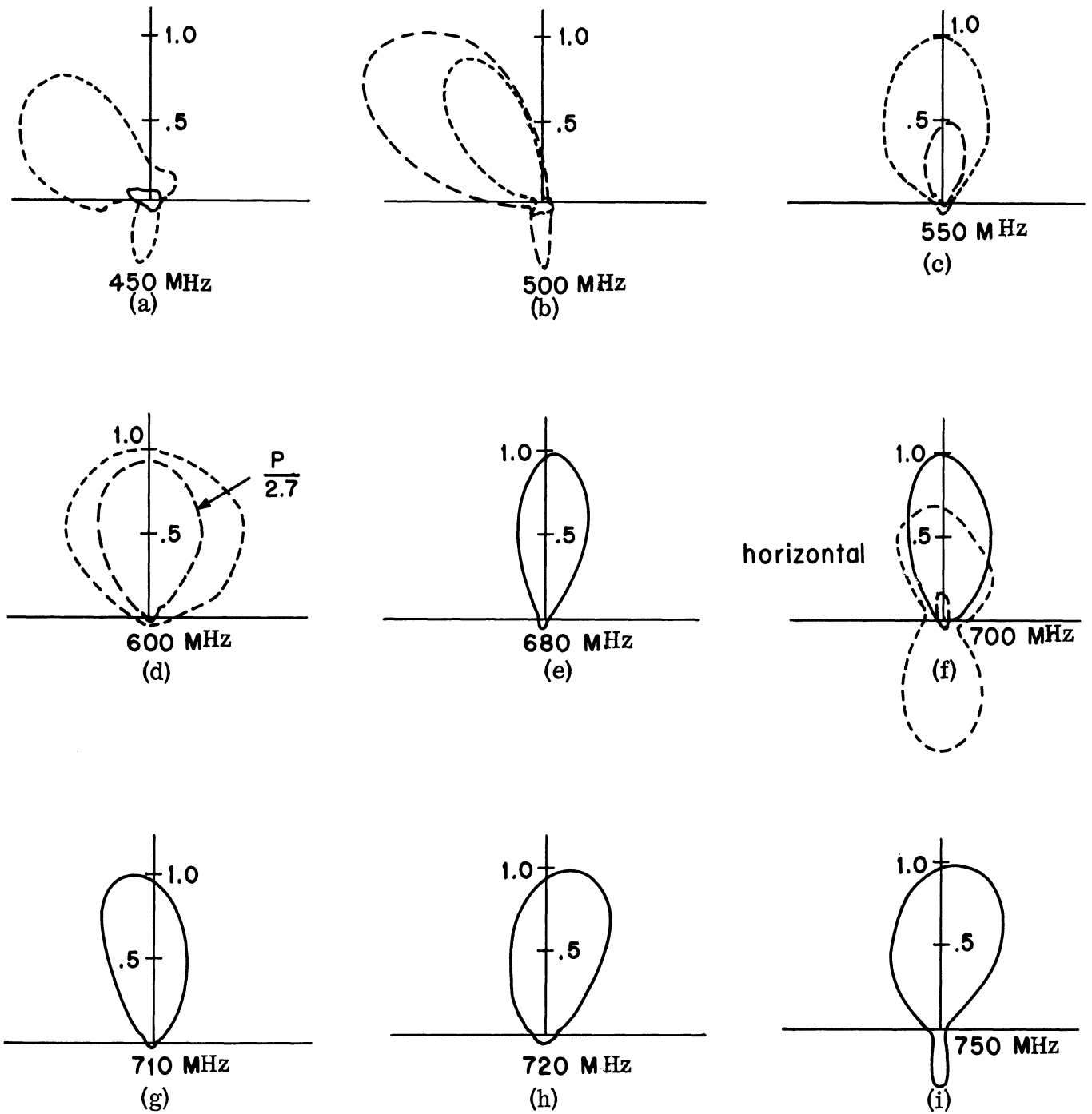
FIG. 2-12: BIFILAR HELIX (No. 213) ANTENNA PATTERNS. LOADED VS UNLOADED. E_θ^2 = LINEAR POWER. θ = POLAR ANGLE, P = POWER RECEIVED, —— AIR LOADED, ———— FULL CORE FERRITE POWDER LOADING, — — — .5" INTERIOR LAYER FERRITE POWDER LOADING.

check on the theoretical formulations being done. A major parameter of interest is the thickness of loading necessary in order to achieve good antenna reductions, since a full core loading may weigh too much.

In assessing the effectiveness of loading (i. e., the "best" loaded frequency versus the "best" unloaded frequency) from far field patterns, many criteria are available, such as maximum radiation efficiency, pattern shape, specific pattern requirements such as beamwidth or front-to-back ratio, etc. In addition, either the lowest frequency for acceptable operation or a center frequency may be chosen as the "best frequency". Unfortunately, not all criteria give the same reduction. Two criteria will be used to compute reduction factors:

1) The center frequency for maximum radiated power on axis; (for a fixed net input power, after allowance for mismatch).

2) The lowest frequency for reasonably axial, backfire antenna patterns. The first criteria evaluates the backward wave radiation characteristics, and will prove more applicable in extrapolating to a conical helix performance, since the "active zone" of the conical helix (discussed in the next section) is a zone of maximum radiation. The second criteria above applies to helical antennas, but is not readily extrapolated to conical helices, since the low frequency operation of a helix corresponds to the operation of the tip, or apex of the conical helix. The apex is not a critical region in conical helix design.

Table II-2 shows the center frequencies (criterion No. 1) for loaded helices, taken from data not shown in the figures. Normalizing the thicknesses to wave-lengths and the frequency reduction to a fraction, the reduction factors for criterion No. 1 (from Table II-2) and for criterion No. 2 (from Figs. 2-5 to 2-10) are shown in Table II-3, along with the theoretical reduction factors from Appendix B.

Two important things are summarized in Table II-3. First, a reduction factor for a helix antenna diameter can be achieved which approximates, but is

TABLE II-2:

FREQUENCIES OF PEAK RADIATED POWER
LOADED BIFILAR HELICES

| Antenna | Loading Thickness, t | | Loading | Frequency for Maximum |
	(Inches)	$(\frac{t}{\lambda})$	Material	Radiated Power, MHz
No. 217	0	.	Air	730
"	1/16	.0033	Ferrite	625
"	1/8	.0064	"	600
"	1/4	.0116	"	550
"	Full Core			450
No. 213	0		Air	820
	1/2	.0238	Ferrite	560
	1/2 (Outside)	.0216	"	510
	Full Core		"	530
No. 217	0		Air	730
	1/8	.0064	Dielectric	610
	1/4	.012	"	570

Note: a) Thickness relative to λ is taken at the center frequencies listed in column two.

b) Layers are inside and within .04" of the conductor, unless specified otherwise.

c) Frequencies for best circular polarization were usually lower; e.g., for 1/8" dielectric, 550 MHz was the best frequency.

TABLE II-3:

REDUCTION FACTORS FOR LOADED HELICES

Loading Material	Inside Loading Thickness ($\frac{t}{\lambda}$)	Experimental Reduction Factor		Sheath Theoretical Factor (Eq. B.29)
		Lowest Freq.	Center Freq.	
Ferrite	Full Core	.7	.64	.58
"	.022 (Outside)	.7	.62	~.58
"	.024	.78	.68	~.58
"	.012	.7	.75	~.58
"	.006	.75	.82	
"	.003	.8	.85	
Dielectric	Full Core	-	-	.45
"	.012	.74	.78	~.45
"	.006	1.0	.83	

always larger (less reduction) than the full core theory for thick layers of ferrite.
Second, thick layers greater than .25-.5 of the radius behave as full core loading
while thinner layers can be used with less than full core diameter reduction. The
layer-effect predictions of theory, given in Eq. (B.45), show that layers of .015λ
thick, (for the helices used) should give approximately full core loading. Table
II-3 partially verifies this.

In addition, these are two indications from the data that contradict the sim-
plified theoretical approach used;

1) The effect of the dielectric was not as great as theory predicts, although
about equal to the ferrite. This contradicts later near field measurements as well.
Notice that, due to a lack of material, thick layers of dielectric have not yet been
tried.

2) The outside loading of ferrite appears considerably more effective in size
reduction than the inside loading, although in Section VII, efficiency is shown to be
reduced with outside loading. Intuitively one might expect trouble with interfer-
ences at the outside ferrite-air boundary, causing poorer patterns and smaller
radiated power than with inside loading.

Further data will be required on the above two contradictions. In addition, the
reduction factors shown with either criterion are not as good as those achieved for
the pyramidal helices discussed later, nor are they as good as the phase measure-
ments on the helix. In general, the antenna pattern measurements of loaded
helices do not allow as good a prediction of loaded conical helix operations as first
anticipated.

A monofilar antenna (No. 215, Fig. 2-13) was constructed similarly to the
bifilar helices. Although most of the theory in this report applies only to back-
ward wave radiation, it is certainly expected that a decrease in current phase
velocity will decrease the diameter of a monofilar phased for forward radiation.
The patterns in Fig. 2-14 (vertical polarization) show that based on criterion
No. 2, the lowest operating frequency of the monofilar helix has been reduced
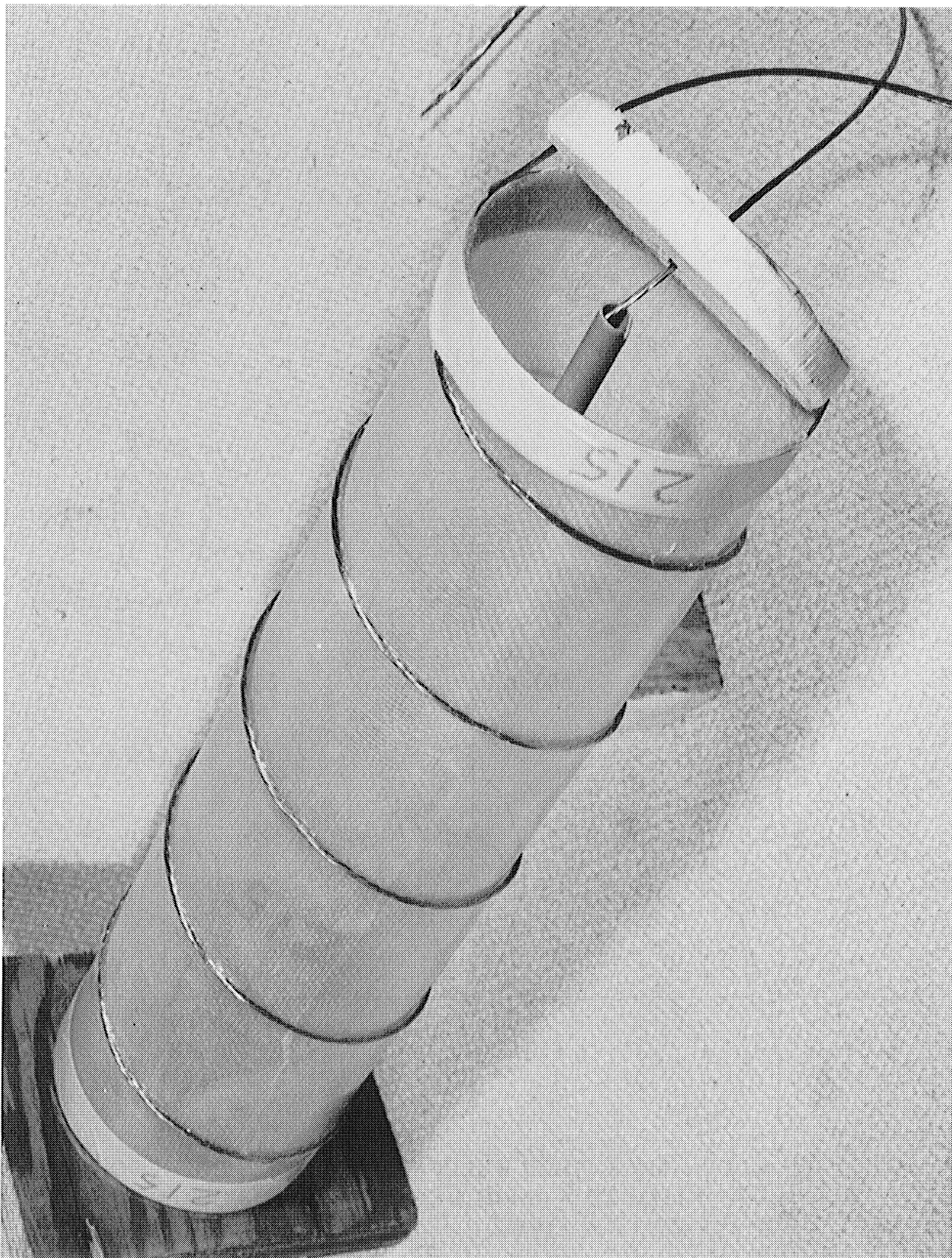
FIG. 2-13: MONOFILAR 4" HELIX WITH SMALL TUBE FOR CENTER
CONDUCTOR NO. 215.
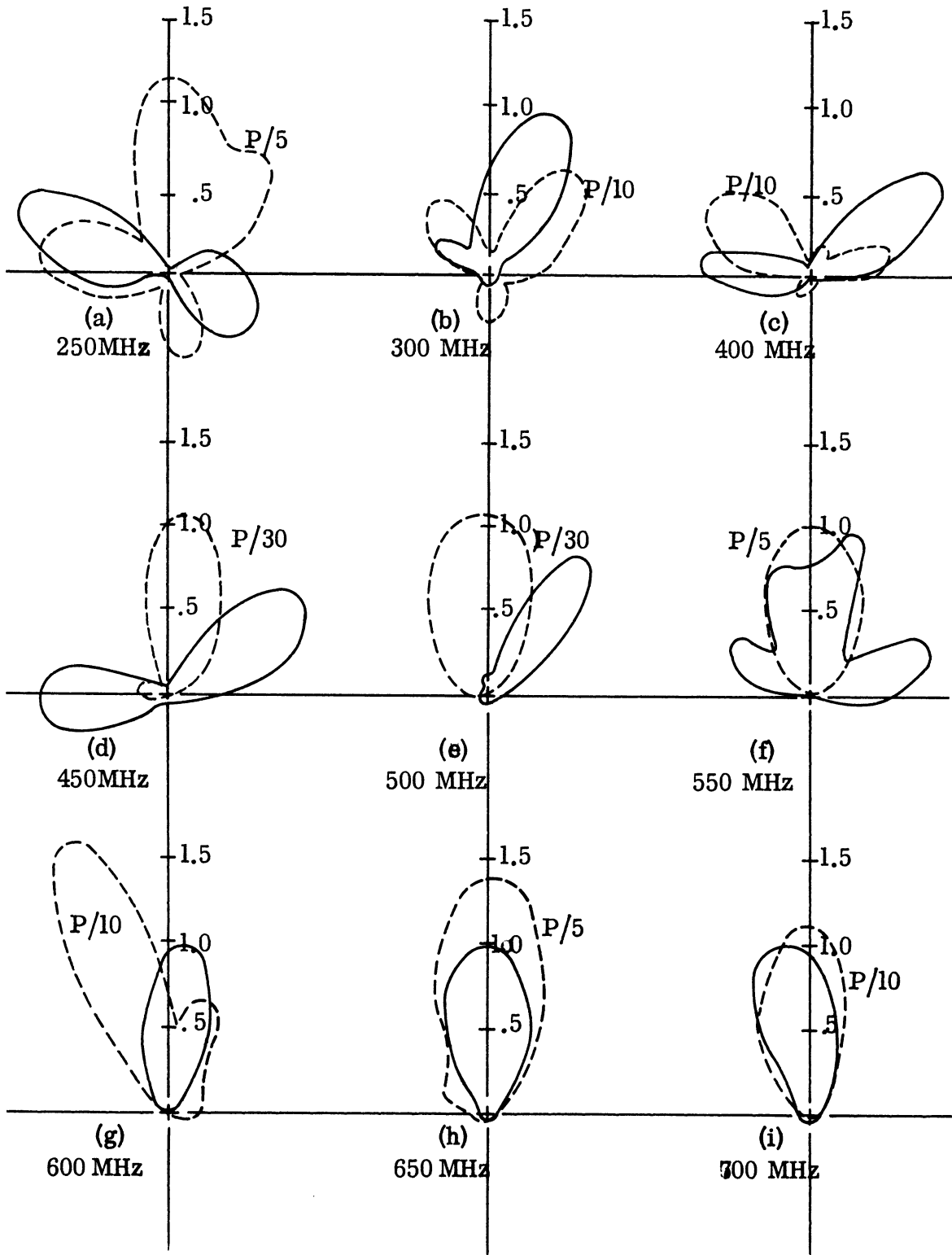
FIG. 2-14: 4" DIA. MONOFILAR HELIX (NO. 215) $|E_\phi|^2$ LINEAR POWER .
— UNLOADED --- FULL CORE FERRITE POWDER LOADED.
P = POWER RECEIVED.

from the 650 - 700 MHz to the 450 MHz region. This is more reduction than the bifilar helix experienced for criterion No. 2. Data for the use of criterion No. 1 has not yet been taken. Figure 2-15 shows similar plots for a horizontally polarized receiving dipole. These patterns are far worse than Fig. 2-14; they resulted from early data when great interference from ground reflections existed on the antenna range. It is felt that these poor patterns are due to reflection problems that have since been greatly reduced.

2.1.3 Near Field Measurements

2.1.3.a Probing Equipment. The preliminary measurement method used for the near field pattern for helical and log-conical antennas was similar to that of other workers (Dyson, 1965), (Patton, 1962). These measurements were made with surface current measurement facilities of the Radiation Laboratory. The facilities involve an anechoic chamber, a magnetic probe with its carriage system, and receiver-recorder system. The block diagram of the set-up for the near field phase measurement is shown in Fig. 2-16. The details of the anechoic chamber are described fully in the literature (Knott, 1965). The picture of the facility Fig. 2-17 shows the probe assembly hanging from ceiling. The probe carriage above the ceiling is shown in Fig. 2-18. Figure 2-19 shows the near field amplitude set-up.

The shielded vertical loop probe was used throughout the measurement. It has a diameter of 0.131". The highest frequency used in the measurement.was 1600 MHz; thus, the pick-up error due to E-field is assumed very small (Whiteside, 1962).

2.1.3.b Near Field Amplitude Measurements. The bifilar helix (No. 213) was measured as shown in Fig. 2-20. Figure 2-21 shows a result without loading from which it can be predicted that the bifilar helix will probably have a backfire radiation at 700 and 800 MHz (which is confirmed by radiation patterns). At 600
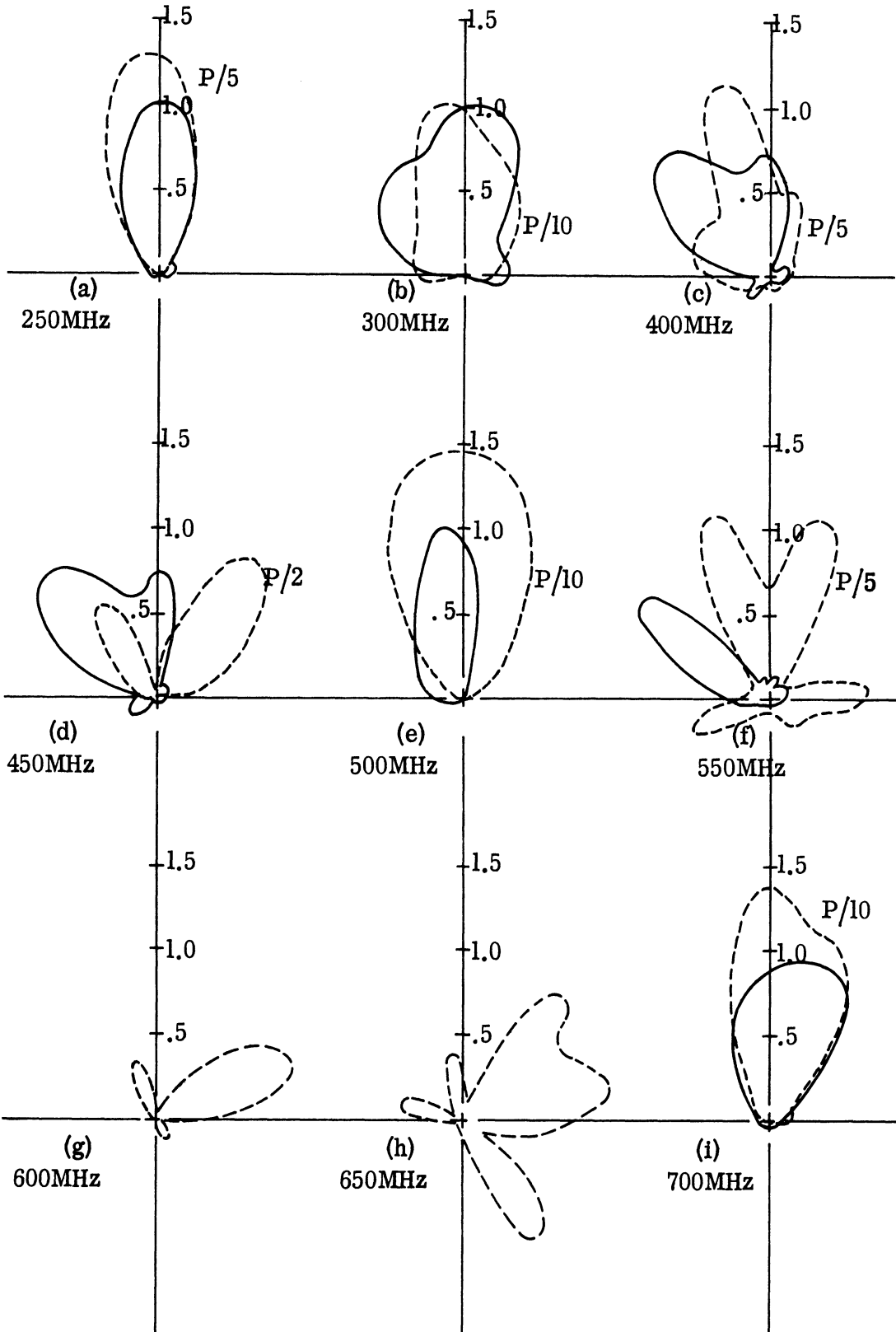
FIG. 2-15: 4" DIA. MONOFILAR HELIX (NO. 215) $|E_\theta|^2$ LINEAR POWER.

— UNLOADED, --- FULL CORE FERRITE POWDER LOADED.

P = POWER RECEIVED.
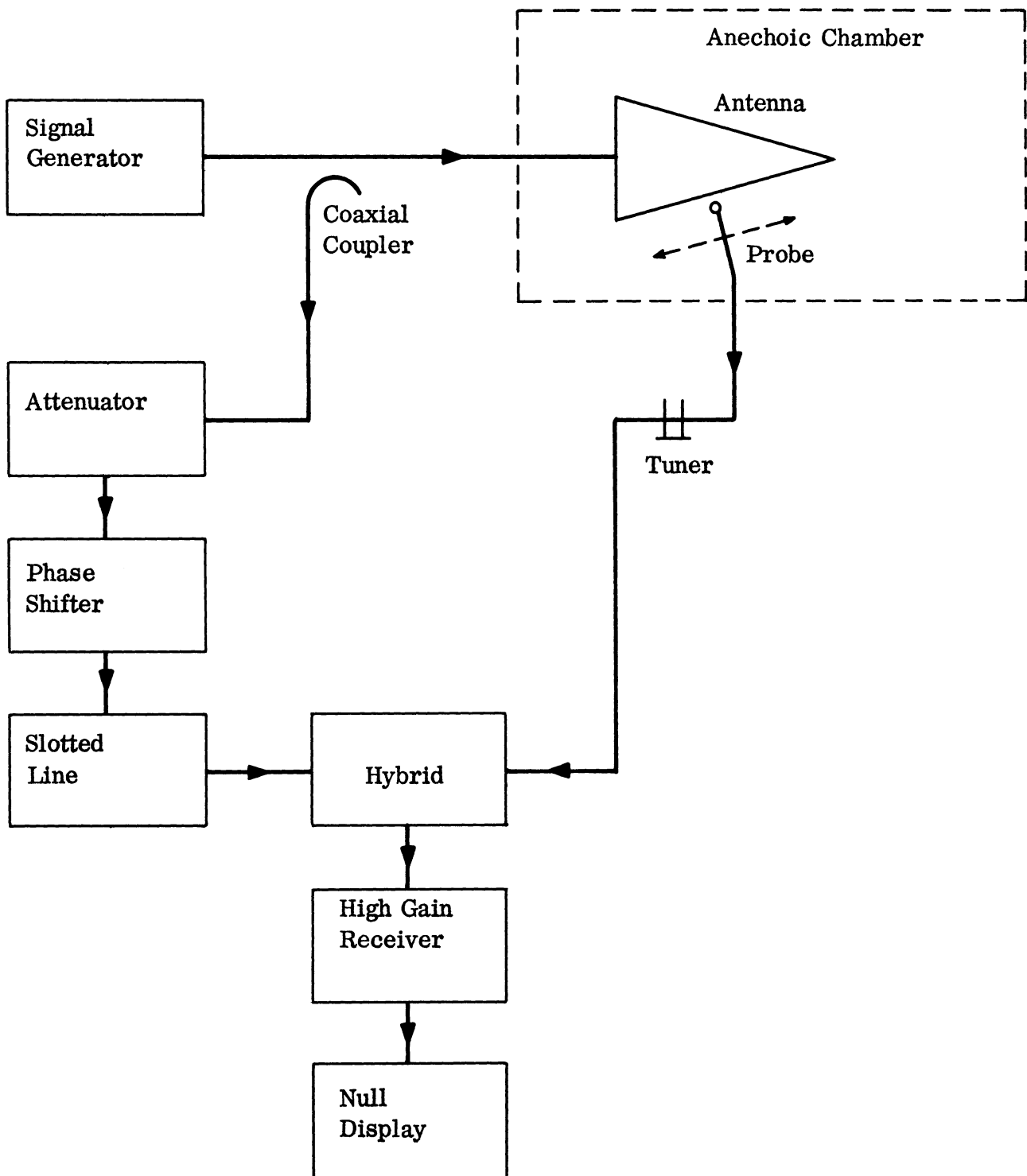
FIG. 2-16: BLOCK DIAGRAM FOR NEAR FIELD PHASE MEASUREMENTS.
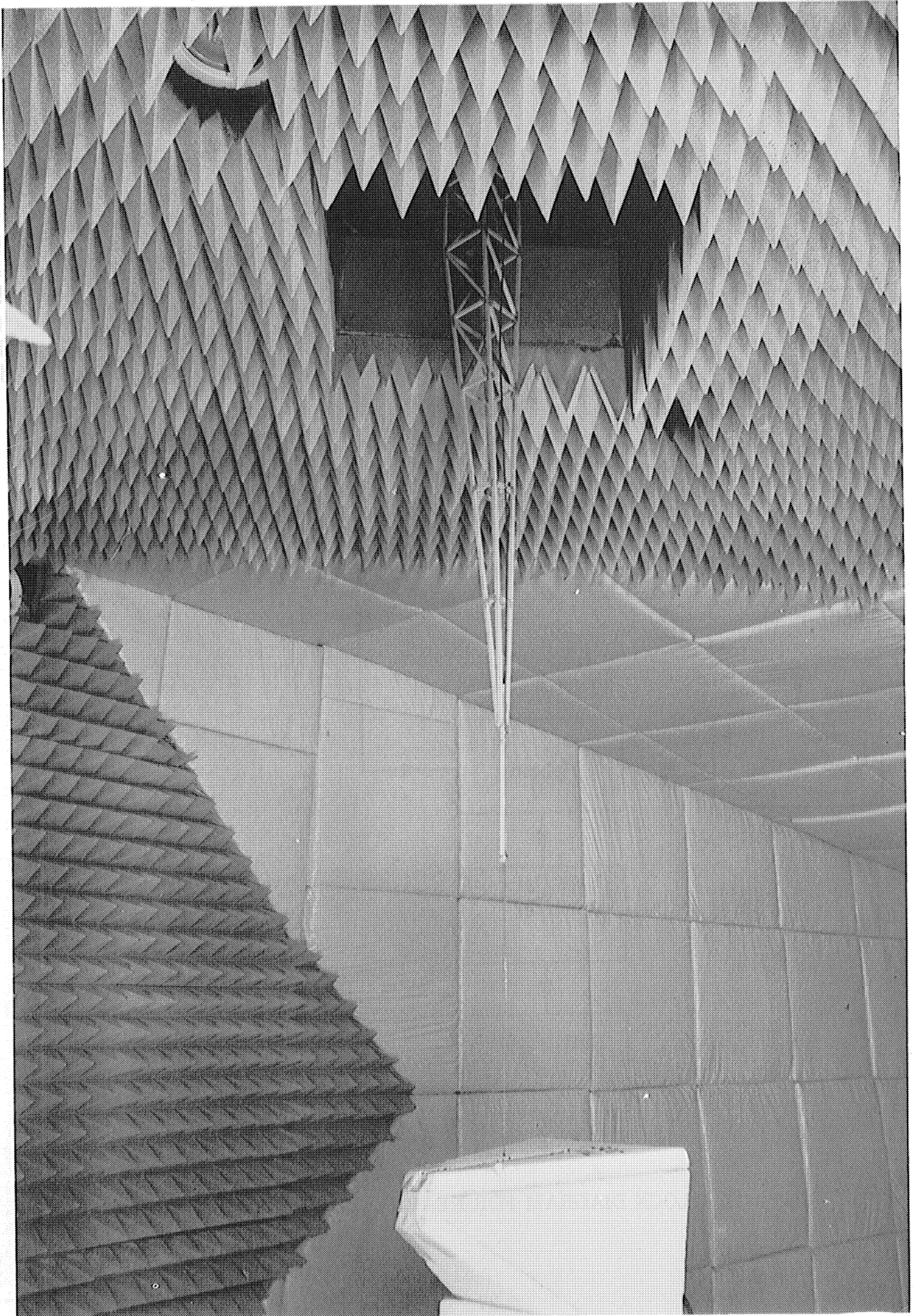
FIG. 2-17: ANTENNA NO. 223 WITH MAGNETIC PROBE ABOVE THE SURFACE; SHOWN IN ANECHOIC CHAMBER
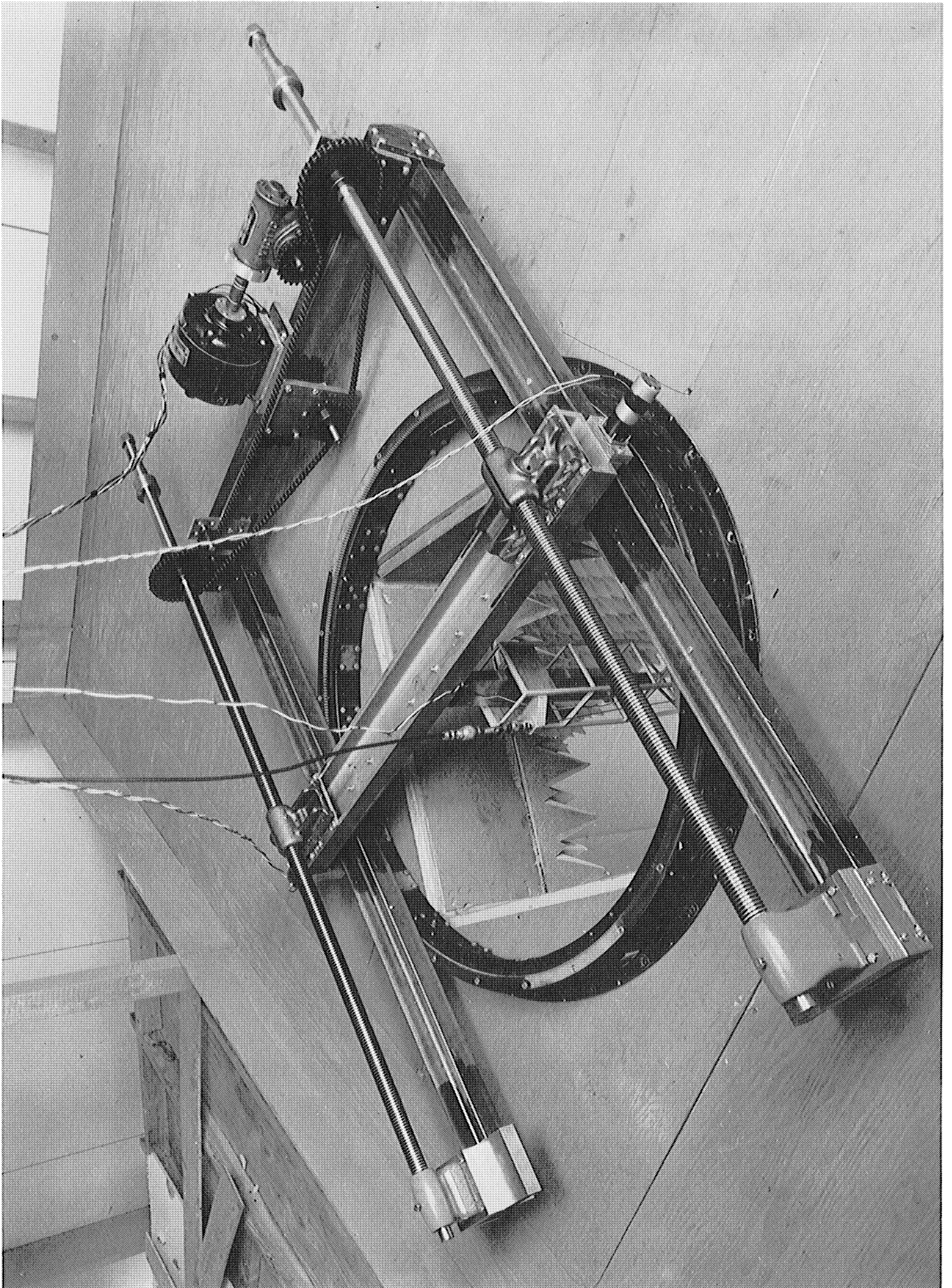
FIG. 2-18: PROBE CARRIAGE SYSTEM ON TOP OF ANECHOIC CHAMBER
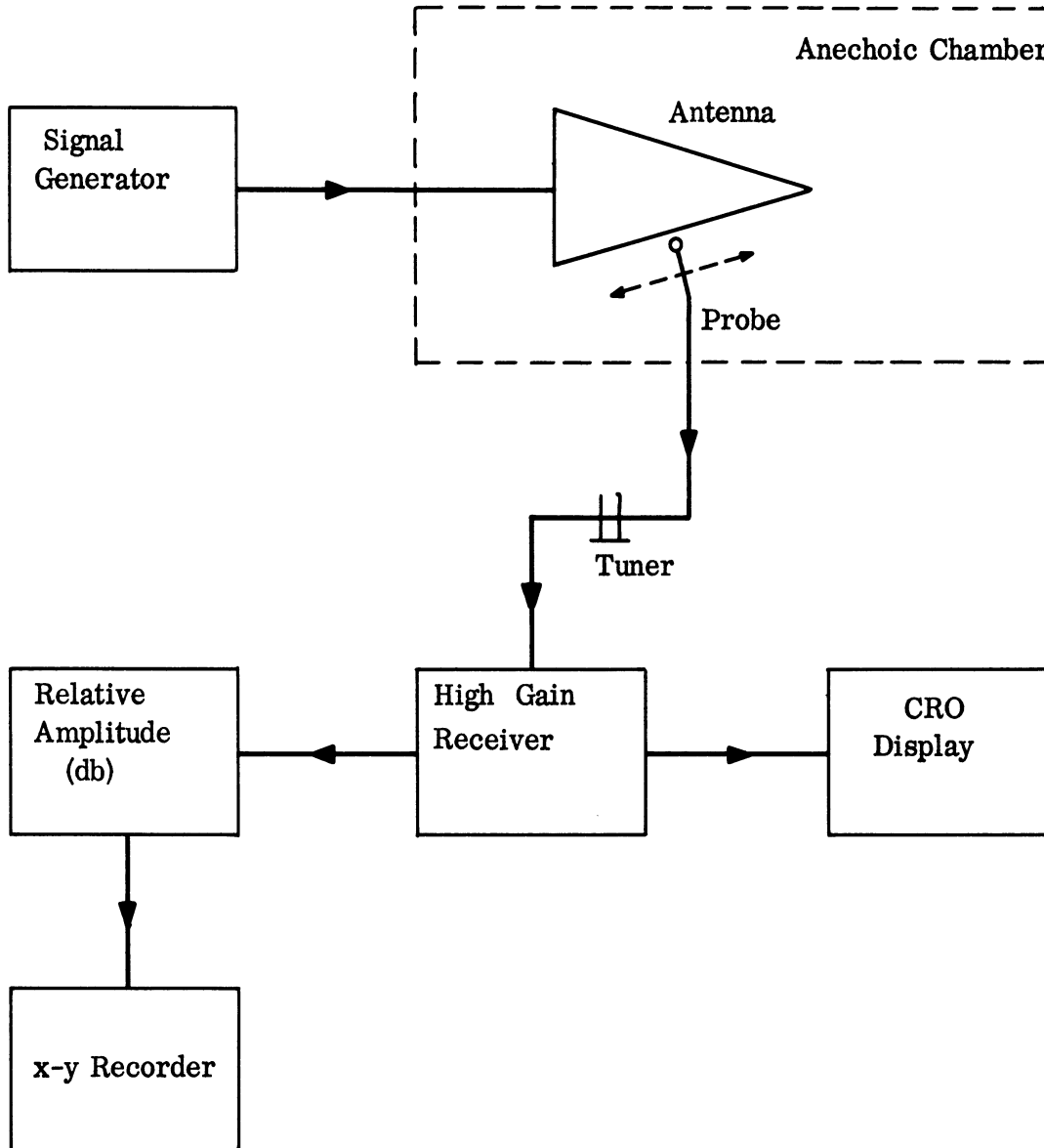
FIG. 2-19: BLOCK DIAGRAM FOR NEAR FIELD AMPLITUDE
MEASUREMENTS.

FIG. 2-20: ANTENNA NO. 217 WITH MAGNETIC PROBE IN POSITION
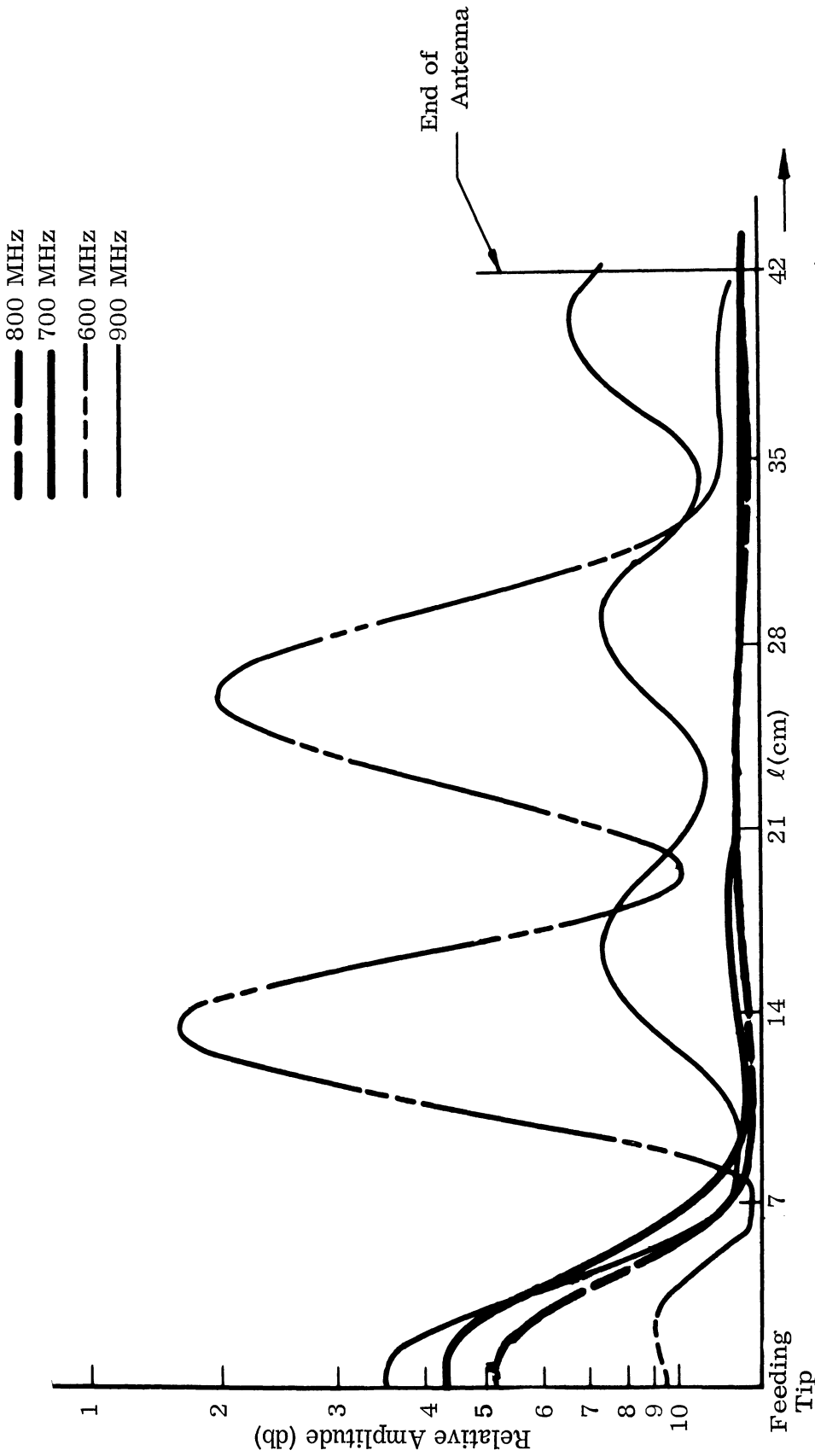
FIG. 2-21:NEAR FIELD AMPLITUDE OF ANTENNA NO. 217. PROBE POSITION $\lambda/6$ ABOVE ANTENNA SURFACE.

and 900 MHz the standing wave patterns due to the interference of higher order
modes suggest the lower and upper bounds for the backfire radiation. Neverthe-
less, from Figs. 2-5 - 2-8, it can be seen that the axial patterns remained good
below 600 MHz and above 900 MHz (no axial ratio information is available). Notice
that the radiation axial power level did peak at 730 MHz, from Table II-2. This
indicates, as stated before, that axial radiation power level may be a good far
field measure of antenna reduction. The measurements were repeated for the
same antenna by loading with a ferrite shell of 3/8" (.02λ) thick. Figure 2-22
shows that the frequencies of operation have now changed to between 550 - 700
MHz. Table II-2 shows a 3/8" layer has a center frequency of 520 MHz from
antenna pattern criterion No. 1. The radiation, and possibly the lossy nature
of ferrite at the higher frequencies, explain the observed decay of the standing
wave patterns toward the base of the antenna. The comparison of Figs. 2-21
and 2-22 shows a reduction factor of about 0.78 in the near field amplitude pattern
due to a 3/8" ferrite layer.

    2.1.3.c Near Field Phase Measurements. The relative phase shift for the
bifilar helix No. 217 was measured above the antenna conductor along the axial
direction of the antenna for both the air core and ferrite loaded cases. The results
are plotted in Fig. 2-23 for 500 MHz and Fig. 2-24 for 900 MHz. An almost
linearly changing phase shift was obtained for both cases. The effect of the ferrite
shell was to increase the phase shift constant β_1 by a factor of approximately
1.68 corresponding to a decrease in size of 0.6.

    The near field phase measurement contains information that the amplitude plot
alone cannot predict. First of all, the rate of increasing or decreasing phase angle
determines whether there is a forward wave or backward wave as seen by Figs.
2-23 and 2-24. The bifilar helix No. 217 supports a backward wave at 500 MHz
and a forward wave at 900 MHz. The loading effect is readily seen by comparing
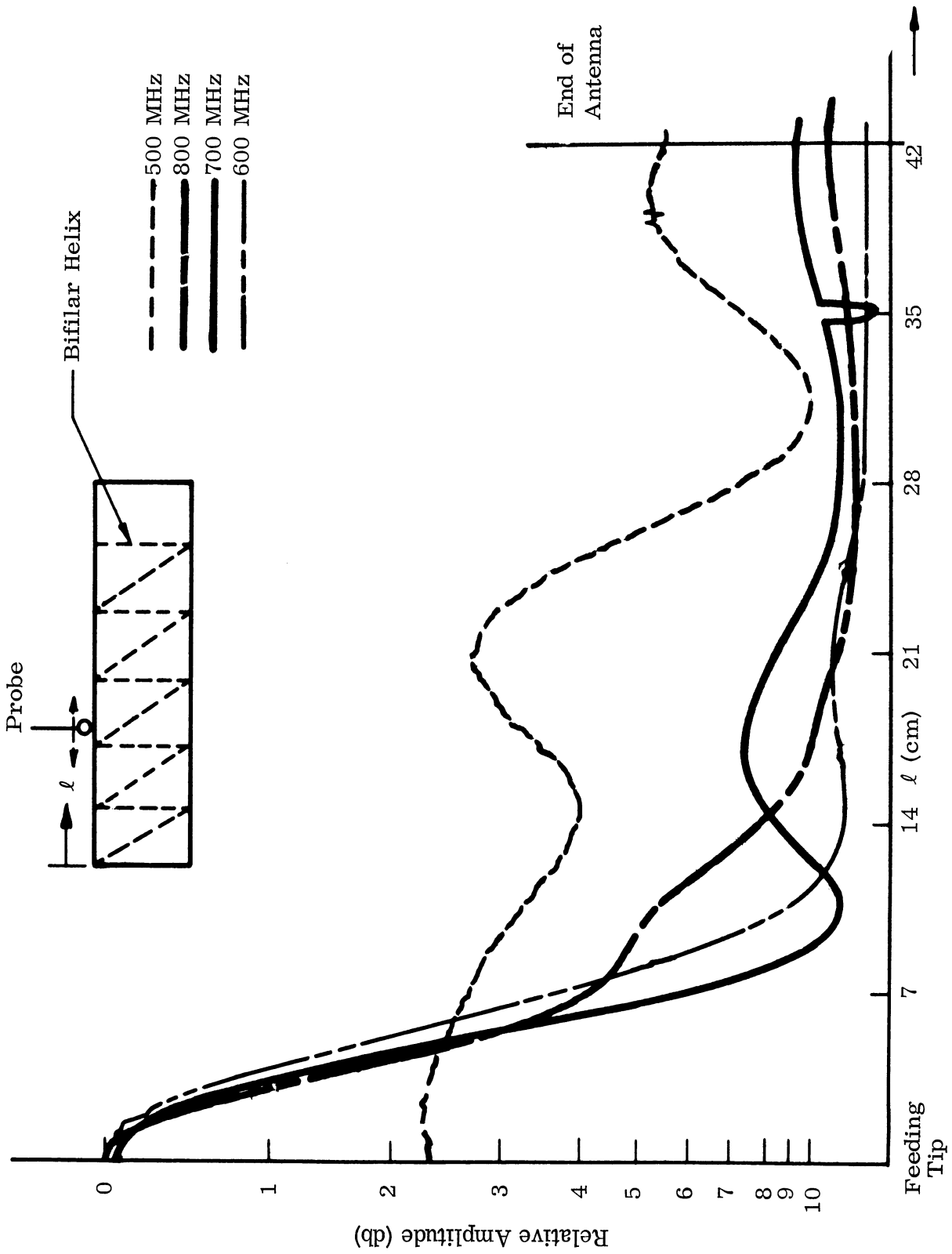
FIG. 2-22: NEAR FIELD AMPLITUDE OF ANTENNA NO. 217 WITH FERRITE LAYER. PROBE POSITION λ/5 ABOVE ANTENNA SURFACE.
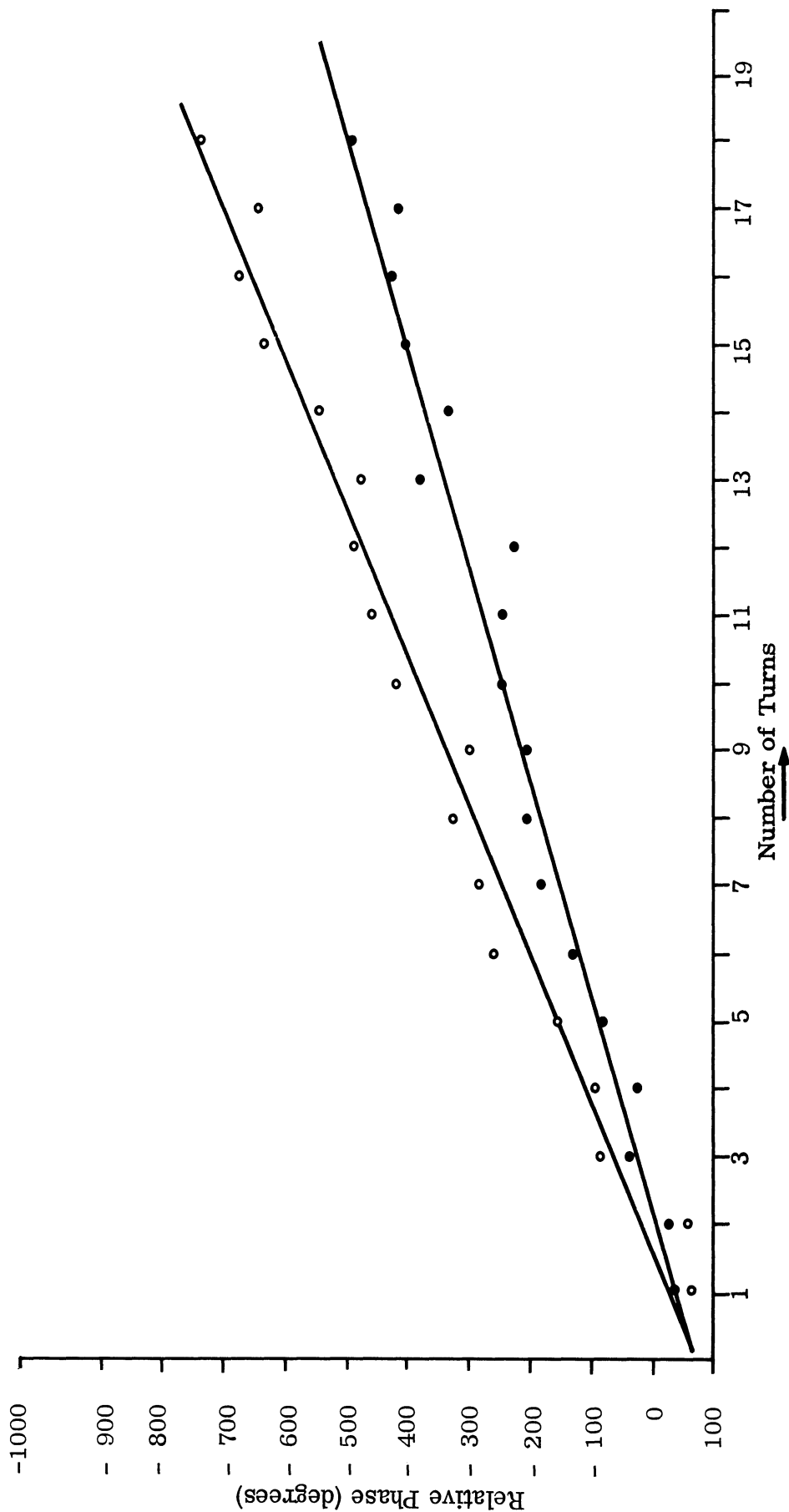
FIG. 2-23: PHASE SHIFT FOR BIFILAR HELIX NO. 217 AT 500 MHz, 0.9 cm ABOVE THE SURFACE. (○ ○) FERRITE LOADED, (● ●) AIR CORE.
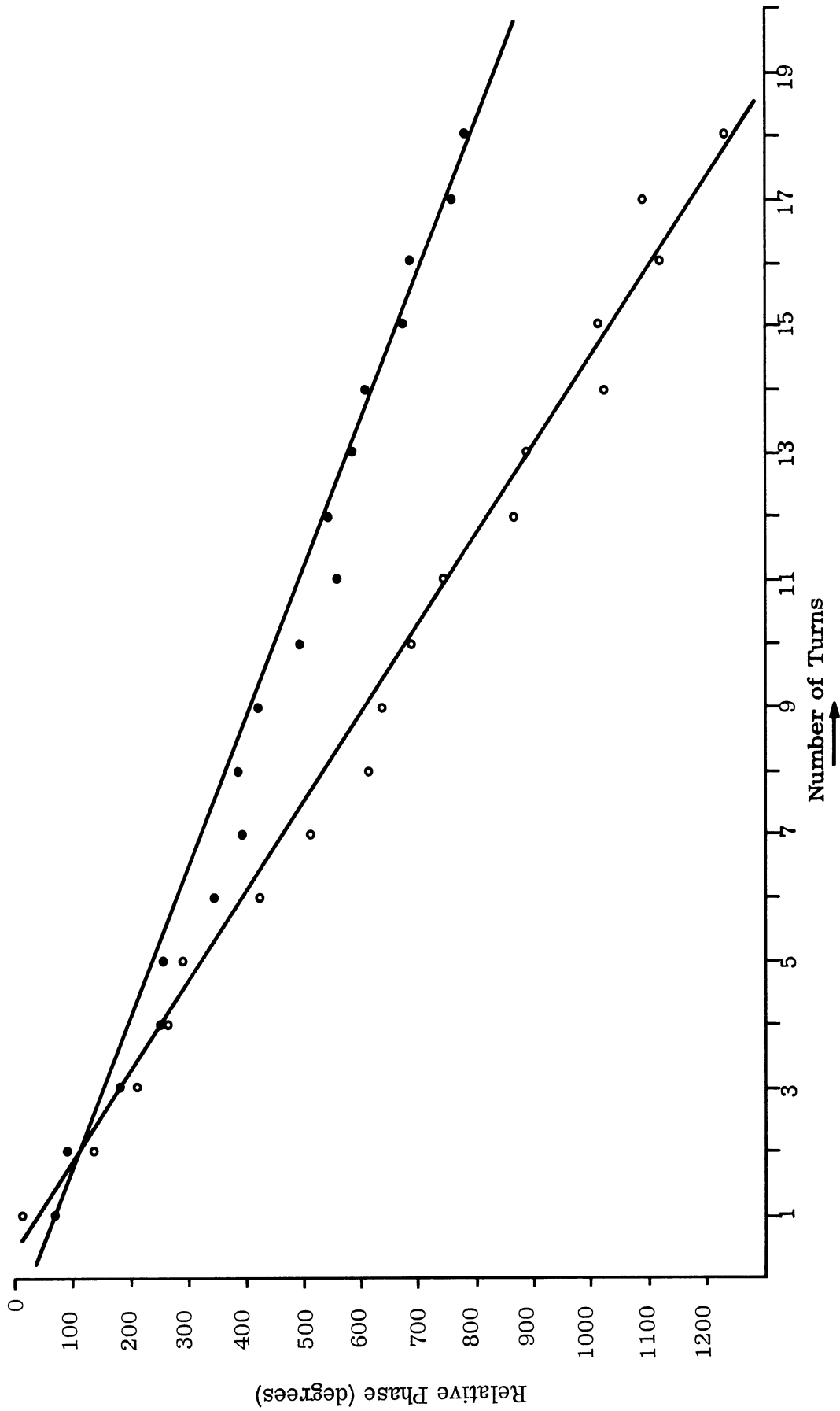
FIG. 2-24: PHASE SHIFT FOR BIFILAR HELIX NO. 217 AT 900 MHz, 0.5 cm ABOVE THE SURFACE
(o o) FERRITE LOADED (• •) AIR CORE

the change of the phase shift constant β_1. This provides the information for the effect of the ferrite loading or, for the same frequency, the factor will correspond to the size reduction factor due to the ferrite loading of the antenna. The reduction in size (0.6) is close to the theoretical reduction factor for full core loading (0.58) and is greater than the very approximate antenna pattern reduction factors. Thus, a good check of sheath theory is provided from phase measurements. Nevertheless, phase measurements alone are not sufficient to measure the whole active region problem with loading; in particular, it does not give any idea of radiation attenuation.

2.2 Loaded Conical and Pyramidal Antennas

A possible theoretical analysis of the loaded log-conical helix can be made by way of the loaded helix solution. Although no extension of the loaded helix solution has yet been tried, the method is indicated in Appendix A.

The experimental effort began with the construction of two pyramidal-helix antennas, described in Table II-4. These have been shown to operate approximately as conical helix antennas (Tang, 1962). Antenna No. 223 used a styrofoam construction to minimize any fiberglass loading. The antennas had identical properties except for wire width, feed, and apex truncation. Near field data of both in air, as discussed later, show that the fiberglass construction shifted the active region by no more than several per cent. However, some consistent differences such as beamwidth and active zone size have not yet been completely explained.

The loading experiments of these antennas have just begun; only one loading type was done for each antenna, and not all measurements have yet been made even on these. Nevertheless, significant conclusions can be drawn particularly from the near field measurements. First, near field measurements are especially important in tapered antennas, since the far field patterns are extremely insensitive to changes in active region position; only by going below cutoff frequencies of the

TABLE II-4:

SPECIFICATIONS OF CONICAL-HELIX ANTENNAS

Dimension	I.D. Number 221	223
Base, Side	9.47"	9.47"
Apex, Side	1.56"	.47"
Height	13.44"	15.38"
Apex (cone) Angle	45°	45°
Pitch Angle	85°	85°
Turns	8.5	14.75
Outer Conductor	RG 58-U	No. 20 Enamel Coated Wire
Feed	Infinite Balun	Wideband Hybrid
Nominal Frequency Range, Unloaded	500-900 MHz	500-3000 MHz

Note: Both antennas were pyramidal with a square cross-section. Construction of No. 221 consisted of two-layer fiberglass epoxy layers forming the inside supporting pyramid upon which the coax was wound. Antenna No. 223 was made of 1" thick styrofoam layers forming the outside supporting pyramid, with the antenna conductor cemented inside with epoxy.

antennas can one make any significant change in the patterns.

It is worthwhile noting that criterion No. 1 for evaluating antenna patterns (see helix section) is not available here; the data indicates that the normalized radiated power does not vary much with frequency. The cutoff frequency for "fair" antenna pattern shape or a rapid change in beamwidth will be used as the far field measure of loading effect.

2.2.1 Far Field Measurements

Both antenna Nos. 221 and 223 were first measured in air and then with a tapered loading of the Emerson and Cuming, Inc. material ($\mu = 1$, $\epsilon = 10$). The results and descriptions of the loading are shown in Figs. 2-25 and 2-26. Figure 2-25 shows that with 1/4 radius (constant ratio), partial-height loading, the antenna patterns are acceptable down to 250 MHz. Air patterns below 400 MHz on antenna No. 223 have just recently been taken, but are not shown in Fig. 2-25. Severe disturbances below 350 MHz were noted. Complete collapse of the patterns of Antenna 221 is shown in Fig. 2-26.

The poor pattern region in Fig. 2-25 from 500 - 600 MHz has not yet been fully explained. However, the near field measurements discussed later show that in this frequency region;

1) The near field amplitude has several major peaks rather than one.
2) The total active region width does not decrease with loading, causing the forward radiation zone to be excited.
3) The near fields extend into the unloaded region past the dielectric, although at a low amplitude.

Any of the above cause pattern disruption. The major unanswered question is whether there is a basic loading limitation indicated by the double-peaked near field.

Figure 2-26 shows the patterns for a somewhat unusual loading on antenna No. 221, an attempt to load only the low frequency, (large size) portion of the

Outer layer
of styrofoam

antenna
conductors

1/4 radius loading, $\epsilon = 10$, $\mu = 1$

Antenna No. 223

200 MHz

250 MHz

290 MHz

330 MHz

400 MHz

500 MHz

600 MHz

700 MHz

900 MHz
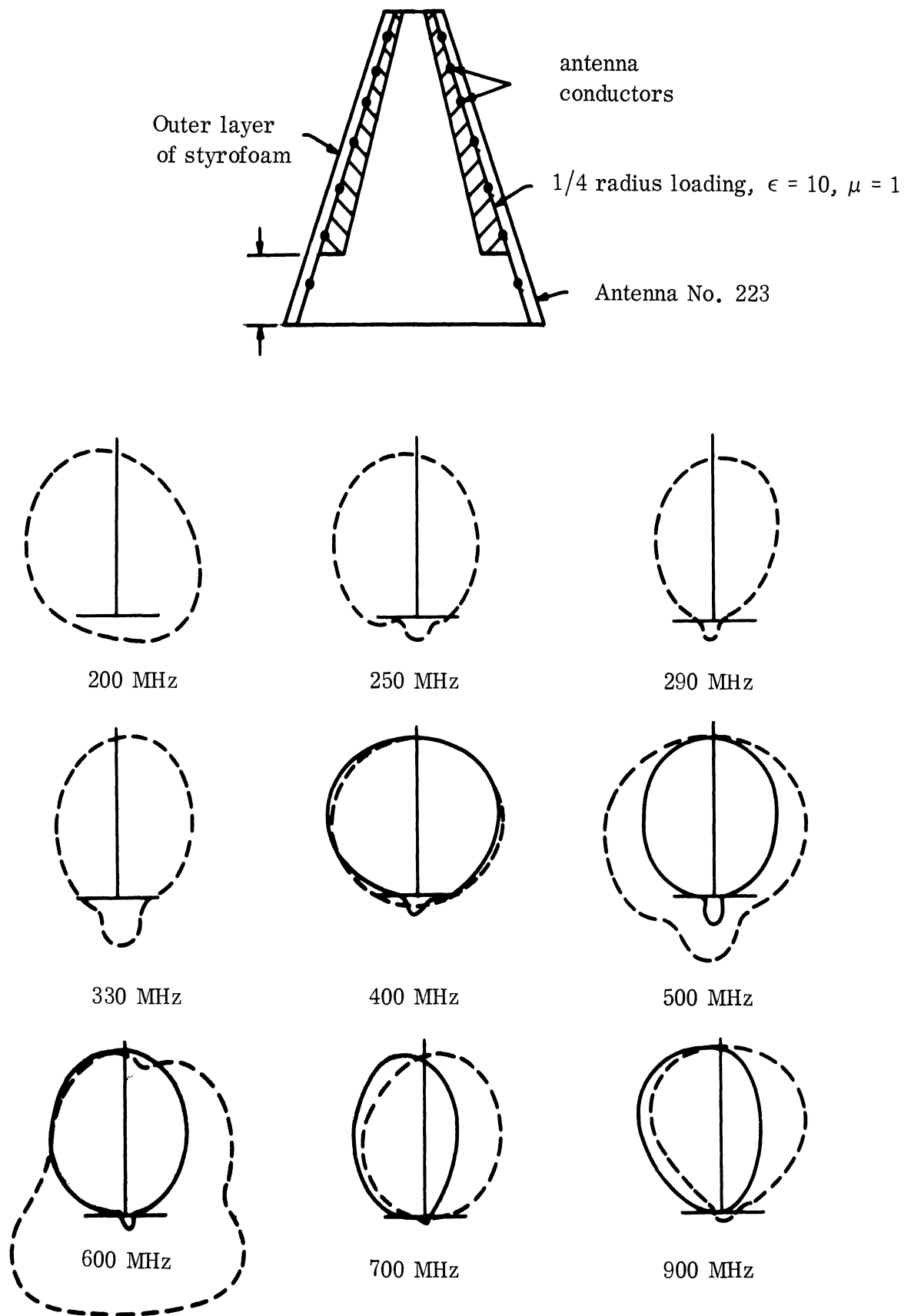
FIG. 2-25: TAPERED LOADING OF PYRAMIDAL HELIX NO. 223

————— unloaded, - - - - loaded, plots of $(E_\phi)^2$

Loading
Material
$\mu=1$, $\epsilon=10$

Antenna No. 221

1/4 a

a

230 MHz.

300 MHz

350 MHz

400 MHz
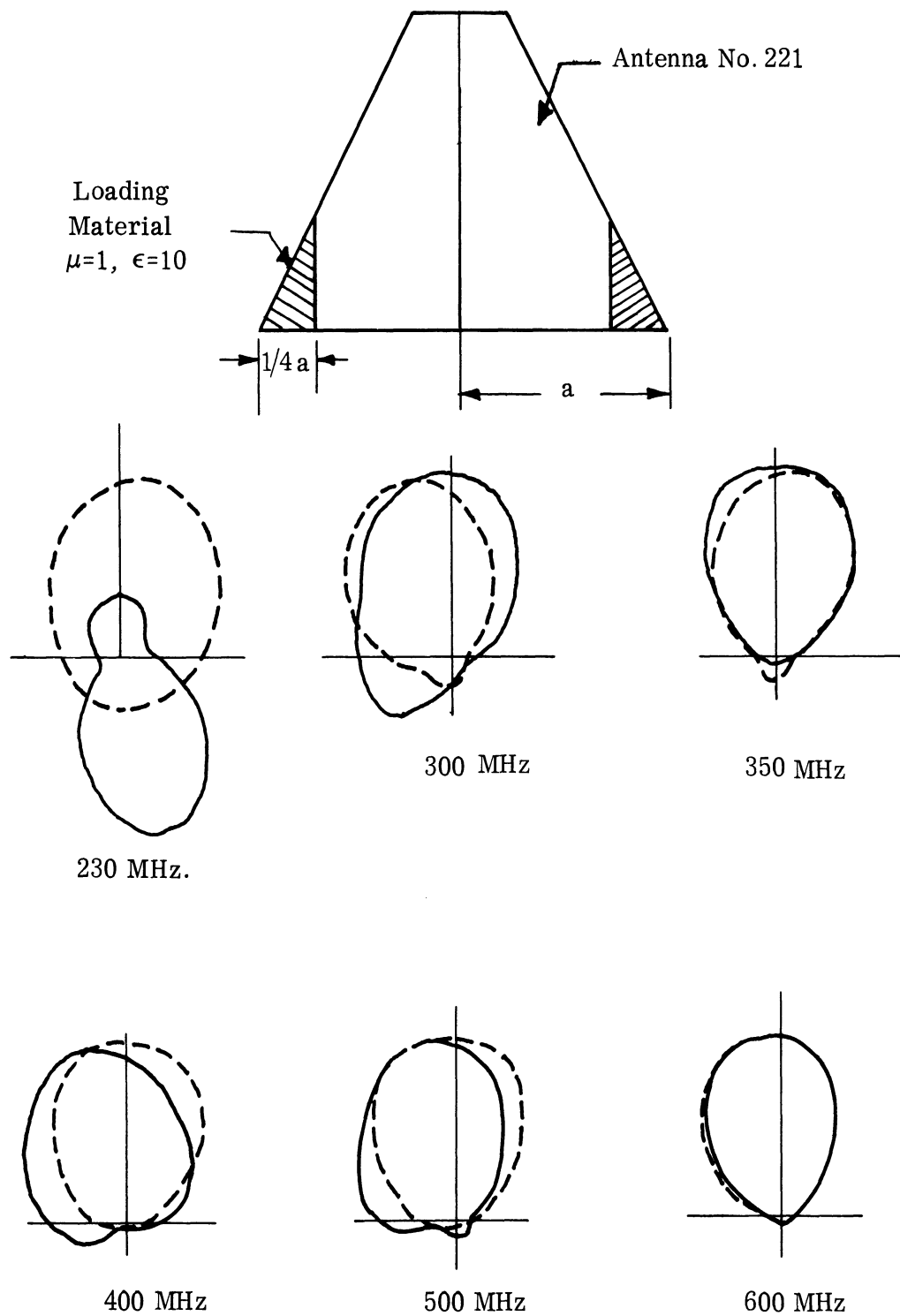
500 MHz

600 MHz

FIG. 2-26: TAPERED LOADING ON PYRAMIDAL HELIX (221)

———— unloaded,   — — — — dielectric loaded

antenna. Because of the infinite balun, the air patterns of No. 221 have some beam tilt and lack of symmetry below 600 MHz whereas the patterns of No. 223 are fairly good to 400 MHz (with some increase in beamwidth). Nevertheless, the loading on No. 221 was very successful, decreasing the frequency for fairly good patterns to 230 - 250 MHz. Near field patterns have not yet been taken.

Only a very approximate conclusion on reduction with loading can be made from far field patterns. Using the lowest frequency for an acceptable pattern as a criterion, a reduction factor of approximately 0.66 - 0.76 is obtained with the loadings shown, compared to an approximate factor of 0.74 - 0.83 with the loaded helices. The above factors are very pessimistic, since the air patterns in Fig. 2-26 were clearly disturbed below 600 MHz, but 350 MHz was chosen as the lowest acceptable air pattern. Actually a first-pattern-disturbance criterion would give a reduction from 600 MHz down to 300 - 350 MHz, (reduction factor 0.5). Similar reduction factors are obtained by taking the frequency at which a large increase in beamwidth (without beam tilt) occurs with and without loading.

2.2.2 Near Field Measurements

2.2.2.a Amplitude Measurements. The log pyramidal helix antenna (No. 223) was first measured without any loading (Fig. 2-27). Several probe positions were tried to find an optimum distance for showing the active zone clearly. Figure 2-28 a, b, and c shows data for probe positions of 1/8", 1/2", and 1" respectively above the unloaded antenna surface for various frequencies; the well known shift of the center of the active region toward the feed point as the frequency is increased is readily apparent. The greater smoothness of the near field patterns at 1" is evident, since the probe is far enough away to integrate and smooth the individual wire contributions. At closer distances, large probe signal variations are seen due to individual wire contributions. For a given effect, probe distance must be measured in wavelengths; thus as frequency is lowered for a constant probe distance, the wire
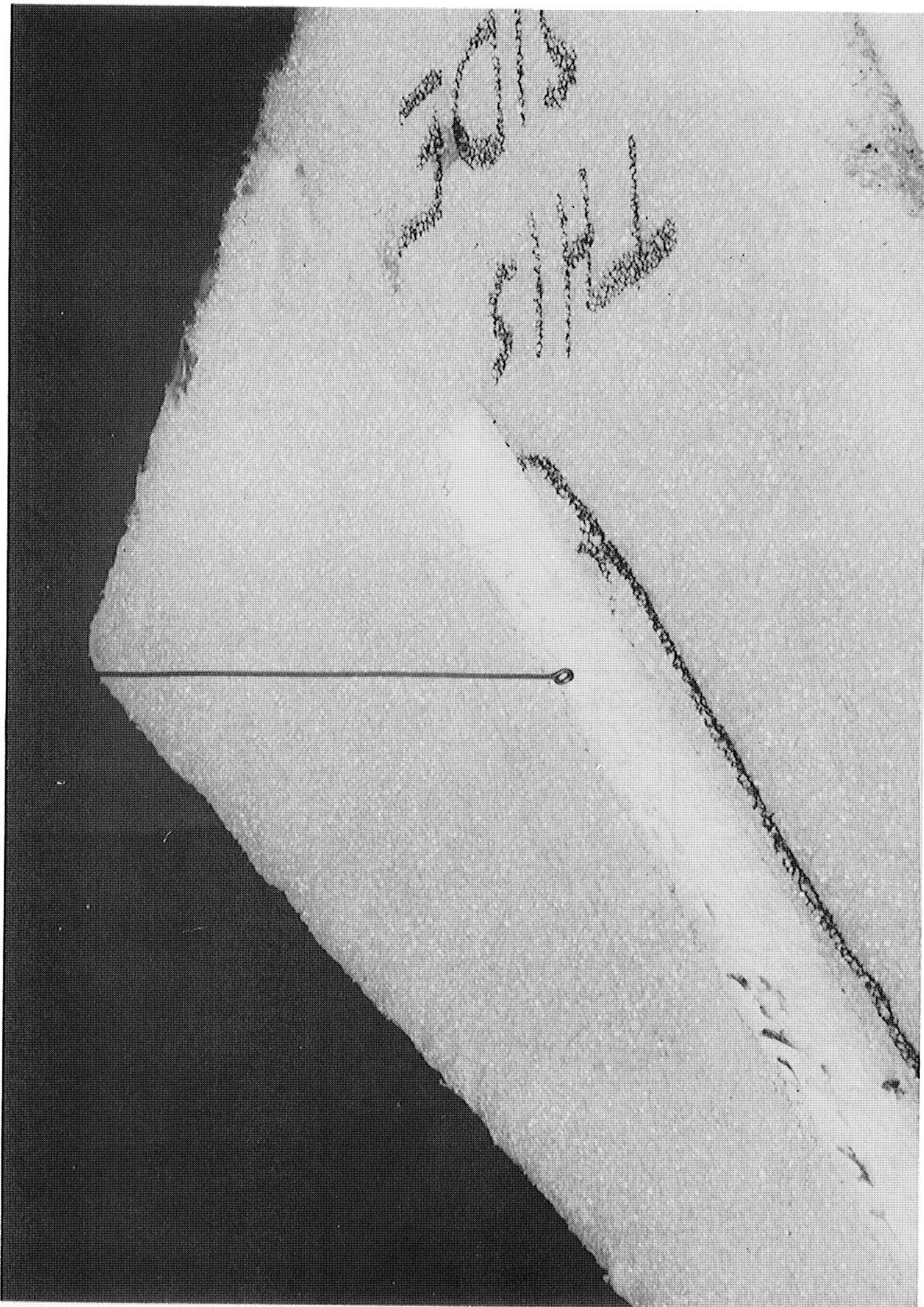
FIG. 2-27: ANTENNA NO. 223 WITH MAGNETIC PROBE IN POSITION.
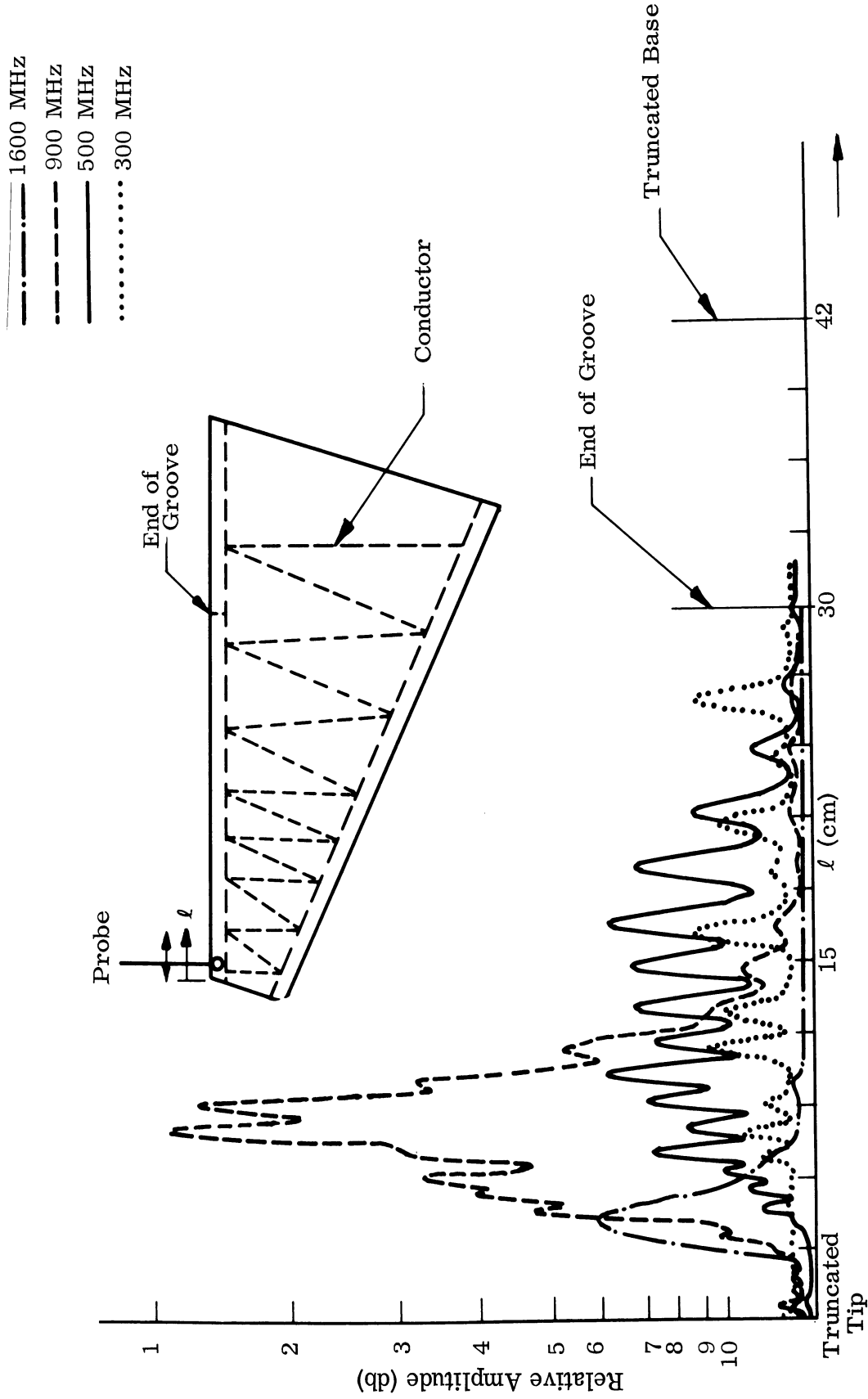
FIG. 2-28a: NEAR FIELD AMPLITUDE OF ANTENNA NO. 223. PROBE POSITION 1/8" ABOVE ANTENNA SURFACE, UNLOADED
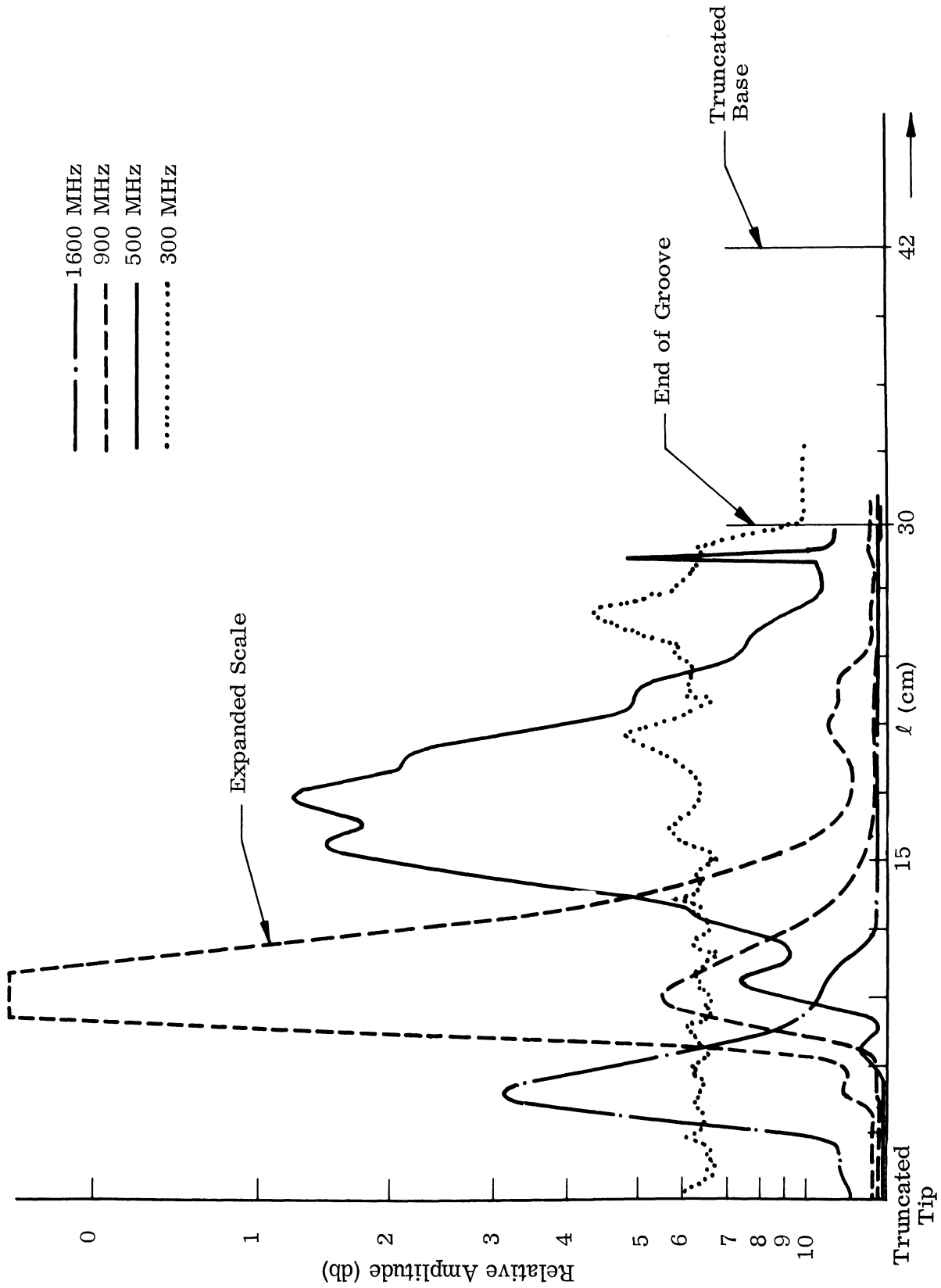
FIG. 2-28b: NEAR FIELD AMPLITUDE OF ANTENNA NO. 223, UNLOADED;
PROBE POSITION 1/2" ABOVE ANTENNA SURFACE.
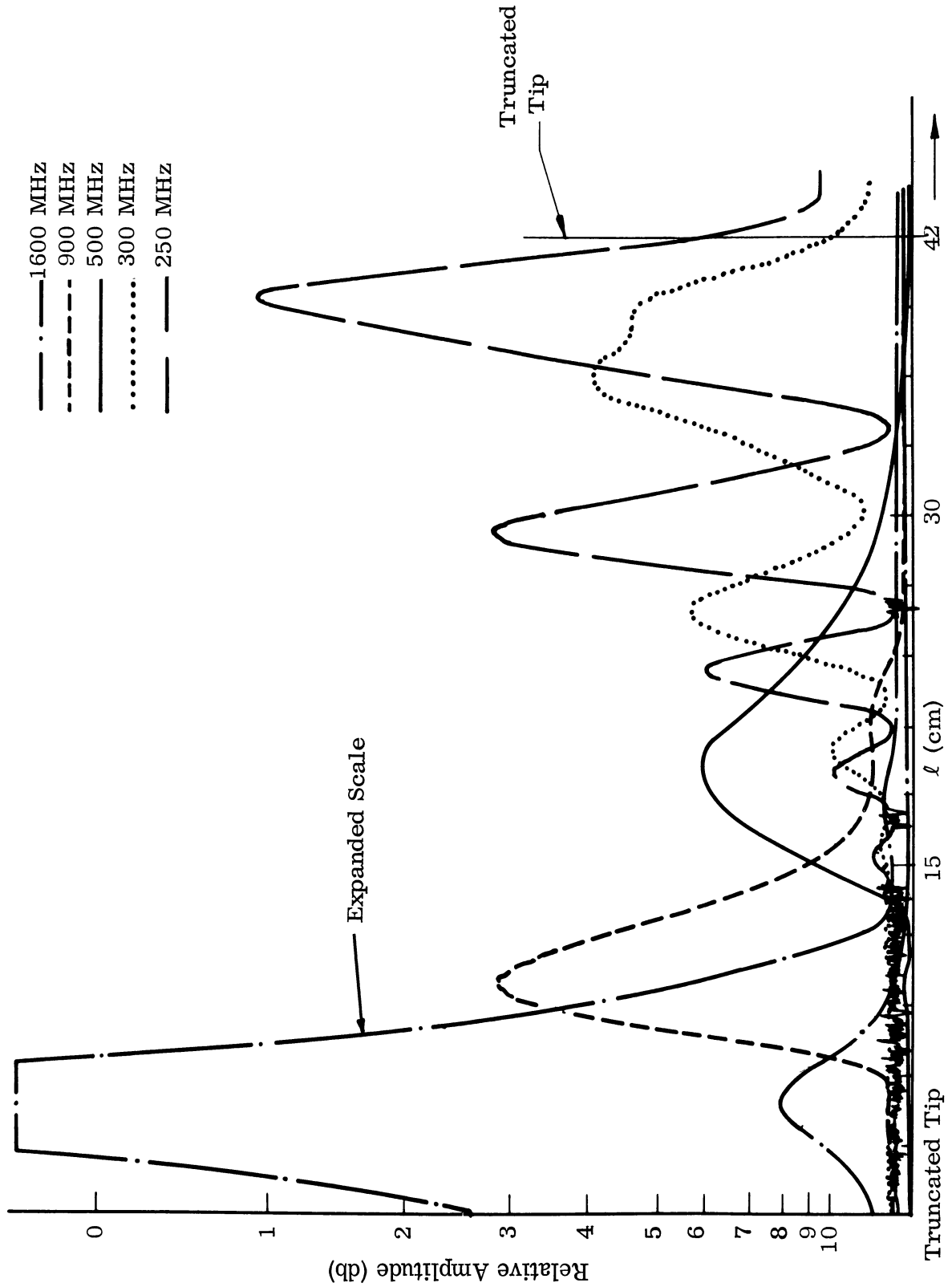
FIG. 2-28c: NEAR FIELD AMPLITUDE OF ANTENNA NO. 223, UNLOADED;
PROBE POSITION 1" ABOVE ANTENNA SURFACE.

variations become larger (see, for example, 250 MHz versus 500 MHz in Fig. 2-28c). The variations in probe signal due to passing individual wires is a local perturbation effect and should not be confused with standing waves due to traveling waves in opposite directions. The observed probe signal at 300 MHz was so weak near the tip of the antenna that considerable noise was seen in the plot, but an increasing standing wave amplitude is seen toward the base of the antenna. The groove length was not sufficiently long to allow a full-length plot at this close probe position. Due to the frequency response of the receiver, measurements were not taken above 1600 MHz. Therefore, higher order mode active regions cannot be observed in this plot. It was found from these plots that the probe distance of $1/20 \sim 1/5$ wavelength above the antenna surface provides good information on the location of the center and the width (3-db width) of the active region.

The same antenna (No. 223) was measured again with dielectric loading. The result is shown in Fig. 2-29 for a fixed probe position and 2-29b for a probe position of $\lambda/11$ above the antenna surface. The comparison of Fig. 2-29a versus 2-28c clearly points out the shift of the active region for the same antenna due to dielectric loading. The amount of dielectric material available permitted the loading to extend only to within 8 cm from the base of the antenna. The effect of this discontinuity can be seen from Fig. 2-29a and b. The centers and width of the active region for antenna No. 223 are measured and tabulated in Table II-5 for comparison. The shift of the center of the active zone of No. 223, when loaded, corresponds to a reduction factor of 0.57 at 900 MHz and 0.53 at 500 MHz. This is a very important result. The reduction factor with 1/4 radius loading is almost .5, and much more than is indicated from either helix loading experiments or far field patterns of the pyramidal helices, with the exception of the first-pattern-disturbance criterion. This measured reduction factor (0.55) is felt to be the most accurate and basic measurement made yet.
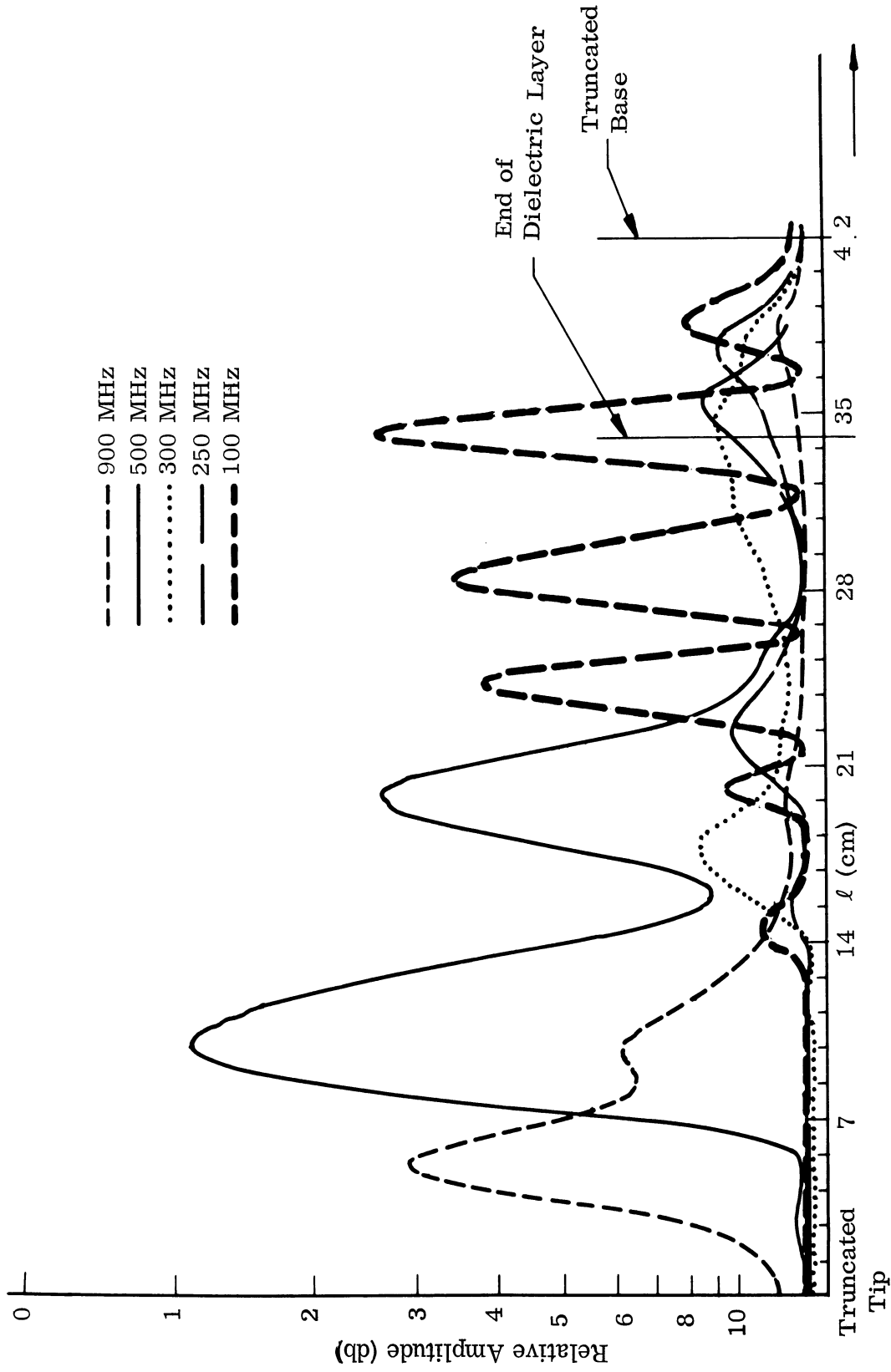
FIG. 2-29a: NEAR FIELD AMPLITUDE OF ANTENNA NO. 223 WITH DIELECTRIC LAYER. PROBE POSITION 2.8 cm ABOVE ANTENNA SURFACE.
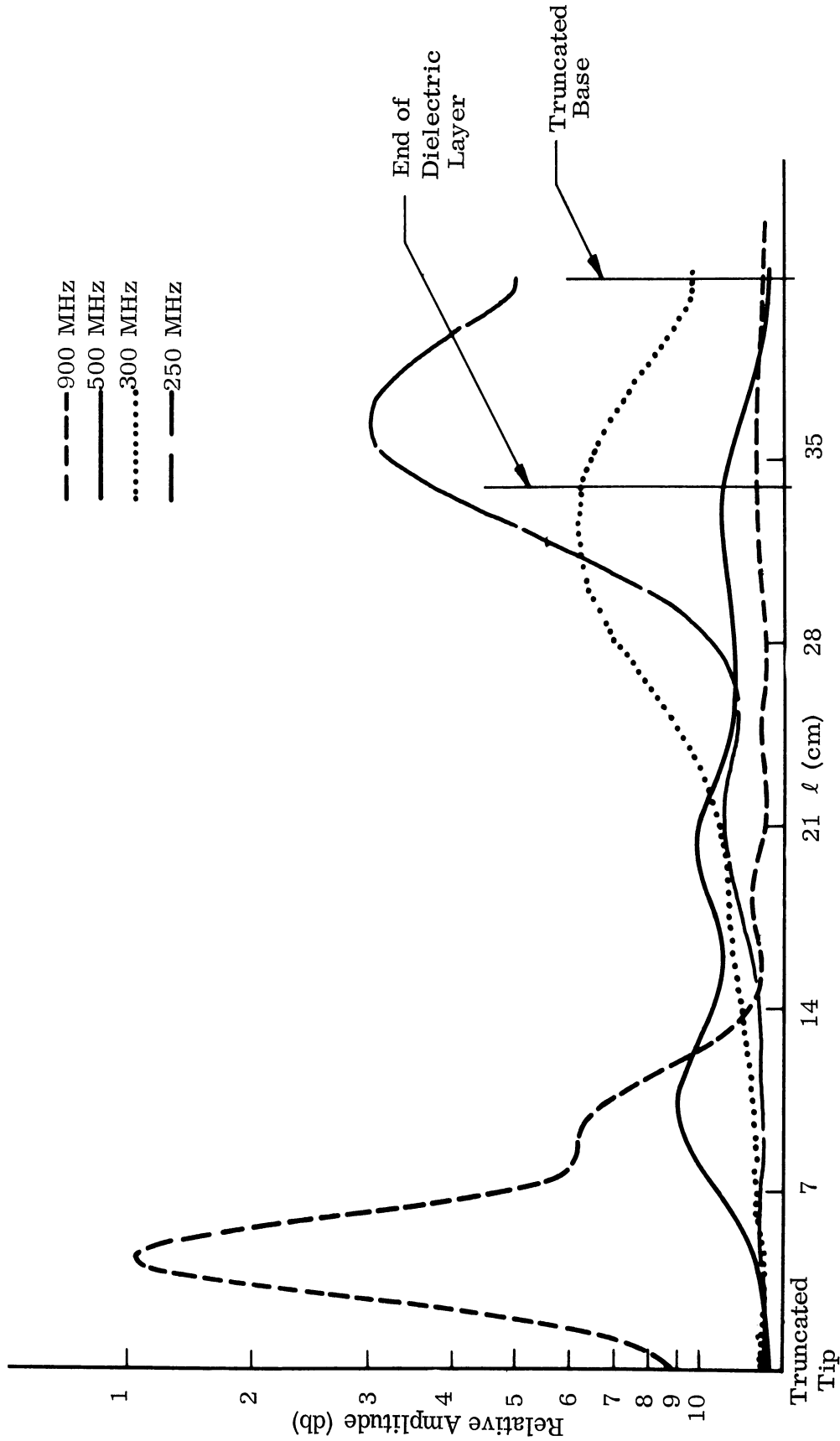
FIG. 2-29b: NEAR FIELD AMPLITUDE OF ANTENNA NO. 223 WITH DIELECTRIC LAYER. PROBE POSITION $\lambda/11$ ABOVE ANTENNA SURFACE.

TABLE II-5: CENTER AND WIDTH OF ACTIVE REGION FOR ANTENNA
NO. 223

Frequency f (MHz)	Air Core			Dielectric Shell Loading		
	Center (cm)	3 db Width (cm)	f x Width (GHz-cm)	Center (cm)	3 db Width (cm)	f x Width (GHz-cm)
1600	4.3	2.13	3.40	-	-	-
900	9.5	3.88	3.49	5.18	4.1	3.69
500	19.0	7.00	3.50	9.8	6.52	3.26
300	-	-	-	30.1	11.6	3.48
250	-	-	-	36.4	-	-

The breakup of the near field into several peaks, on the other hand, is a very serious problem. In the zigzag Section (III), this same phenomenon is discussed. It appears that some of the energy transmitted along the antenna wires is getting past this first mode radiation zone, and radiating in other regions, including the first mode forward-fire region. It is also possible that the second peak in the near field plots is not "active" (i.e., radiates poorly).

Although near field patterns of No. 221 loaded are not yet available, the setup and measurements of the unloaded antenna are shown in Figs. 2-30 and 2-31. It may be seen from a comparison of Figs. 2-31 and 2-28c that the epoxy-fiberglass, material used to construct antenna No. 221 has no significant effect on the antennas active region position (assuming the polystyrene foam plus epoxy glue construction of antenna No. 223 has no effect). The centers and widths of the active regions are tabulated in Table II-6.

It is found from Tables II-6 and II-7 that when the product of the frequency and the 3 db width of the active region is taken, it remains fairly constant for either antenna. In other words the active region width in free space wavelengths is approximately constant at 0.1 for antenna No. 223. This is indeed a very important and interesting result. The loading of a dielectric does not appear to change the normalized active zone width. This perhaps explains the band narrowing effect of a conical antenna after loading. If we define band narrowing factor to be:

$$\frac{\left(\dfrac{\text{Upper bounds - lower bounds}}{\text{center frequency}}\right)_{\text{air}}}{\left(\dfrac{\text{Upper bounds - lower bounds}}{\text{center frequency}}\right)_{\text{loaded}}}$$

then the factor for antenna No. 223 is 1.47. Notice that the active zone width used above is a total width, including both peaks.
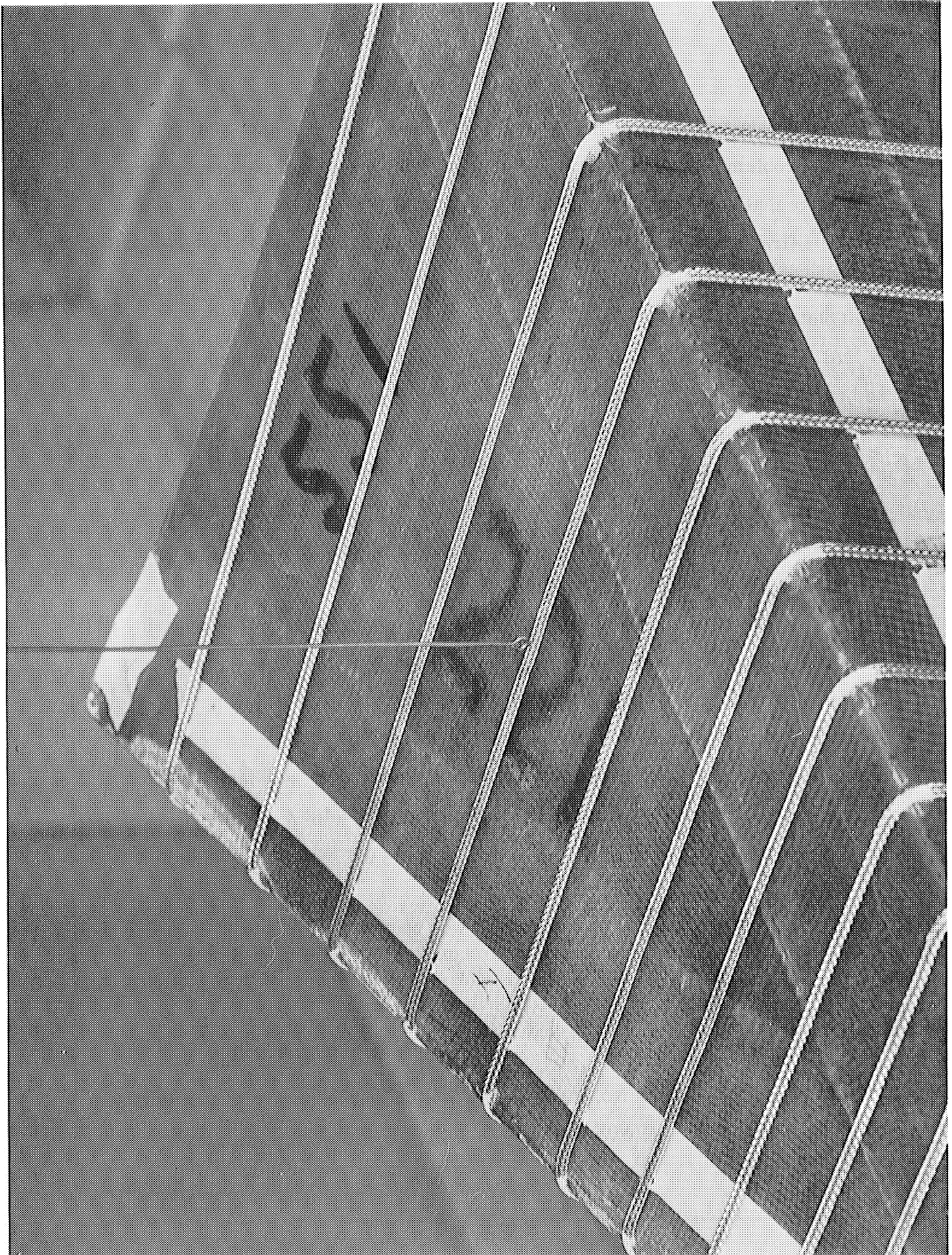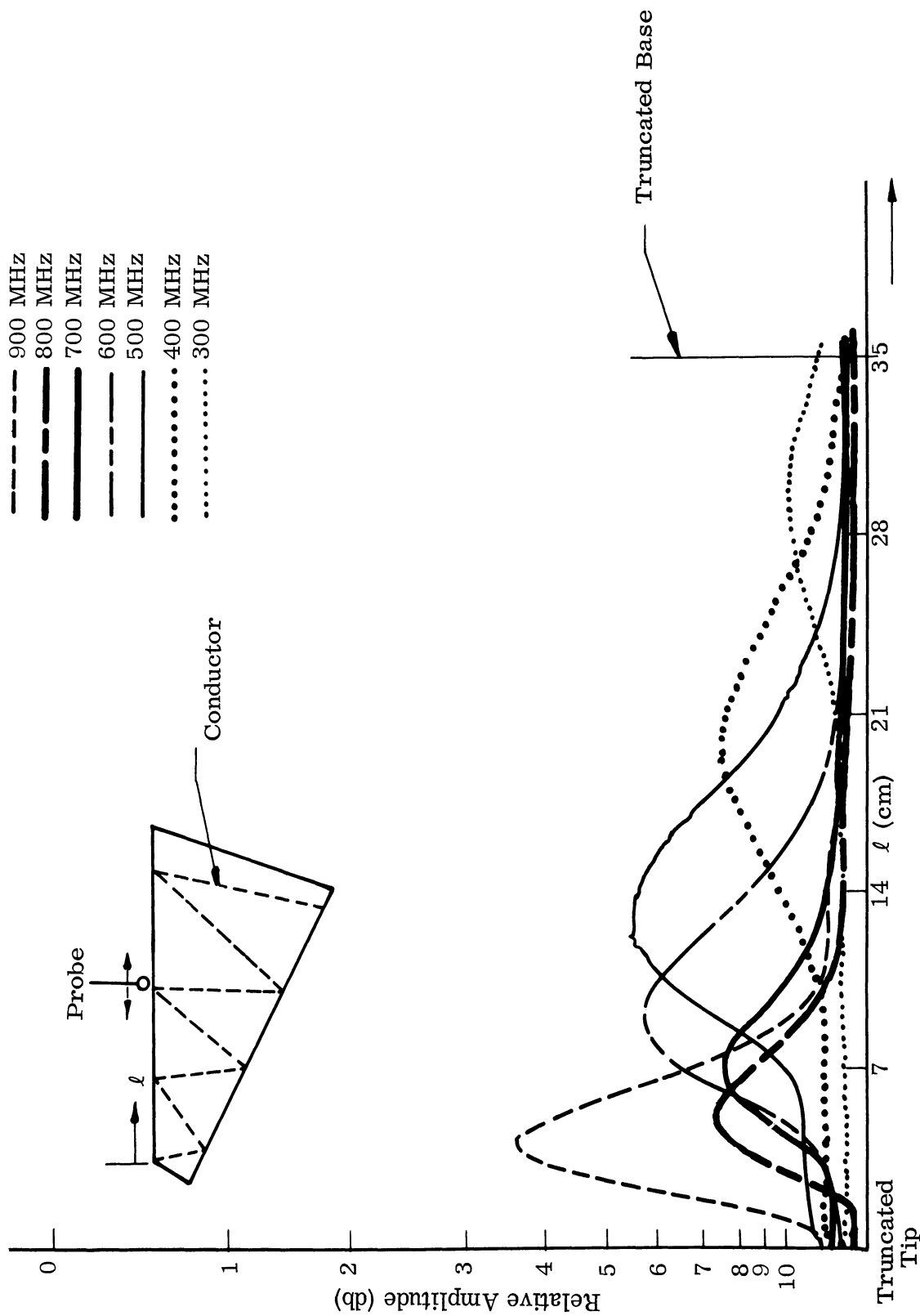
FIG. 2-31: NEAR FIELD AMPLITUDE OF ANTENNA NO. 221, UNLOADED PROBE POSITION λ/12 ABOVE ANTENNA SURFACE.

TABLE II-6:

CENTER AND WIDTH OF ACTIVE
REGION FOR ANTENNA NO. 221

Frequency (MHz)	Center (cm)	3 db Width (cm)	fx Width (GHz-cm)
900	4.1	4.82	4.34
800	5.18	5.6	4.48
700	7.10	6.2	4.35
600	9.10	7.8	4.68
500	12.6	9.6	4.80
400	19.6	11.3	4.52
300	29.4	—	—

TABLE II-7

VSWR OF LOADED LOG PYRAMIDAL
HELICES NO. 221

Frequency (MHz)	VSWR AIR	LOADED
250	—	3.3
300	—	3.4
350	—	3.7
400	2.5	1.6
500	1.9	2.1
600	1.7	1.6
700	1.9	1.5
800	2.3	1.3
900	1.7	1.3

2.2.2.b Phase Measurements. The unloaded log pyramidal antenna (No. 221) was next measured on all four antenna faces above the wires along the antenna without any loading. Figure 2-32 shows the results at 500 MHz. The phase angle decreases toward the truncated base and stays fairly constant over the active region. When the frequency was increased to 900 MHz, the phase angle decreases first and levels off over the active region and then increases rapidly toward the truncated base as shown in Fig. 2-33. Thus, the regions of backward, active and higher order mode standing waves are distinguishable. The phase shifts along each wire are plotted in Figs. 2-34 and 2-35. The dotted line indicates a net shift of 2π degrees. The actual phase shift should be continuous and increasing toward the truncated base; the phase velocity calculated from $\frac{\omega}{\beta}$ along the wire is found to be very close to the velocity of light as shown in Figs. 2-36 for wire 2. Phase measurements again show good potential for indicating effects of loading on antenna active regions.

Table II-7 is a record of VSWR of the antenna No. 221 with and without loading. The loading does not affect VSWR greatly, and with impedance corrections, the effect would be less.

2.3 Conclusion

Table II-8 shows a very abbreviated list of the best results obtained with various loadings and measurement methods. All of the loadings shown are inside. Outside loadings (with the exception of the one promising factor, .62 for a 1/2" outside shell on a helix) have yet to be investigated. A reduction factor of 0.5 appears within reach.

The breakup of the near field with loading seems to be the most serious loading problem yet uncovered. It must be thoroughly investigated. The fact that the active zone region in free space wavelengths (or the frequency-width product) was observed to be a constant may place a basic limitation on the minimum antenna size
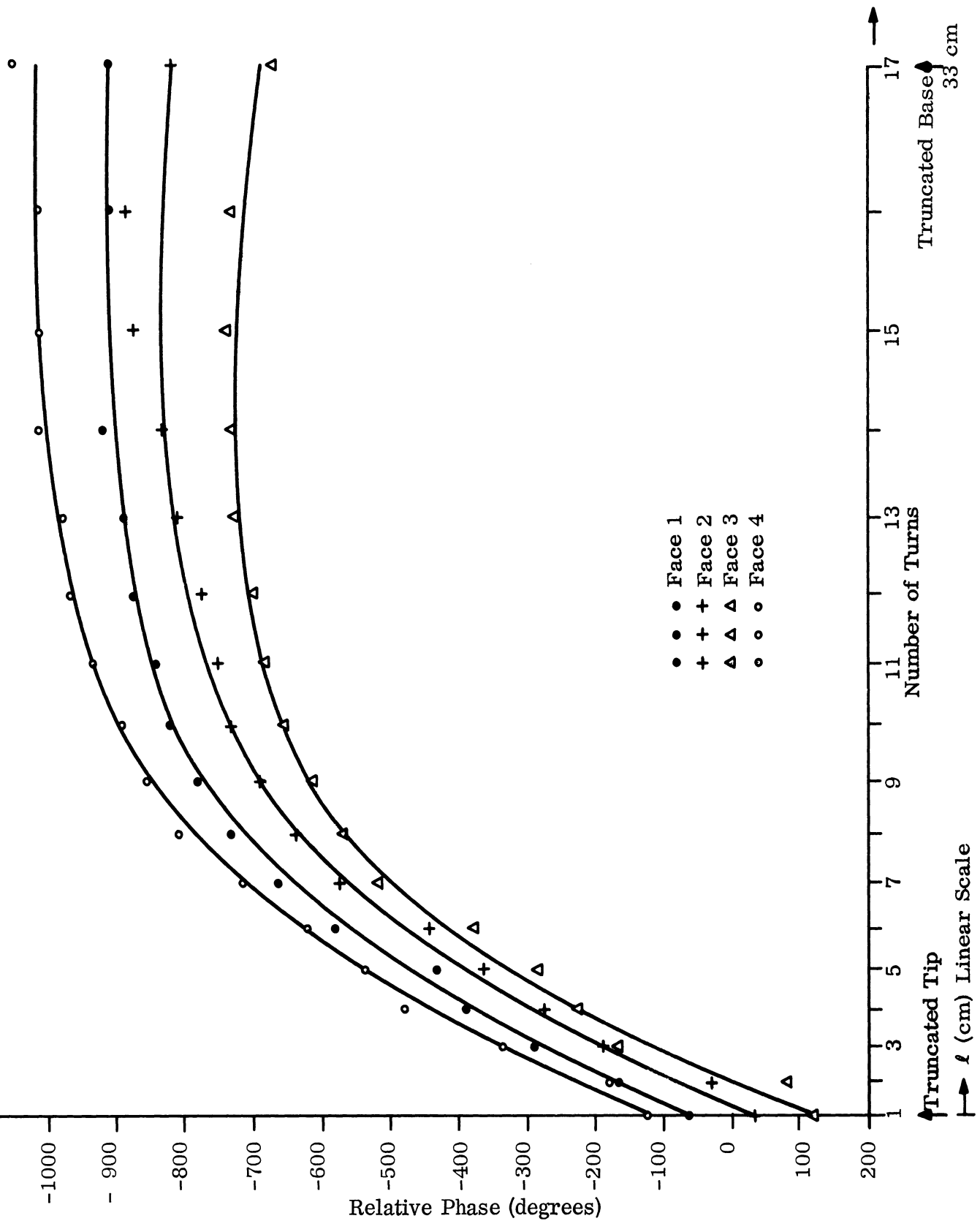
FIG. 2-32: PHASE SHIFT FOR ANTENNA NO. 221 AT 500 MHz, 0.9 cm ABOVE
THE SURFACE FOR FOUR DIFFERENT FACES, UNLOADED.
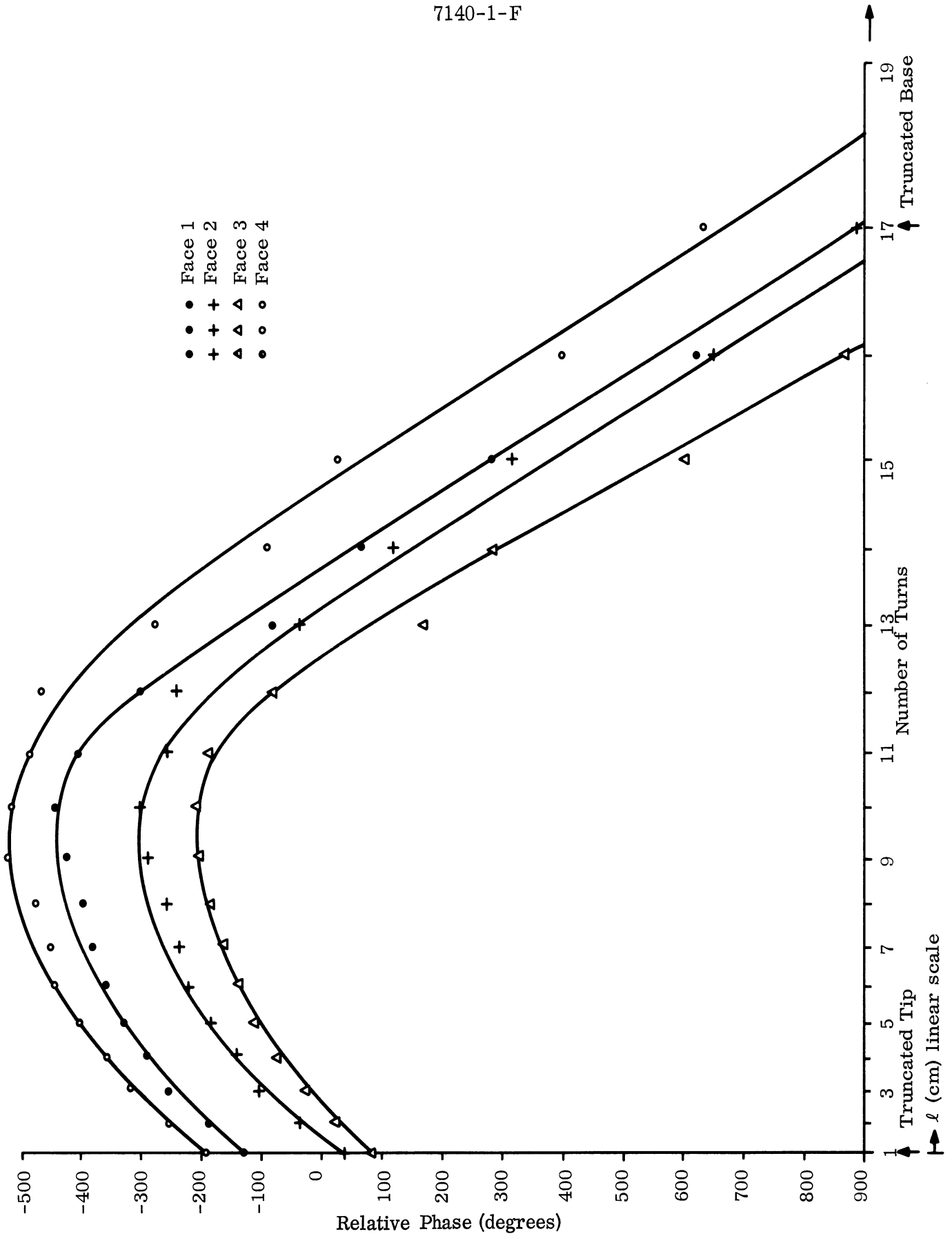
FIG. 2-33: PHASE SHIFT FOR ANTENNA NO. 221 at 900 MHz, 0.5 cm ABOVE THE
SURFACE FOR FOUR DIFFERENT FACES, UNLOADED.
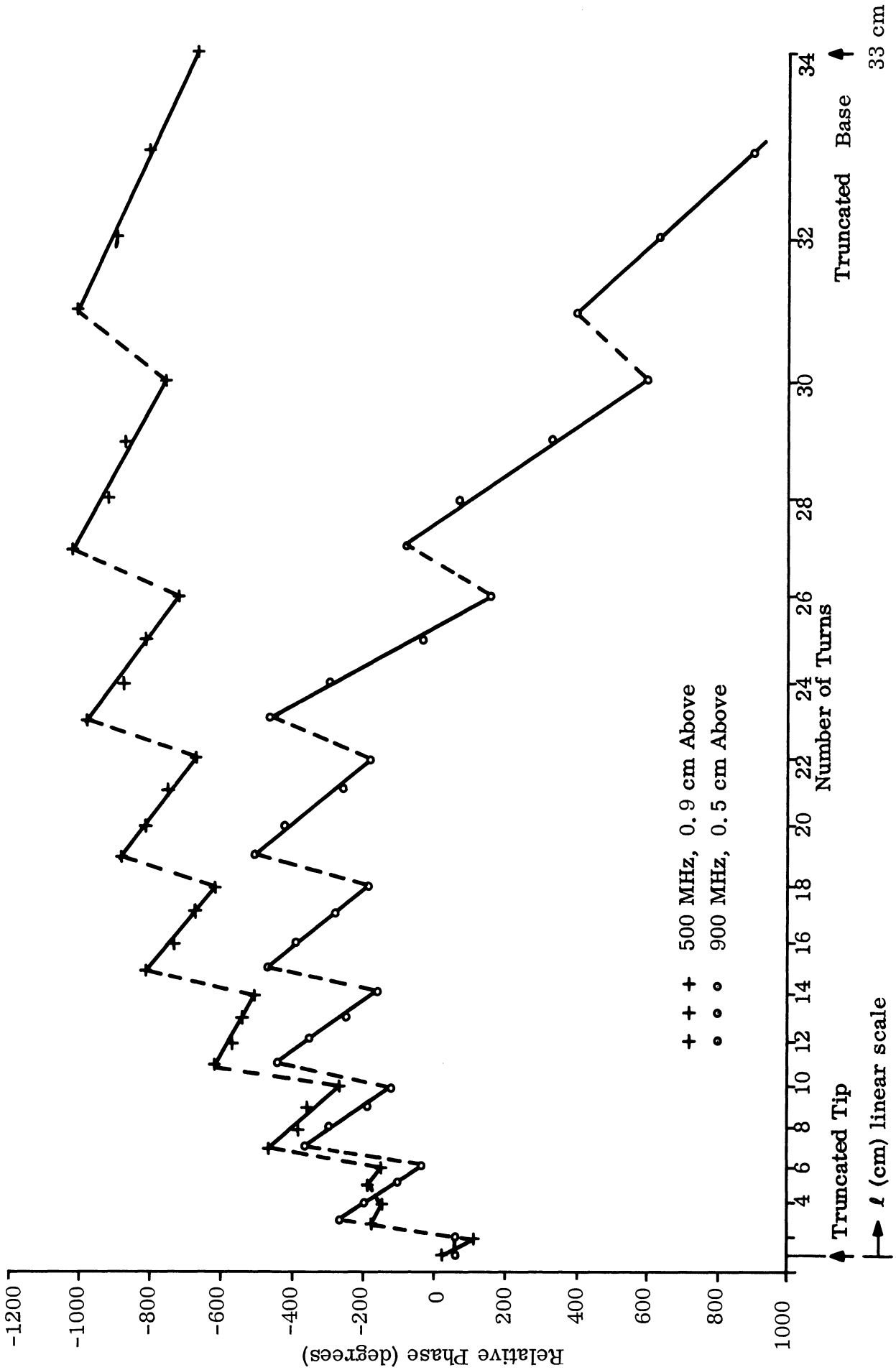
FIG. 2-34: PHASE SHIFT FOR ANTENNA NO. 221 ALONG THE WIRE 1, UNLOADED.
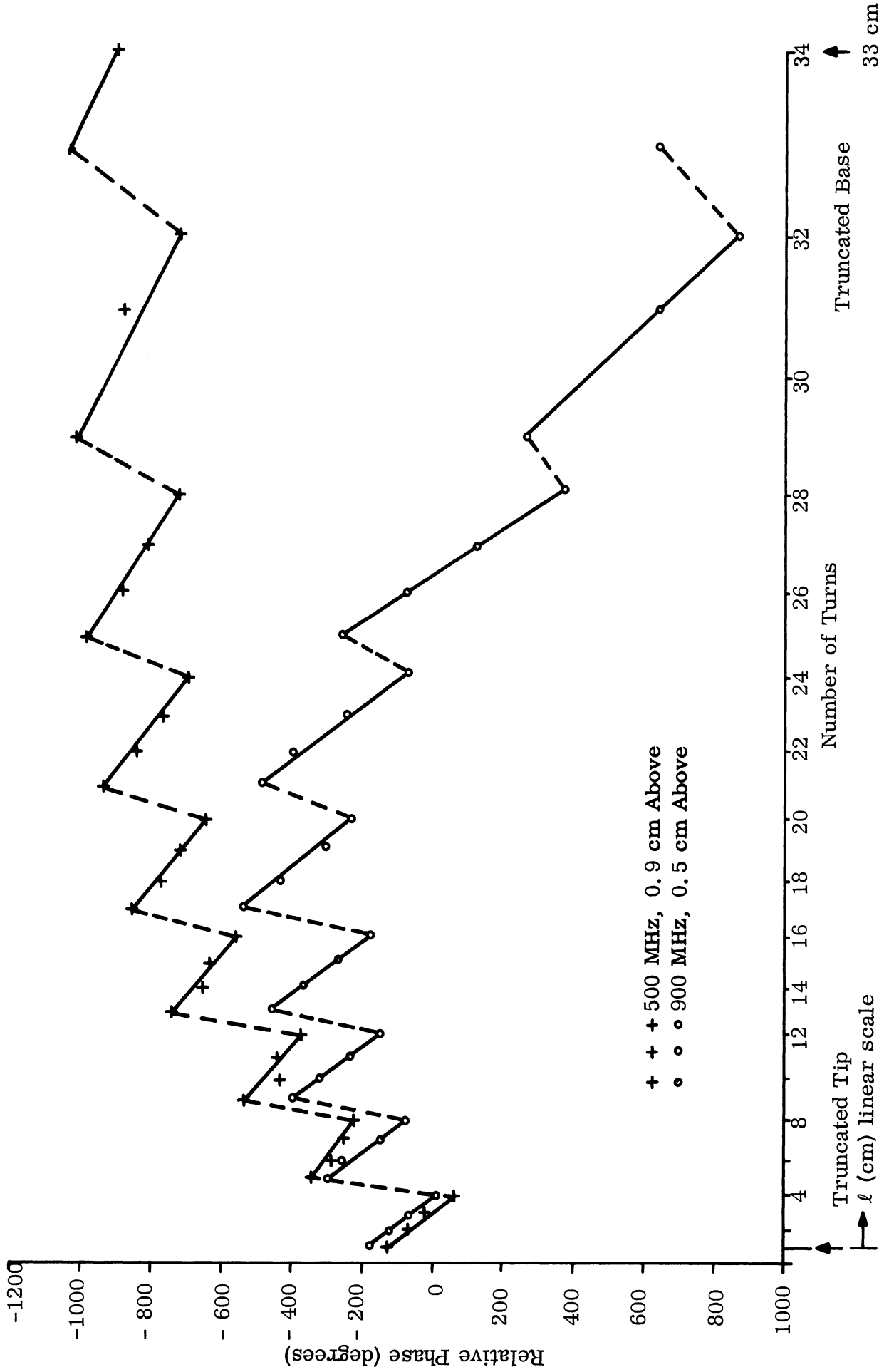
FIG. 2-35: PHASE SHIFT FOR ANTENNA NO. 221 ALONG WIRE 2, UNLOADED.
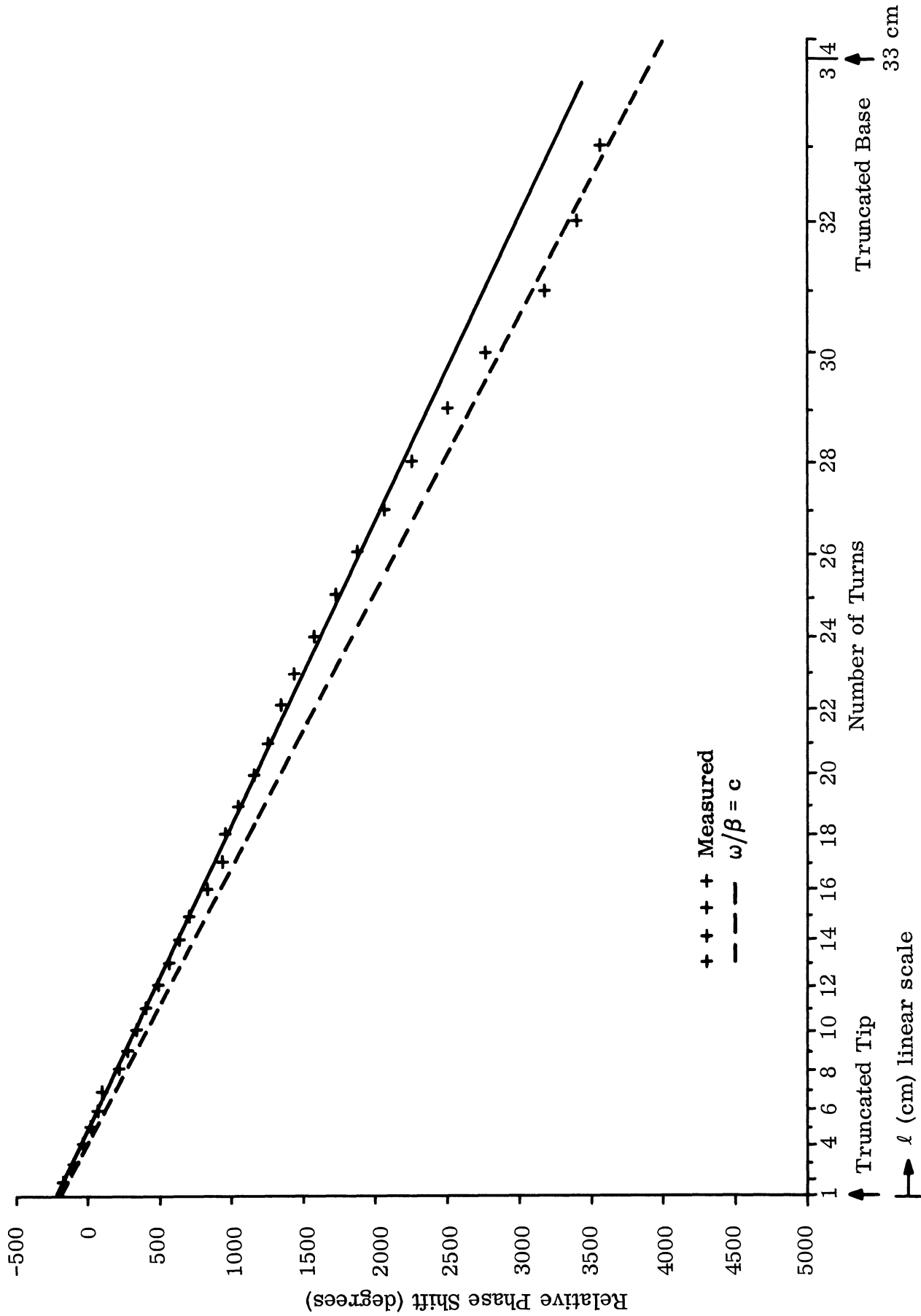
FIG. 2-36: PHASE SHIFT FOR ANTENNA NO. 221 AT 900 MHz, 0.5 cm ABOVE THE SURFACE ALONG WIRE 2, UNLOADED.

TABLE II-8:

Antenna	Measurement Type			Sheath Theory, Full Core
	Patterns (criterion 2)	Near Field Amplitude	Near Field Phase	
Helix-Ferrite	.62	.78	.7	.58
Helix-Dielectric (1/18 Radius Max.)	.78	—	—	.45
Pyramidal Helix (Dielectric) 1/4 Radius Max.)	.5 - .7	.55	—	.45

for a given pattern. Nevertheless, this width is only 0.1λ; thus, considerable reduction may yet be possible.

The near field measurement method has proved very useful in measuring the effects of loading of antennas. Antenna patterns have proved a somewhat less sensitive measure of loading effects, although normalized radiation amplitude appears to be a useful measurement.

III

BIFILAR LOG PERIODIC ZIGZAG PYRAMIDAL ANTENNAS

3.1 Far Field Patterns

Figure 3-1 shows the H-plane patterns of a solid-ferrite loaded log zigzag antenna No. 225, the characteristics of which are shown in Table III-1. The log zigzag is fed at the small end with two coaxial cables from a wideband hybrid junction. As the wave travels along the zigzag conductor, the period increases progressively with distance along the antenna axis. As the frequency increases, the active region moves up along the antenna axis. Figure 3-1 shows that EAF-2 ferrite loading patterns at 500 MHz and 600 MHz are bi-directional. At frequencies higher than 800 MHz, the radiation patterns with and without ferrite become nearly the same, since the ferrite loading did not extend to the apex and did not cover the active zones at these frequencies. Figure 3-2 shows patterns of the loading effect of the solid EAF-2 ferrite material at 700 and 800 MHz on two different log zigzag antennas, Nos. 219 and 225, described in Table III-1.

3.2 The Near Field Amplitude Measurement of Log Periodic Zigzag Antenna

The near field amplitude was measured on antenna No. 225, loaded with powdered EAF-2 ferrite as shown in Fig. 3-3. The near field pattern, Fig. 3-4, shows a backfire radiation from higher than 900 MHz down to about 450 MHz. At 400 MHz the near field amplitude begins to deteriorate. Thus, the overall frequency band of this unloaded antenna is about 450 MHz and the center frequency is approximately 680 MHz.

The antenna was then loaded with the ferrite powder layer with the thickness of 3/8" as shown in Fig. 3-3. The near field amplitude was measured and is shown in Fig. 3-5a and Fig. 3.5b. The near field amplitude does not have a single peak as did the unloaded case; however, it is still possible to observe the effect of the

300 MHz

400 MHz

500 MHz

600 MHz

700 MHz

800 MHz
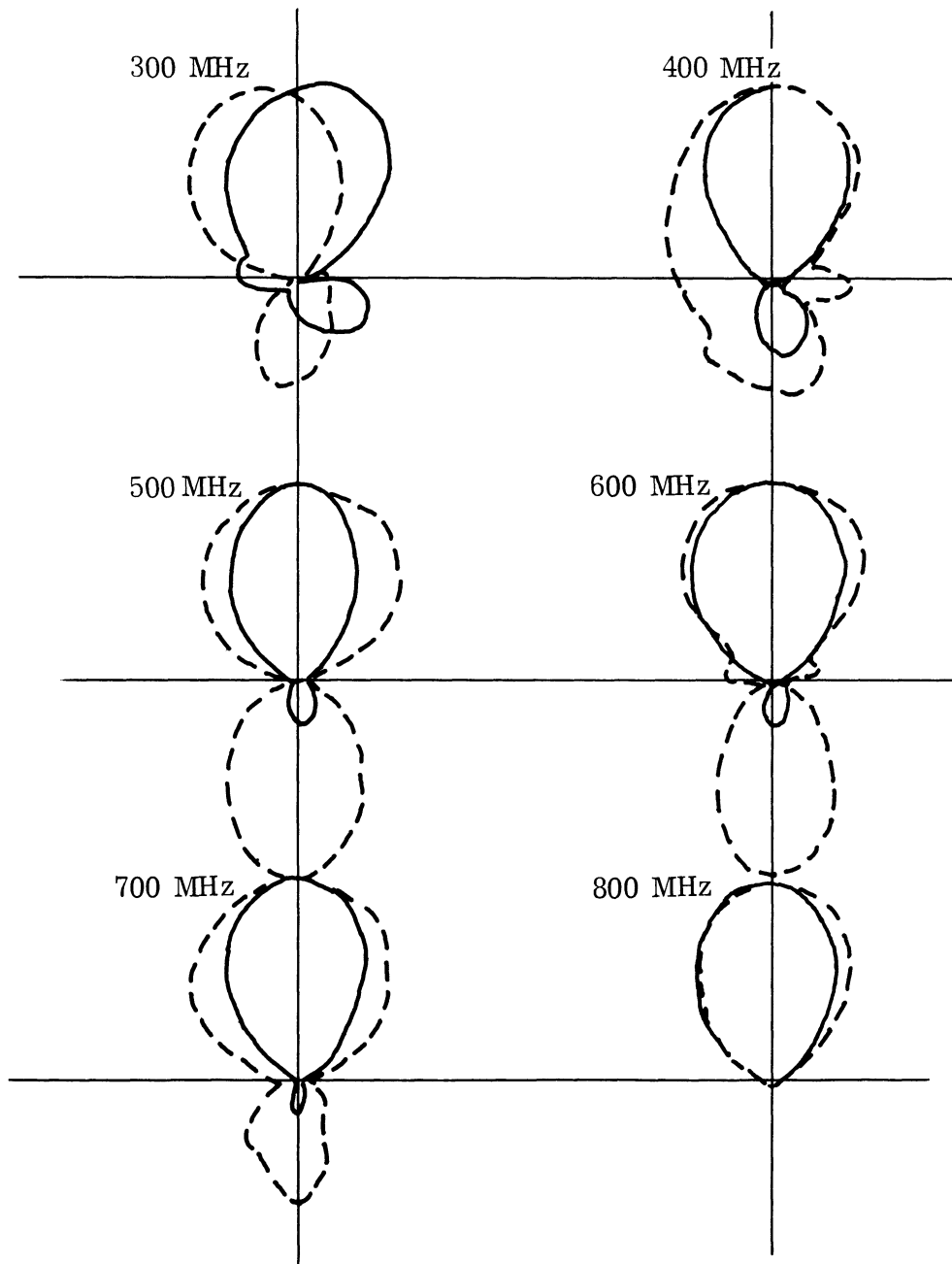
——————— Air Loaded

— — — E A F 2 Ferrite Loaded

FIG. 3-1: H-PLANE PATTERNS OF LOG ZIGZAG ANTENNA (No. 225)
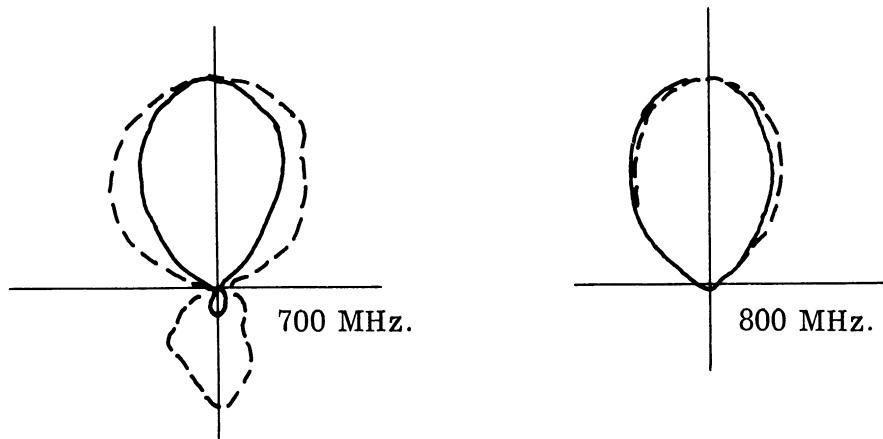
(a) Log Zig Zag Antenna (No. 225)

$\alpha = 12^{\circ}$ $\gamma = 10^{\circ}$ $\tau = 0.85$ 10 cells on each side
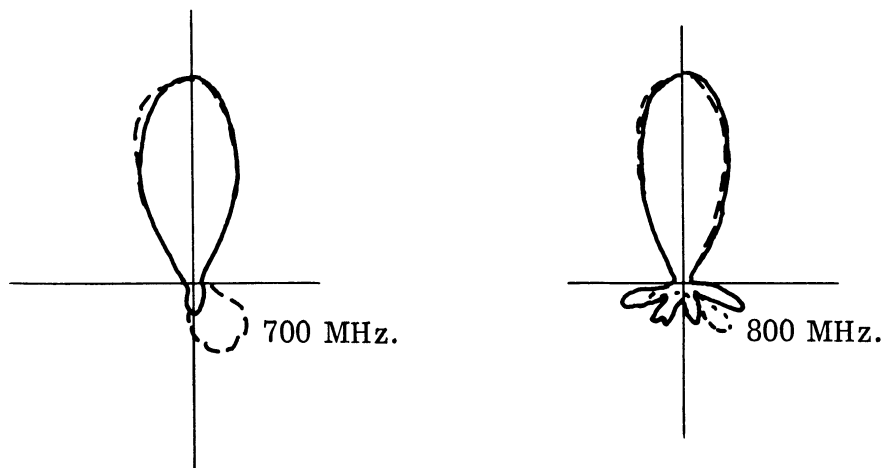
(b) Log Zig Zag Antenna (N. 219)

$\alpha = 10^{\circ}$ $\tau' = 0.7$ 6 cells on each side

———— Air Loaded

– – – – E A F 2 Ferrite Loaded

FIG. 3-2: H-PLANE PATTERNS LOG ZIGZAG ANTENNAS AT
700 MHz. AND 800 MHz.

TABLE III-1:

BIFILAR LOG-ZIGZAG PYRAMIDAL ANTENNA SPECIFICATIONS

	Antenna Numbers 219	225
Apex Angle, 2α	20°	24°
Growth Factor, τ	.7	.85
Pitch Angle, ψ	—	10°
Base Width	32. x 32. cm	32.5 x 32.5 cm
Apex Truncated Width	16 cm	6.4 cm
Height	44.2 cm	10
No. of Cells Per Arm	6	10
Length on Plane of Conductors	45 cm	62 cm
1) from truncated tip	45 cm	62 cm
2) from virtual tip	92.5 cm	77.5
Loading Material	EAF-2 Solid Ferrite Along Entire Length	EAF-2 Solid Ferrite (antenna Pattern); powdered ferrite EAF-2 (near field meas.)
Loading Configuration	1/2" Inside Layer From Base to Tip	3/8" Inside Layer from Base to Tip (Fig. 3-3), powdered ferrite EAF-2

$$\alpha - 12^{\circ}$$

$$\gamma = 10^{\circ}$$

$$\tau = \frac{R_n - 1}{R_n} = .0.85$$
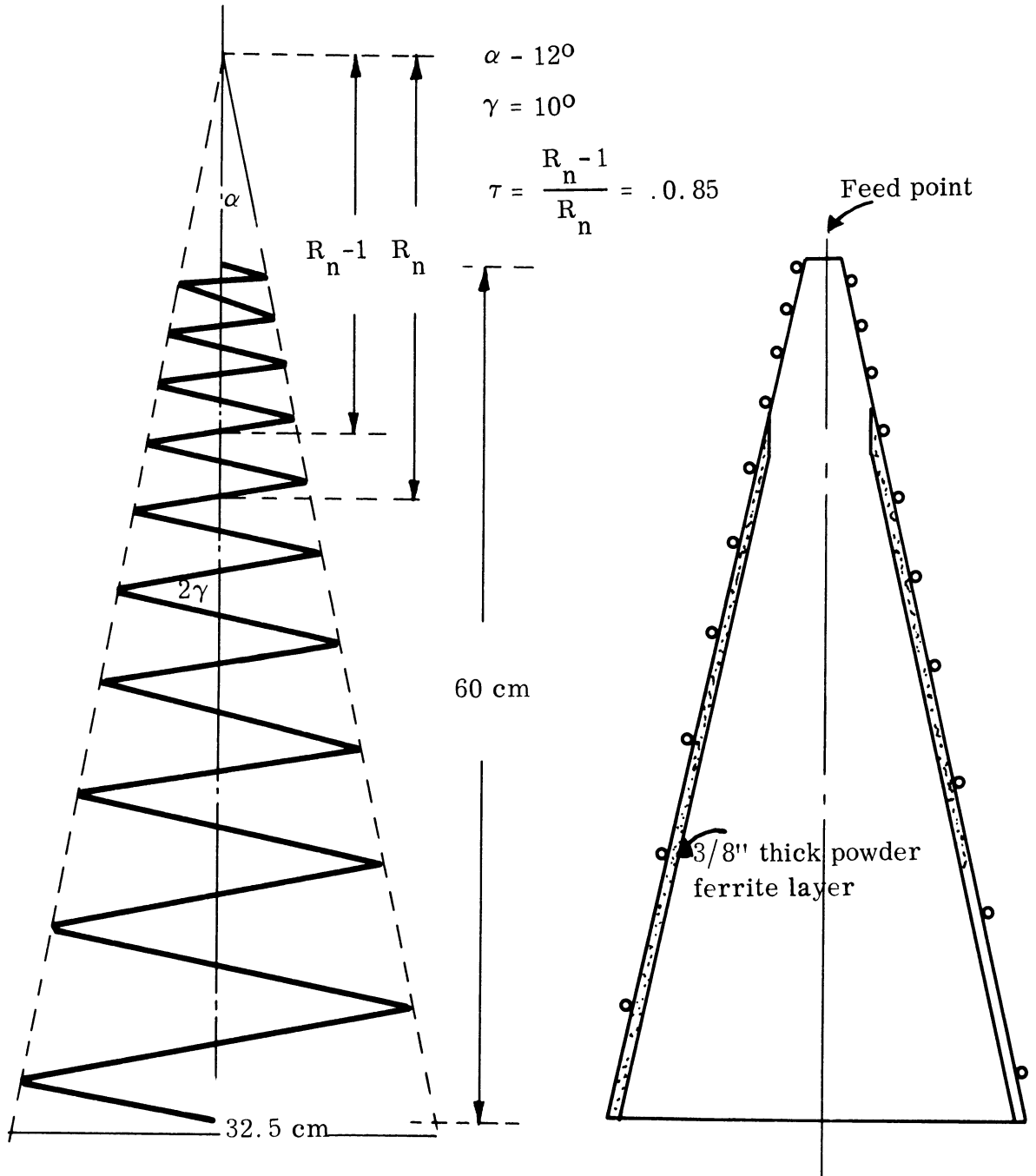
FIG. 3-3: LOG ZIGZAG ANTENNA
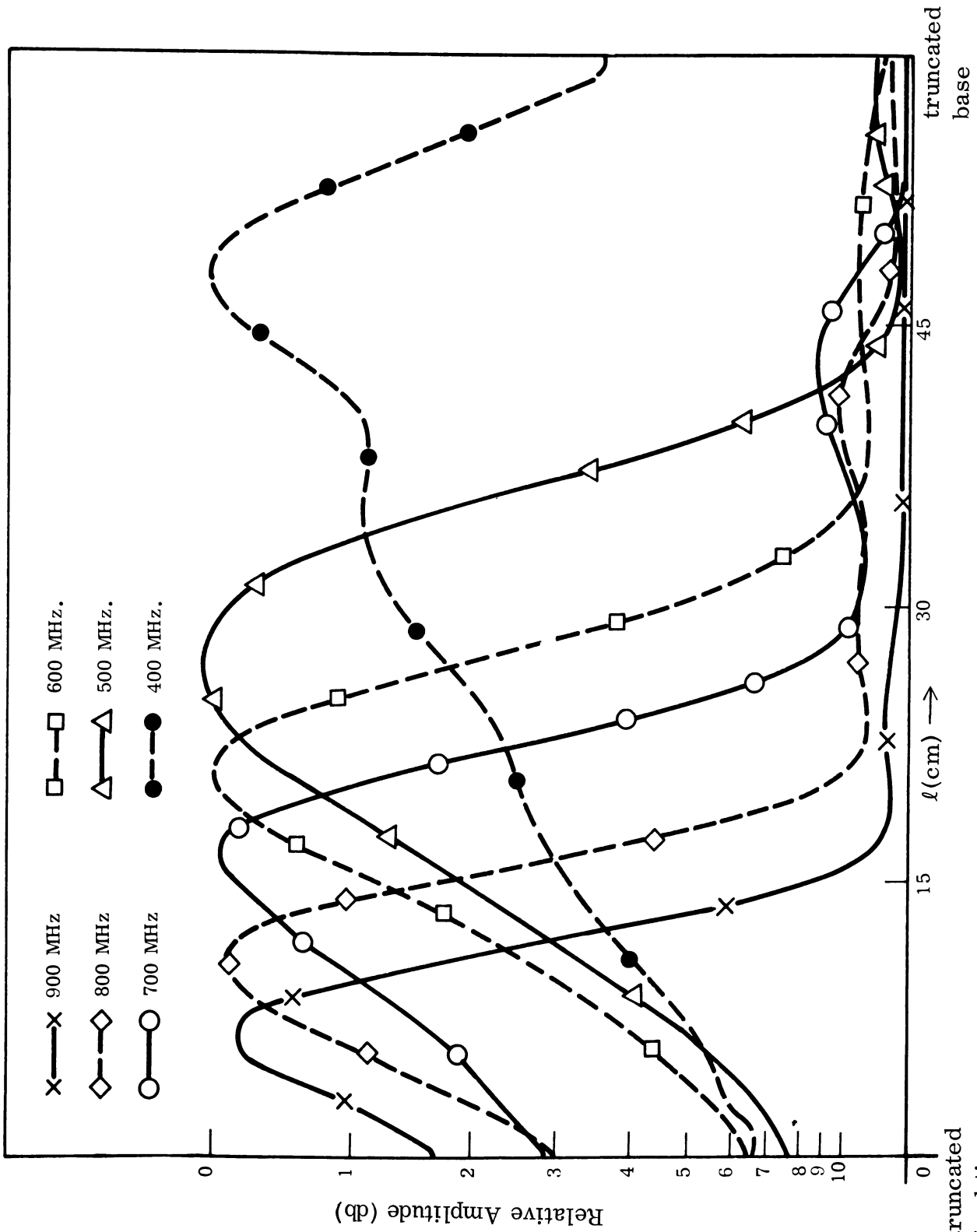
FIG. 3-4: NEAR FIELD AMPLITUDES OF ZIGZAG ANTENNA NO. 225 UNLOADED
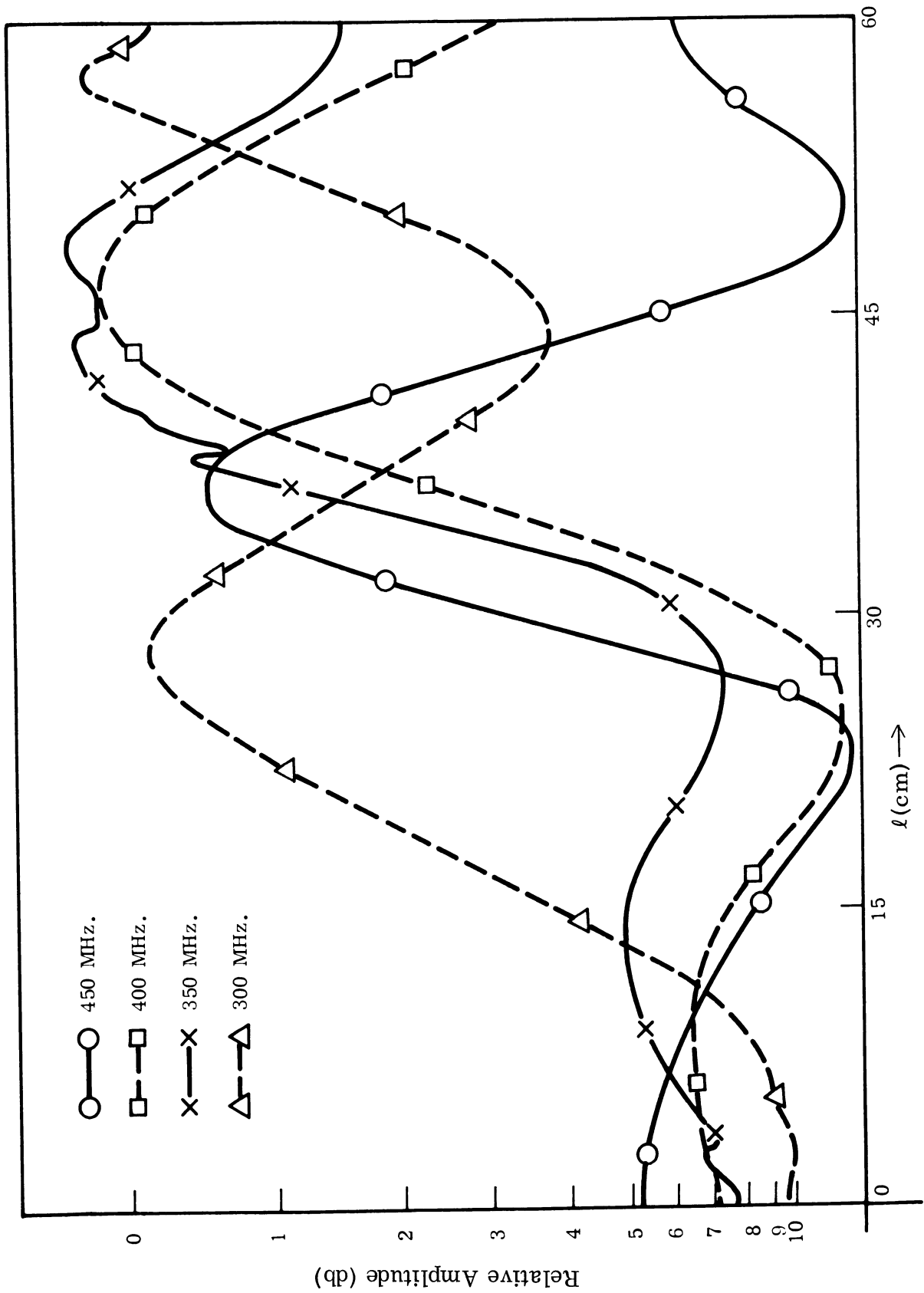
FIG. 3-5a: NEAR FIELD AMPLITUDE OF ZIGZAG ANTENNA NO. 225
LOADED WITH 3/8" INSIDE LAYER OF FERRITE POWDER

FIG. 3-5b: NEAR FIELD AMPLITUDE OF ZIGZAG ANTENNA NO. 225
LOADED WITH 3/8" INSIDE LAYER OF FERRITE POWDER

ferrite loading for different frequencies.

First of all, we observe that two or more active regions usually appear. The first (left or closest to the tip) one is shifted by a reduction factor of approximately .57 toward the left, or apex, of the zigzag. For example, the first peak of 300 MHz for the loaded case (Fig. 3-5a) is practically at the same position as the 500-600 MHz peak in air (Fig. 3-4). Also the first peaks for 350, 400, and 450 MHz (Fig. 3-5a), (the small ones on the left hand side) are roughly at the same position as 700, 800, and 900 MHz in air (Fig. 3-4).

In addition, patterns taken on the pyramidal helices show forward fire as well as backfire radiation. Thus, in conclusion, the loading appears to produce the un-desirable effect of allowing much of the energy to pass the desirable first mode backfire region without being radiated. This energy then passes into regions of forward fire for the first order modes and to other radiation regions, thus destroy-ing the antenna pattern. These results are undoubtedly dependent upon the pitch and cone angle of the antenna to be loaded. They will be thoroughly studied.

IV

FERRITE LOADED WAVEGUIDE SLOT ARRAY

The ferrite loading of a waveguide array cannot reduce the length of the array; however, the cross-section of the waveguide is reduced considerably (Jones, 1965). The loading of an individual slot with ferrite can reduce the resonant length of the slot, thus reducing the proximity of the slot to its neighbors. Hence the mutual coupling effects can be reduced (Kay, 1956). Furthermore, electronic scanning of the array pattern is possible through magnetic bias control on the ferrite without additional ferrite devices (Cheo, 1965).

Some preliminaries have been commenced in the utilization of ferrite filled slots in a short linear array. The array has been designed to have a pattern with side lobes down 26 db (i.e. the side lobe field level should be 0.5 per cent of the main lobe field) and a beam width of 25° at half power points. The efficiency is to be determined with these requirements fullfilled. The pattern will be scannable by variation of the magnetic bias. The ferrite material used for loading is the Q-3 ferrite supplied by Indiana General in the form of 7.16 cm x 1.246 cm x 0.3 cm (2.82" x 0.49" x 0.12") sticks. The center frequency has been chosen to be 200 MHz, which is within the range for Q-3 ferrite as published by Indiana General.

4.1 Preliminary Design and Tests

The Q-3 ferrite material was tested for μ_r and ϵ_r and loss tangent values for frequencies from 100 to 300 MHz. The account of these tests along with the complete procedure is given in Section VI of this report. The results of the μ and ϵ tests are summarized as follows:

TABLE IV-1:

f	μ_r	ϵ_r
100 MHz	12.5	7.96
200 MHz	14.3	7.81
300 MHz	16.0	7.7

The measured values of μ_r and ϵ_r at 200 MHz were used in the preliminary design of the waveguide assuming cutoff frequency at 126 MHz and a TE_{10} mode.

The waveguide width "a" is, (Fig. 4-1)

$$a = \frac{3 \times 10^{10}}{2 \times 126 \times 10^6 \sqrt{\mu_r \epsilon_r}} = 11.23 \text{ cm.}$$

The dimension "b" was assumed to be 0.3 cm which is the height of one ferrite stick. The dimension a = 11.23 cm. can exactly accommodate nine ferrite sticks widthwise and this is the reason to choose the cutoff frequency at 126 MHz with a cutoff ratio of

$$\frac{fc}{f} = \frac{1}{1.59} \quad .$$

With these values then:

$$Z_{TE_{10}} = \frac{377 / \sqrt{\mu_r \epsilon_r}}{\sqrt{1 - \left(\frac{1}{1.59}\right)^2}} \tag{4.1}$$

$$= 45.75 \ \Omega$$

$$\frac{1}{4}" \text{ Thick} \atop \text{Aluminum Plate}$$

Ground Plane
(upper plate of waveguide)

3-I(a)

$$Z_{loop} = \frac{138}{\sqrt{\epsilon}} \log_{10} \frac{4h}{d}$$

Insulation

Insulated Feed Loop

0.3 cm

ferrite
piece

ferrite
piece

11.23 cm

Coaxial feed
from the side

Grounded to the
bottom plate
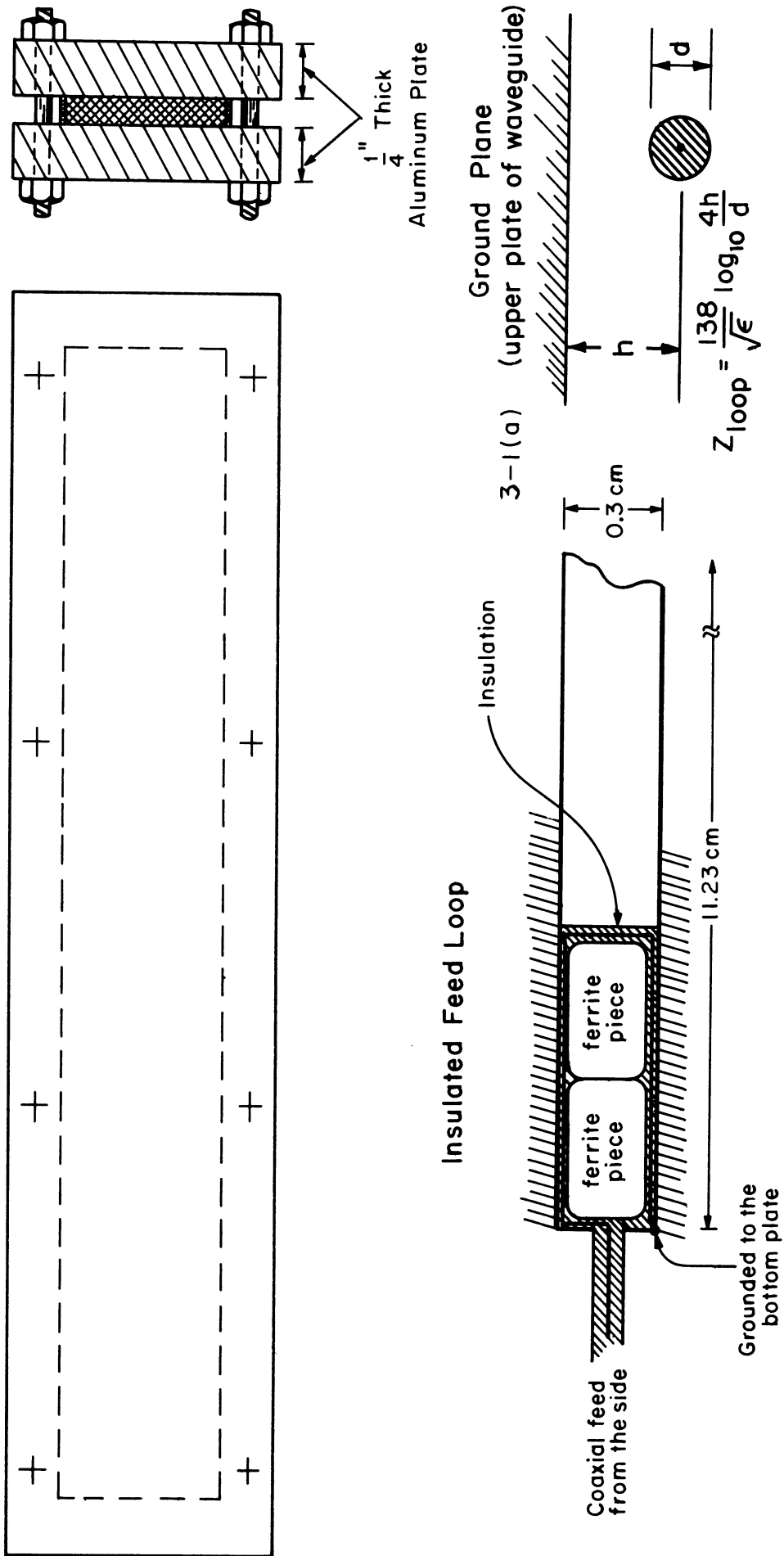
FIG. 4-1: PROPOSED MECHANICAL CONFIGURATION FOR WAVEGUIDE TEST.
a) DETAILS OF THE FEEDING LOOP

$$\lambda_g = \frac{\lambda_o}{\sqrt{\mu_r \epsilon_r - \left(\frac{\lambda_o}{2a}\right)^2}}$$

(4.2)

$$\lambda_o = 150 \text{ cm at } 200 \text{ MHz}$$

Then

$$\lambda_g = \frac{150}{\sqrt{112 - 44.5}} = 18.25 \text{ cm.}$$

The waveguide was tested for insertion loss. The waveguide was excited with a current loop. This method of exciting the waveguide was chosen on account of its convenient form considering the odd assemblage of ferrite sticks. A rectangular strip was used instead of a round wire for the loop. With this loop arrangement a voltage standing wave ratio of 1.95 was obtained at 200 MHz with the other end of the guide short circuited. The length of the guide used for this test was 1.08 meters.

For the insertion loss test, a hybrid junction was connected at the input end and the other end was short circuited. The input power and the reflected powers were measured then:

$$P_{in} \exp(-2\alpha\ell) = P_{out}$$

(4.3)

The attenuation constant, a, in nepers/cm was calculated from the reading of P_{in} and P_{out} (the reflected power).

P_{in} was measured at port B with a matched load connected at port D; the output power was measured at port D with the matched load on port B (see Fig. 4-2).
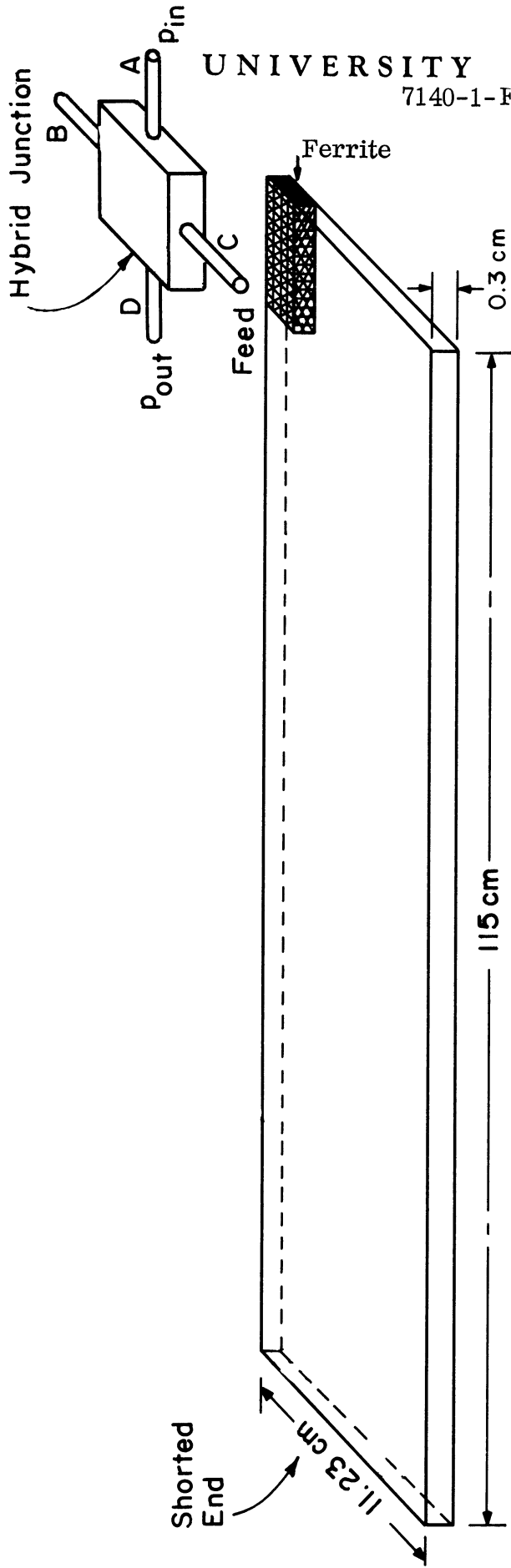
FIG. 4-2: EXPERIMENTAL DETAILS TO DETERMINE INSERTION LOSS OF WAVEGUIDE.

The observations are tabulated below:

TABLE IV-2:

f (MHz)	P_{in}(mw)	P_{out}(mw)	VSWR	Reflection Coefficient	Insertion Loss Per Foot
160	3.6	2x0.4	3.65	0.57	0.92 db/ft.
180	3.6	2x0.22	2.10	0.354	1.28 db/ft.
200	3	2x0.11	1.95	0.322	1.6 db/ft.
220	0.45	2x0.004	2.15	0.358	very high

The insertion loss is high. The above readings show that a better center frequency would be either 160 or 180 MHz instead of 200 MHz.

4.2 Array Design Procedure

The array is designed to have 5 slots separated by distance of $\frac{\lambda_o}{2}$ at 200 MHz. The slots are to be in the broad wall of the waveguide. The array will be a non-resonant array of resonant slots. As a non-resonant array, $\frac{\lambda_o}{2}$ is not an odd multiple of $\lambda g/2$ at 200 MHz. The slot length is to be chosen such that the reactance of the slot is zero, making the slot resonant. The non-resonant array is chosen because it has a better bandwidth than the resonant array (Jasik, 1961). The slots are to be taken at resonance for the maximum radiated power consideration.

The following types of slots are available for a choice:

1) Series displaced

2) Shunt displaced

3) Series rotated

4) Displaced and rotated

The slots are drawn in the broadface of waveguide in the Fig. 4-3. The first three types above involve a single branch equivalent circuit (Oliner, 1957), either series or shunt; the fourth type involves two branch equivalent series circuits as well as a shunt branch.

The calculations of the first three types are quite complicated but since there are standard computer programs available for solutions, the work is simplified. However, these standard computer programs have to be modified to take account of the high permeability of the ferrite material and the ferrite filling in the slots. Section 4.3 outlines the computer programs for the slot design.

The criterion to be achieved is a side lobe level of 26 db from the five slots in the broadface of the waveguide. Assuming a Dolph-Tchebycheff distribution, the procedure is as follows (Kraus, 1950):

$$20 \log_{10} R = 26$$

$$\text{or } R = 20 \tag{4.4}$$

For five slots the poylnomial chosen is $T_4(x) = 8x^4 - 8x^2 + 1$
then

$$20 = 8x_o^4 - ix_o^2 + 1 \tag{4.5}$$

$$x_o = 1.455 \text{ by a trial and error method}$$

Now

$$E_5 = \sum_{k=0}^{k=2} A_k \cos(2k\frac{\psi}{2}) \tag{4.6}$$
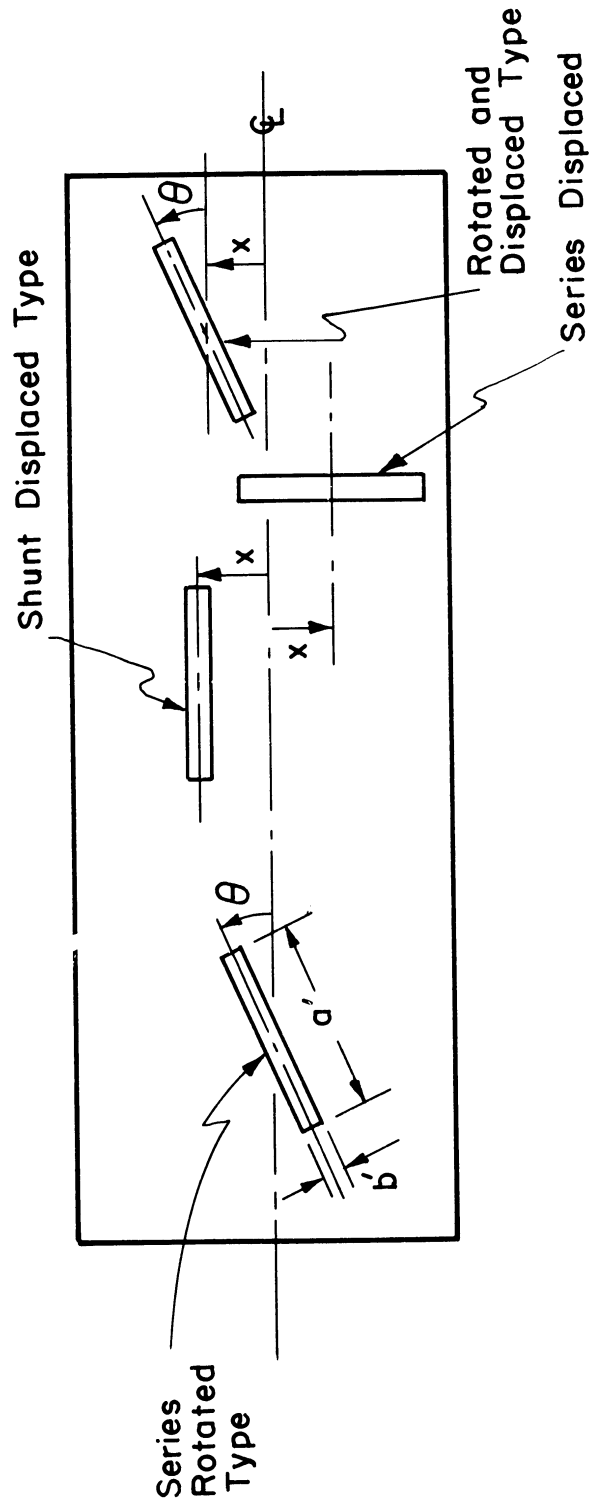
FIG. 4-3: TYPES OF SLOTS AND THEIR PARAMETERS.

$$= A_0 + A_1 \cos 2(\frac{\psi}{2}) + A_2 (\cos 4 \cdot \frac{\psi}{2}) \text{ using } \omega = \cos \frac{\psi}{2}$$

$$E_5 = A_0 + A_1 (2\omega^2 - 1) + A_2 (8\omega^4 - 8\omega^2 + 1) \tag{4.7}$$

where

$$\omega = \frac{x}{x_0}$$

then

$$E_5 = A_0 + A_1 \left(2\frac{x^2}{x_0^2} - 1 \right) + A_2 \left(8\frac{x^4}{x_0^4} - 8\frac{x^2}{x_0^2} + 1 \right)$$

$$= \left(\frac{8A_2}{x_0^4} \right) x^4 + \left(\frac{2A_1 - 8A_2}{x_0^2} \right) x^2 + (A_0 - A_1 + A_2) \tag{4.8}$$

Comparing coefficients with $T_4(x) = 8x^4 - 8x^2 + 1$

$$\frac{8A_2}{x_0^4} = 8$$

giving

$$A_2 = x_0^4 = 4.48 \tag{4.9}$$

$$\frac{2A_1 - 8A_2}{x_0^2} = -8$$

or

$$2A_1 = 8x_o^4 - 8x_o^2 = 19 \qquad (4.10)$$

giving

$$A_1 = 9.5$$

then

$$A_o + A_1 + A_2 = 1 \qquad (4.11)$$

giving

$$A_o = 9.5 + 1 - 4.48$$

$$= 6.02$$

$$2A_o = 12.04$$

Then relative amplitude distribution would be:

$$1 : 2.12 : 2.69 : 2.12 : 1$$

$$A_2 : A_1 : 2A_o : A_1 : A_2$$

Now power radiated is given by:

$$P_{slot} = \left| E \right|_{slot}^2 G \text{ or } = \left| H \right|_{slot}^2 R \qquad (4.12)$$

Hence power distribution would be:

$$1 : 4.48 : 7.2 : 4.48 : 1 \qquad (4.13)$$

$$Ps_1 : Ps_2 : Ps_3 : Ps_4 : Ps_5 \qquad\qquad (4.14)$$

The center slot should radiate 7.2 times as much power as the end slots. Higher values of G will be required to compensate for loss attenuation. Hence a larger value of θ or x (the two slot parameters defined in Fig. 4-3) will be required. The different slots will have appropriate values of θ or x for each location. The difference in the value of θ involves a complication in the calculation of fields, since slightly different polarizations are radiated at various slots. This is a serious drawback of the rotated type of slots. If the polarization of fields is the same for all slots (i.e. discarding rotated type slots), the reduced fields can be very easily calculated from the Smith chart and the design work is simplified greatly. Once the reduced fields are obtained from the Smith chart, then appropriate values of "x" can be chosen to achieve the required power distribution above, thus, achieving the specified power pattern.

The series displaced and shunt displaced type slots are to be explored completely on the computer and then the most suitable resonant slot length will be chosen. One of the two types will be utilized in the final design. A tentative configuration with shunt displaced type slots is given in Fig. 4-4. The effect of mutual coupling between slots has been neglected since the slot resonant length with ferrite filling inside the slots is of the order of 7 cm while the spacing between slots is 75 cm. Experimental verification is underway.

4.3 Computer Programs for Slot Impedance Properties

Computer programs for the first three types of slots mentioned in Section 4.2 need the following inputs:

1) a and b the waveguide dimensions in cm.

2) a' - slot length, Fig. 4-3; a series of values is specified by the - starting value, increment, final value.
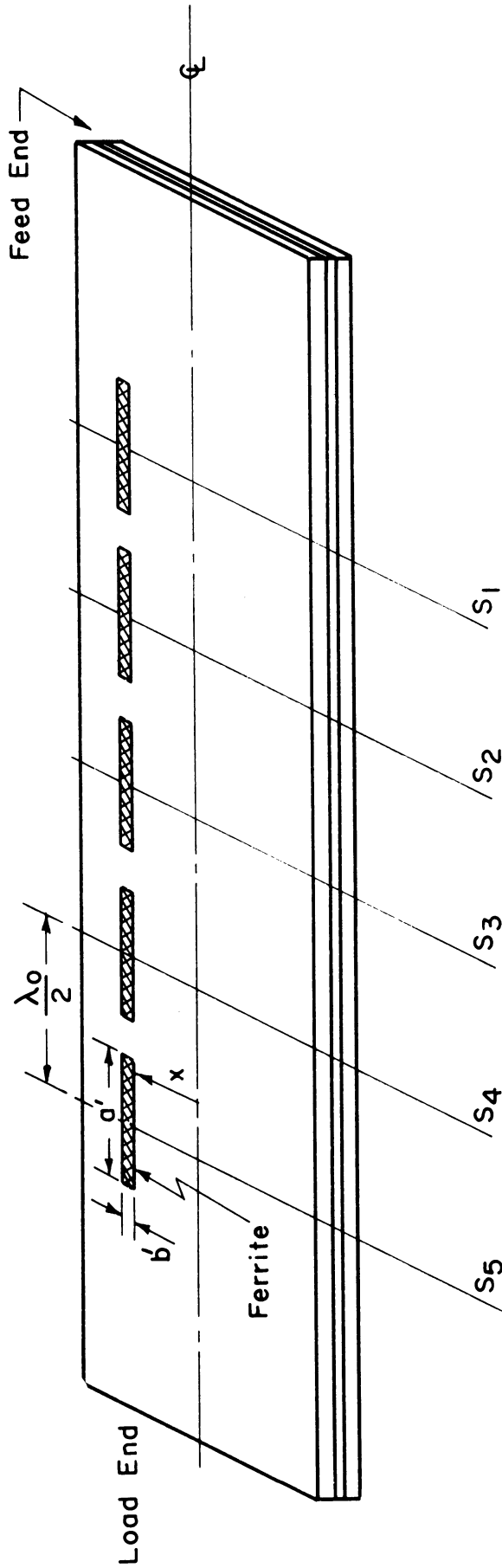
FIG. 4-4: SIMPLIFIED FINAL CONFIGURATION OF ARRAY WITH SHUNT SLOTS

3) b' - slot width in cm.

4) t - slot depth in cm.

5) f - operating (design) frequency.

6) $\mu_r \epsilon_r$ product at operating frequency.

7) θ - slot angle; a series of values is specified by the starting value, increment, final value for rotated series slot. (See Fig. 4-3) or x - starting value, increment, final value for displace series or shunt type slot. (See Fig. 4-3)

The output will be:

a) R and X values versus slot length with θ as a parameter for series rotated type, or with x as a parameter for series displaced type

b) G and B values versus slot length with x as a parameter for a shunt displaced type.

The curves of R and X versus slot length or G and B versus slot length for θ or x as a parameter will indicate the value of resonant slot length. This will be the value of the slot length for which the X or B is zero and R or G is a maximum.

The general behaviour of R and G, symbolizing the radiated power in series and shunt slots respectively, is that R and G increased for increasing values of θ and x at a particular slot length.

4.4 Magnetic Bias Control of Ferrite Array

The array shown in Fig. 4-4 has been designed to demonstrate the usefulness of ferrites in such an antenna. The use of ferrite material offers a possible method for controlling beam shape or position by the application of a magnetic field. For the purpose of demonstrating magnetic control, a still simpler array is contemplated. For this purpose an array having only three slots may be used. The space between adjacent slots will be such that a magnetic field can readily be produced by pole faces placed in these regions. The application of a magnetic field in this

direction offers the possibility of control by causing a phase shift in the transmission mode between each two slots. For the 3-slot array, there are two such intervals for the application of magnetic field. At each of these two locations, the extent of the magnetic pole piece in the direction of propagation would be important. It is through the active width of the magnetic field pole piece that the permeability of the ferrite can be changed (reduced).

V

FERRITE LOADED SLOT ANTENNAS

In this section, two principle ideas are explored. The first part of this section is devoted to a consideration of the production of heat in a ferrite due to the UHF-VHF power supplied to the slot antenna. The second part of this section, indicates a series of studies which show the effect of replacement of certain sections of the slot aperture with balsa wood spacers. Balsa wood acts very nearly as a void since its permittivity is exceedingly low. In some instances, one or more ferrite blocks were covered on the aperture end with metal foil, and thereby, iris effects were produced. The replacement of ferrite blocks with metal blocks produced ridge waveguide effects.

5.1 Power Capabilities of Ferrite Loaded Antennas

In Section VI of this report, information is given on the physical characteristics of some ferrite materials. Of special interest is the temperature dependence of solid ferrite, EAF-2, which has previously been reported (Lyon et al, 1964). Since a sensitivity to temperature change has been observed, it is important to determine the power limitation imposed by this characteristic. For this reason the effect of heating in the UHF-VHF range on a simple ferrite loaded antenna was studied.

5.1.1 Preparation For UHF-VHF Heat Run

A ferrite loaded cavity slot antenna with an aperture 12" x 3" backed by a cavity 9" deep was decided upon as the most typical and most informative construction for studying the power limitation associated with temperature. The cavity was filled with powdered EAF-2 ferrite. The slot was designed for a frequency of 320 MHz. The operating frequency for the heat run was chosen at 338 MHz because of the availability of an adequate power oscillator. The highest available input power

was approximately 9 watts for these tests. In feeding the antenna, a VSWR value of 1.06 was observed. The ferrite loaded slot used is very similar to one previously furnished to WPAFB. Copper-constantan thermocouple temperature probes were inserted 2.5" into the aperture face of the slot. Each thermocouple was 0.04" in diameter. The two wires of each thermocouple were fused at the junction. A Leeds and Northrup Potentiometer was used for the temperature measurements.

The thermocouples were aligned in the direction of propagation along the waveguide, thus having a position at right angles to the electric field. It was observed that the perturbation of the electric field due to the thermocouple insertion was small. The thermocouple elements were inserted so that the thermocouple junctions were spaced 1 - 1/2" apart along the centerline which is parallel to the broad direction of the waveguide (see Fig. 5-1). Such locations should then include a point having very nearly the highest temperature. These locations are essentially interior points of the mass of ferrite material used in this loaded antenna. Temperatures so obtained should be relatively high. Thermocouple No. 4, which is exactly half way across the waveguide and half way in the up and down direction, should give a temperature reading very close to the maximum existing in the mass of ferrite.

5.1.2 Observed Temperatures in Ferrite Loaded Slot

In Fig. 5-2 are shown the experimental observations of temperature versus input power level for the thermocouple temperature readings of thermocouple No. 4 in the middle of the ferrite mass. Measurements were made after sufficient time was allowed for the temperature to stabilize. The input power levels were net values delivered to the antenna. The temperatures correspond to steady state values for cw operation at these power levels. Tests are being extended to higher power levels (up to 100 watts). A 100 watt source is being obtained for this purpose.

Aperture of Slot

Thermocouples are 1.5" apart.
(No. 5 is 1" from No. 4)

1. AIL Generator

2. Direction Coupler (20 db)

3. 20 db Attenuator

4. Power meter

5. Antenna

6. Board with thermocouple switches

7. Bridge for temperature measurements
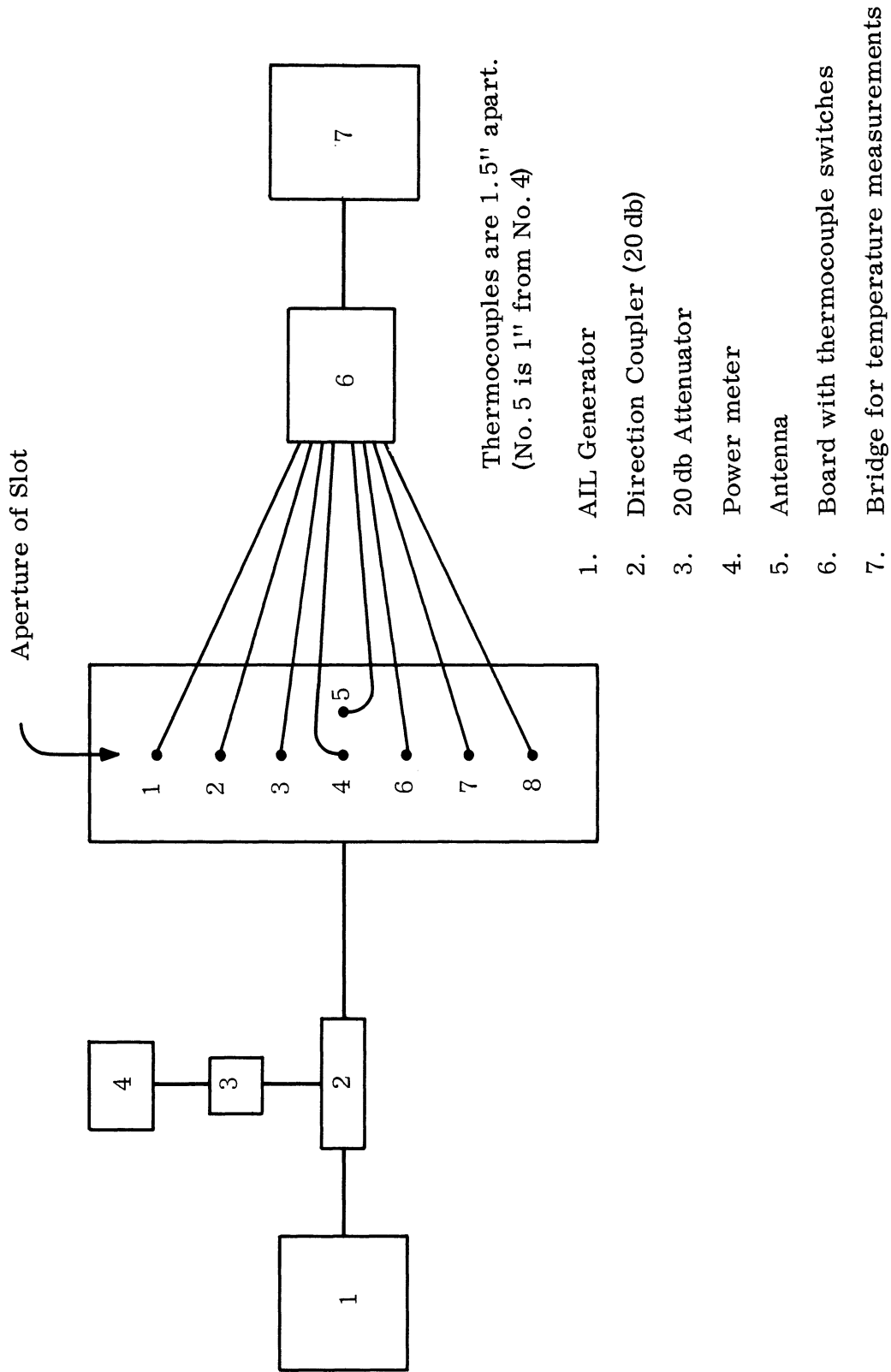
FIG. 5-1: BLOCK DIAGRAM OF POWER-TEMPERATURE MEASUREMENT SET-UP
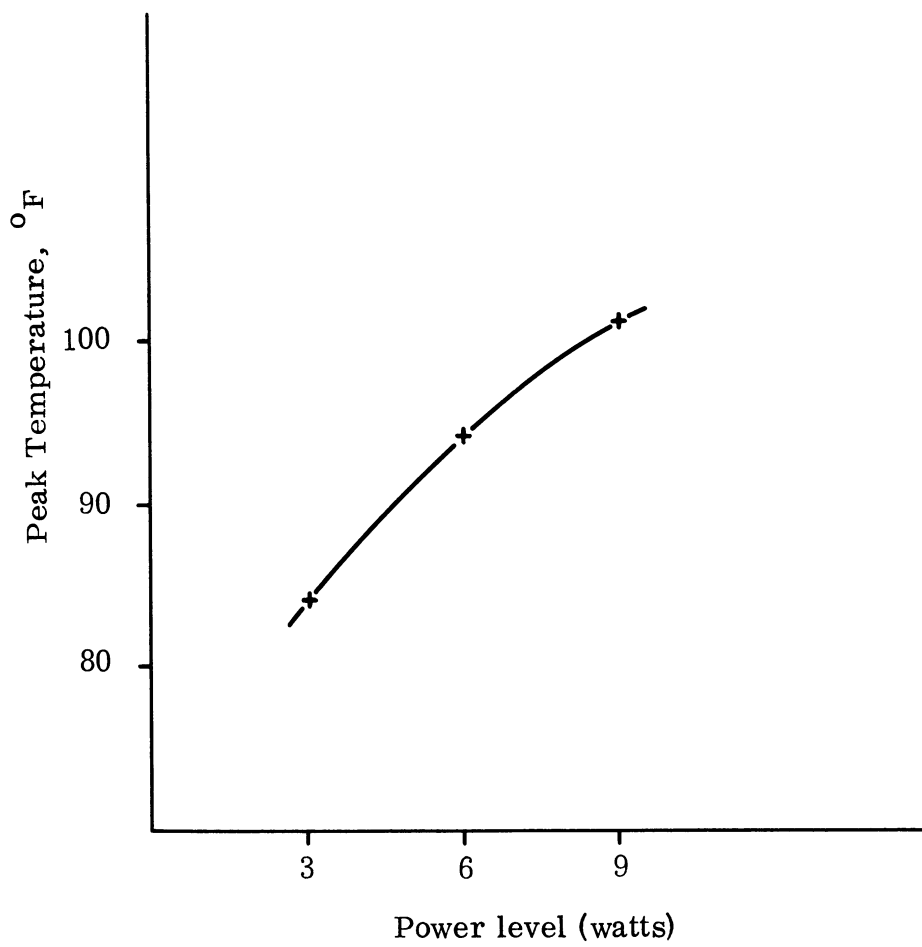
FIG. 5-2: PEAK TEMPERATURE (POSITION 4) VS. POWER LEVEL

Table V-1 presents all of the temperature versus thermocouple position data for various power levels. Figure 5-3 is the most complete display of all such data.

5.1.3 Significance of Observed UHF-VHF Produced Temperatures

The level of temperatures obtained at various interior points of the ferrite mass indicates that for the power levels covered, there is no serious overheating problem for antenna operation. However, as the temperature rises, the values of ϵ'', the loss component of permittivity, and μ'' the loss component of permeability increase. Thus, a simple extrapolation to an 100 watt power input level is not possible. Further work on temperature versus power level is necessary.

Both ferrite filled slot antennas and dielectric filled slot antennas are sensitive to the temperature. However, ferrite permits a better impedance match at the aperture. This permits a higher radiation efficiency with ferrite at moderate electric and magnetic Q factors. Because of the aperture impedance mismatch associated with dielectric loading, a higher electric Q factor is necessary for good radiation efficiency. This narrows the bandwidth. The higher Q of a dielectric cavity makes the dielectrically loaded antenna more sensitive to temperature changes and mechanical deformation. This means there may be a substantial advantage for ferrite filled slot antennas over dielectric filled slot antennas for installations where the ambient temperature changes or where mechanical vibration exixts.

5.2 Slot Antennas With Ridges or Irises

In continuing the research on ferrite loaded slot antennas that was initiated by this laboratory on earlier contracts, it was decided to modify the slot antenna, if possible, to allow a wider bandwidth or lower frequency of operation for the same given outside dimensions of the slot antenna. Well-known properties of the ridged waveguide, as well as preliminary experiments performed last year, indicated a possible potential for broadbanding or lowering the frequency of operation of the

(a)   9 watt power level

Number of Thermocouple	$^\circ$F at Equilibrium
1	88.3
2	89.5
3	95.5
4	101.0
5	92.5
6	94.6
7	90.0
8	88.7

(b)   6 watt

Number of Thermocouple	$^\circ$F at Equilibrium
1	86.2
2	87.5
3	91.8
4	94
5	90
6	91.8
7	87.3
8	86.2

(c)   3 watt

Number of Thermocouple	$^\circ$F at Equilibrium
1	78.8
2	79.4
3	81.8
4	84
5	81
6	81.8
7	78
8	78.7

TABLE V-1: DATA OF THE POWER LEVEL-TEMPERATURE MEASUREMENTS IN FERRITE EAF-2
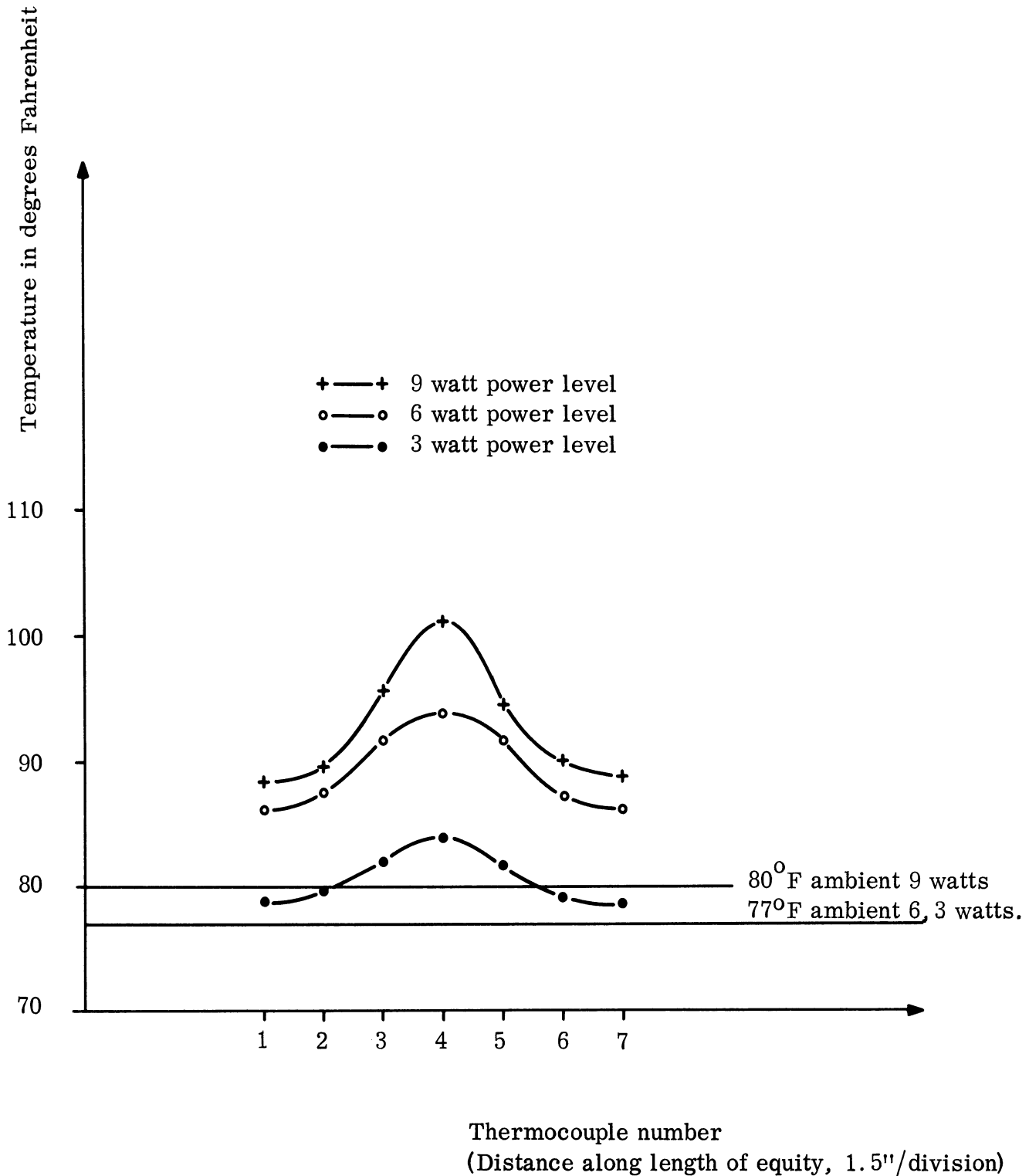
FIG. 5-3: TEMPERATURE VS. POSITION IN CAVITY

slot antenna. The following study was entirely experimental and consisted of inserting various ridges and metal irises into the ferrite-filled slot antenna and noting the changes and impedance as shown in the Smith Chart of the imepdance to the antenna. To reduce the complexity of the data presentation, all Smith Chart grids have been suppressed except for a VSWR scale.

5.2.1 Assumptions of the Study

Several assumptions were made in processing the impedance data for a 'bandwidth'.

1) Tuners were usually not used experimentally.

2) A VSWR circle = 3 was placed about each desired grouping of impedance points to obtain bandwidth (equivalent to the use of a wideband phase shifter and a wideband impedance transformer).

3) No further distortion of the impedance plots by compensation tuning was allowed.

Actually, with compensation tuning, somewhat larger bandwidths might well be obtained.

5.2.2 Solid Ferrite Loaded Antenna

Figure 5-4a shows an impedance diagram of the input impedance for the slot antenna entirely filled with solid ferrite blocks. All ferrite is solid EAF-2 material, the properties of which are summarized in Section VI of this report. The slot antenna with solid ferrite loading was thoroughly analyzed by Adams (1964). The operating frequency of the antenna is 352 MHz and the bandwidth is 18-20 MHz for a VSWR below 3, as may be seen by drawing a circle (VSWR = 3) about the origin of the Smith Chart. Nevertheless, this antenna, with its impedance matched properly, could operate from approximately 333 MHz to 383 MHz (50 MHz bandwidth), as may be seen by shifting the loop located in the upper right-hand portion of the Smith Chart clock-wise to the real impedance axis (e.g. by a wideband phase

all ferrite blocks
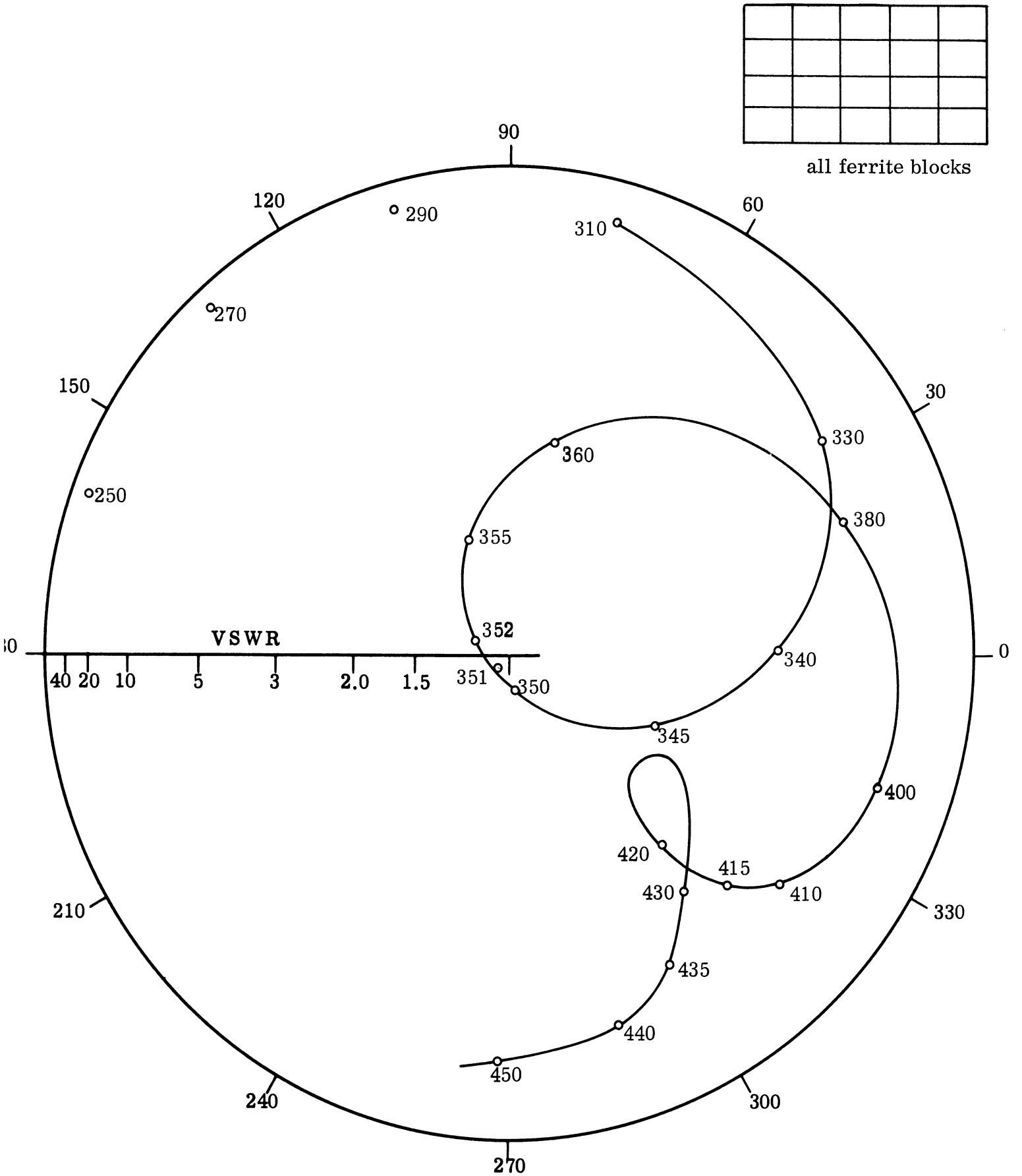
FIG. 5-4a: IMPEDANCE DIAGRAM OF SLOT ANTENNA LOADED ENTIRELY
WITH SOLID FERRITE (Frequency MHz)

shifter) and then drawing a VSWR = 3 circle about this loop, keeping in mind that the diameter of this circle changes with position on the Smith Chart. The 50 MHz bandwidth is therefore roughly the optimum bandwidth that could be achieved by this antenna with a wideband impedance matching without other optimizing circuits. In order to show the effect of a simple, but very narrowband transformer in the form of a double stub tuner, this solid ferrite loaded slot antenna was tuned with a double stub tuner in an attempt to move the upper right-hand loop to the central region. Figure 5-4b shows the resulting input impedance, and indicates a drastic change has taken place in the shape of the curve due to the additional phase shift of the double stub tuner. The phase reference for the original solid ferrite loaded slot antenna was at the input to the 'N' connector mounted directly on the antenna. The phase reference for the antenna shown in Fig. 5-4b with the double stub tuner attached, was at the input to the double stub tuner, a considerable distance from the actual antenna. This caused an additional phase shift shown by a more rapid rotation of the input impedance with change in frequency. This second curve (Fig. 5-4b) has much less optimized bandwidth (approximately 23 MHz) for only slightly lower center frequency. One can conclude that transformation of the input impedance with this particular setting of the double stub tuner, and probably with most other settings, would not be satisfactory for transforming the input impedance in the manner desired for increasing bandwidth or lowering frequency of operation.

5.2.3 Loaded Slot Antenna With Irises

Earlier studies by this laboratory indicated that partial blocking of the loaded antenna aperture significantly changed the input impedance of the antenna such that the bandwidth (as measured by magnitude of VSWR) was improved. Figure 5-5a shows the effect of two irises which are actually aluminum tapes covering the front ends of several of the ferrite blocks used in loading the slot antenna. The actual input impedance (referenced to 50 ohms) is poor by any standard. Nevertheless,

slot loaded entirely
with ferrite blocks
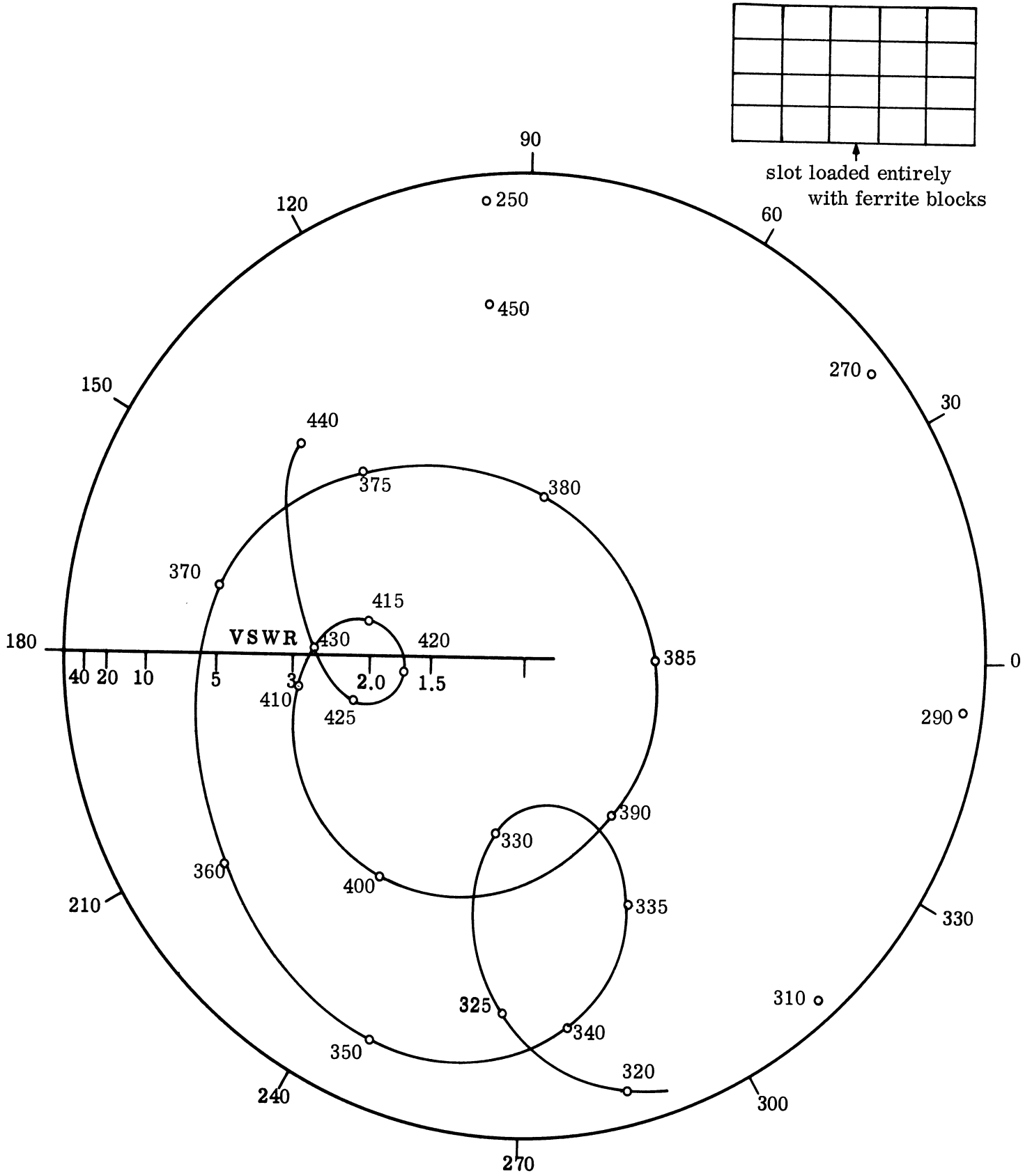
FIG. 5-4b: IMPEDANCE DIAGRAM OF SLOT ANTENNA LOADED ENTIRELY
WITH SOLID FERRITE. DOUBLE STUB TUNER USED. (Frequency MHz)
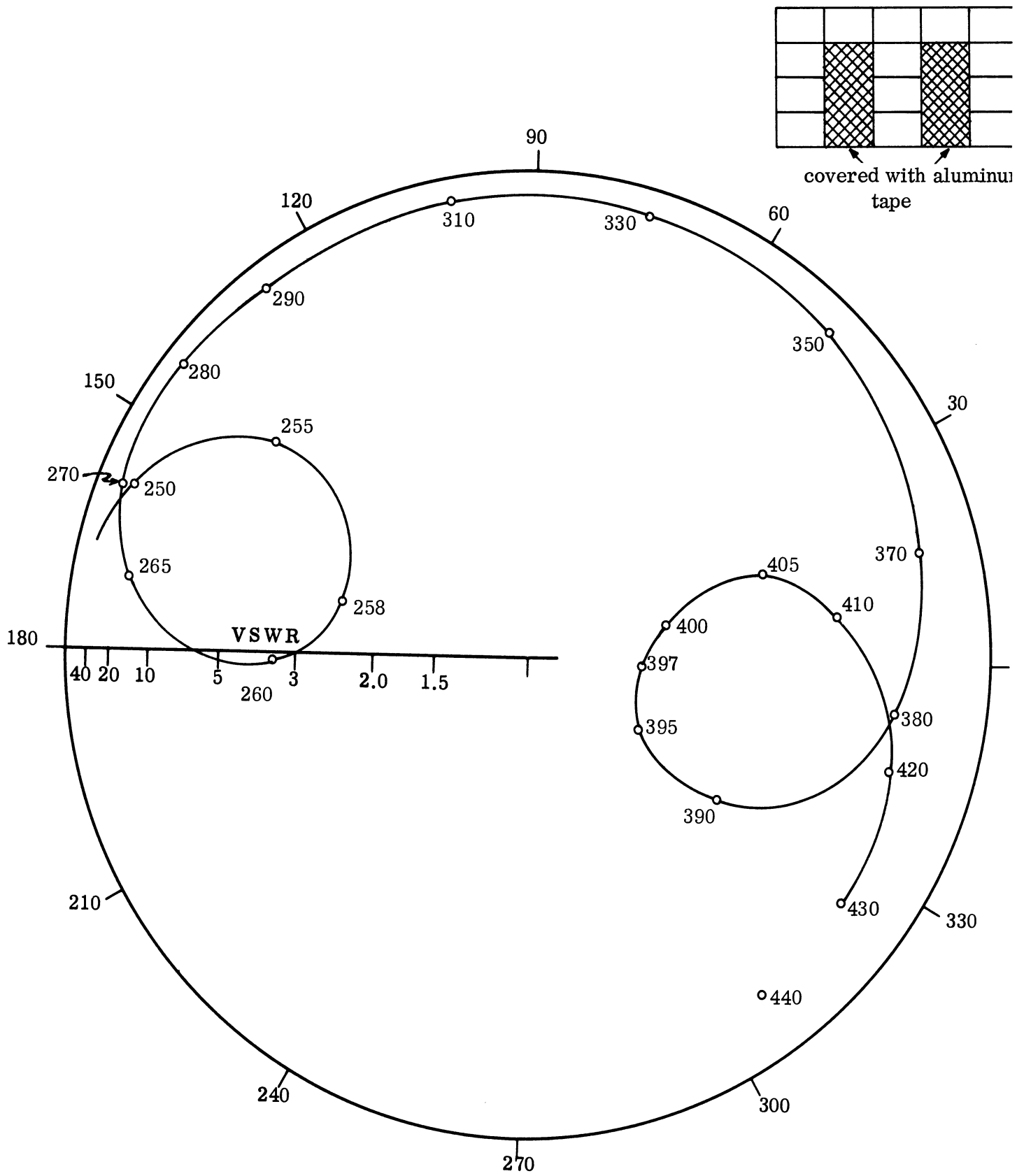
FIG. 5-5a: IMPEDANCE DIAGRAM OF SOLID FERRITE LOADED SLOT
ANTENNA WITH IRIS (Frequency MHz).

the loop on the left is interesting since it occurs at such low frequencies. A circle for VSWR corresponding to three indicates a possible transformed bandwidth of 16 MHz centered approximately at 259 MHz. Another attempt at transforming the impedance diagram with a double stub tuner is shown in Fig. 5-5b, where the lower frequency of operation loop has clearly been moved closer to the center of the Smith Chart. Although the loop is larger in radius, the bandwidth of 20 MHz around 261 MHz is approximately preserved. The reason that the lower frequency of operation loop has not been placed at the center of the chart is an experimental difficulty in controlling the placement of this loop with the double stub tuner (which is essentially a narrow band device). In summary, the possibility of operating at a frequency of approximately 100 MHz lower than the original frequency of the ferrite filled antenna by simply using an iris, is interesting and potentially useful, but it is accomplished at the expense of bandwidth.

Another iris experiment (Fig. 5-5c) involved covering the lower row of ferrite blocks. This produced practically no impedance changes in the lower frequency of operation; a bandwidth of 42 MHz around 356 MHz is shown and this iris was therefore discarded.

In the final iris experiment (Fig. 5-5d), the iris covered the lower three blocks of the center column. The low frequency loop in the upper left diagram has a VSWR = 3 bandwidth of 13 MHz centered around 273 MHz, which is again potentially useful in decreasing the operating frequency, although it drastically reduces the bandwidth.

Experiments attempted using side irises were unsuccessful.

In conclusion, irises appear to act as very narrow band tuners since reflections from the iris (sensitive to frequency) are being used; nevertheless, lower frequencies of operation can be achieved with greater bandwidth than would be obtained with an external tuner.

covered with aluminum
tape

FIG. 5-5b: IMPEDANCE DIAGRAM OF SOLID FERRITE LOADED SLOT ANTENNA
WITH IRIS. DOUBLE STUB TUNER USED. (Frequency MHz)

covered with aluminum
tape

FIG. 5-5c: IMPEDANCE DIAGRAM OF SOLID FERRITE LOADED SLOT ANTENNA
WITH IRIS (Frequency MHz).

covered with aluminum tape

90
120
310
330
60
350
30
265
290
270
150
260
285
370
250
280
273
405
410
180
VSWR
400
380
40 20 10   5   3   2.0   1.5
275
395
390
420
430
330
440
210
240
300
270
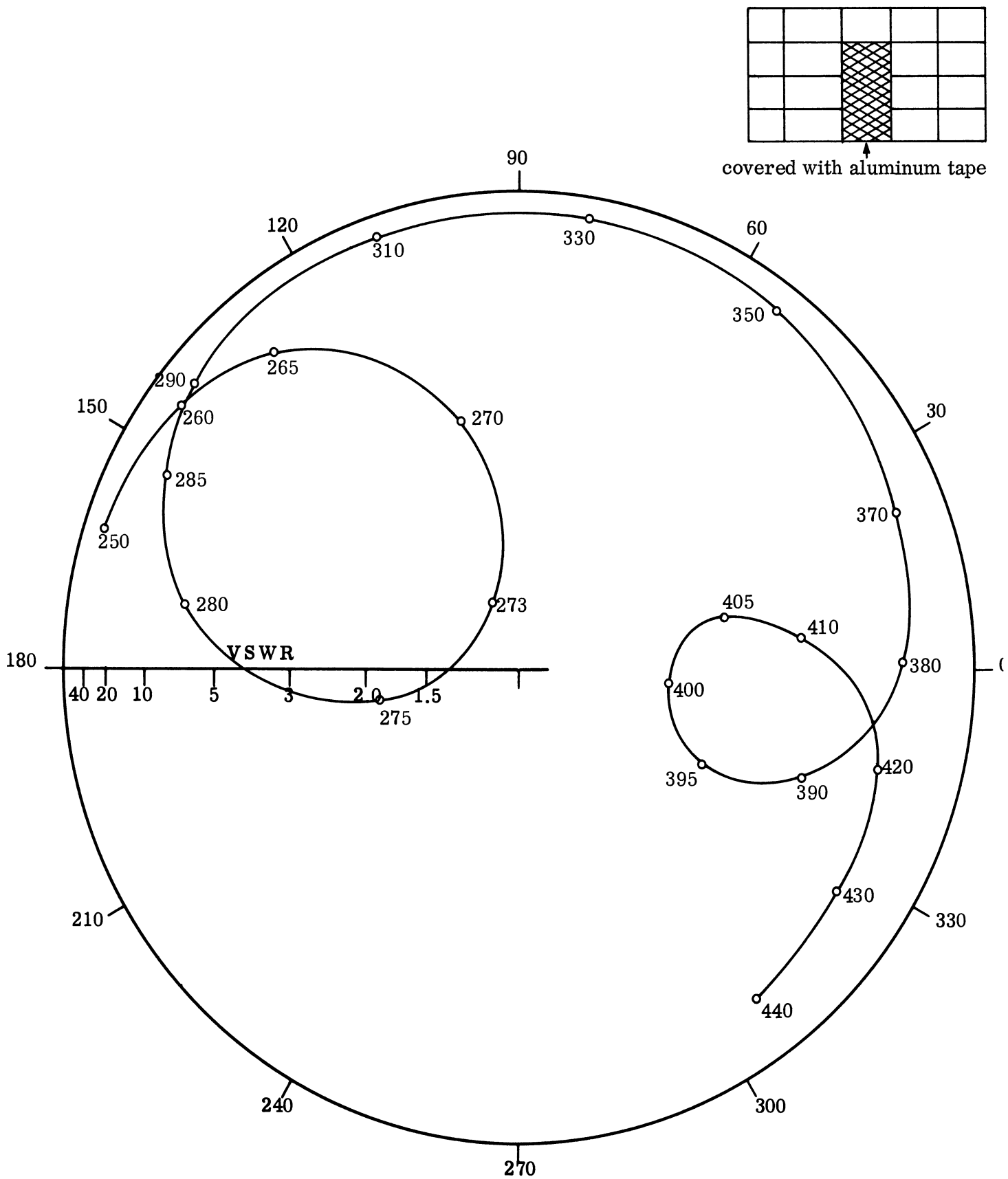
FIG. 5-5d: IMPEDANCE DIAGRAM OF SOLID FERRITE LOADED SLOT ANTENNA WITH IRIS (Frequency MHz).

102

5.2.4 Ridged Loaded Slot Antennas

Because of the increased bandwidth and lower operating frequency of the ridged waveguide, a series of slot loaded antenna experiments was initiated with various ridges created by steel or aluminum blocks replacing the ferrite blocks usually used in loading the slot antennas. It is important to note that the ridges were used without regard for possible improvement in matching the input probe impedance, even though the input probe was specifically designed only for the fully filled ferrite slot antenna. Figure 5-6a (inset) shows two metal ridges extending down to the lower side of the antenna where upper and lower are distinguished in this antenna by the fact that an electric monopole probe feed is used to excite the slot antenna and is inserted into the center of the antenna from the top. Figure 5-6a also shows the effect of the ridges on the input impedance and indicates again a substantial lowering in the lowest operating frequency obtainable from the slot waveguide. A bandwidth of 35 MHz around 291 MHz is achieved. This is felt to be a significant improvement in antenna performance.

The second set of ridges used (Fig. 5-6b) consists of two sets of two steel blocks or ridges substituted for the center ferrite blocks. Figure 5-6b shows the effect on the input impedance of these center ridges and indicates an operating bandwidth of 50 MHz around 330 MHz. The resulting 50 MHz is essentially unchanged from the fully loaded ferrite slot antenna and the center frequency of 330 MHz is not too different from the original 350 MHz. This loading, therefore, is not considered to be particularly useful.

Another double ridge slot antenna (Fig. 5-6c) shows significant improvement in the lower operating frequency with a possible transformed bandwidth of 44 MHz around 317 MHz. This is a shift downwards of 41 MHz in operating bandwidth, a small but possibly useful shift.
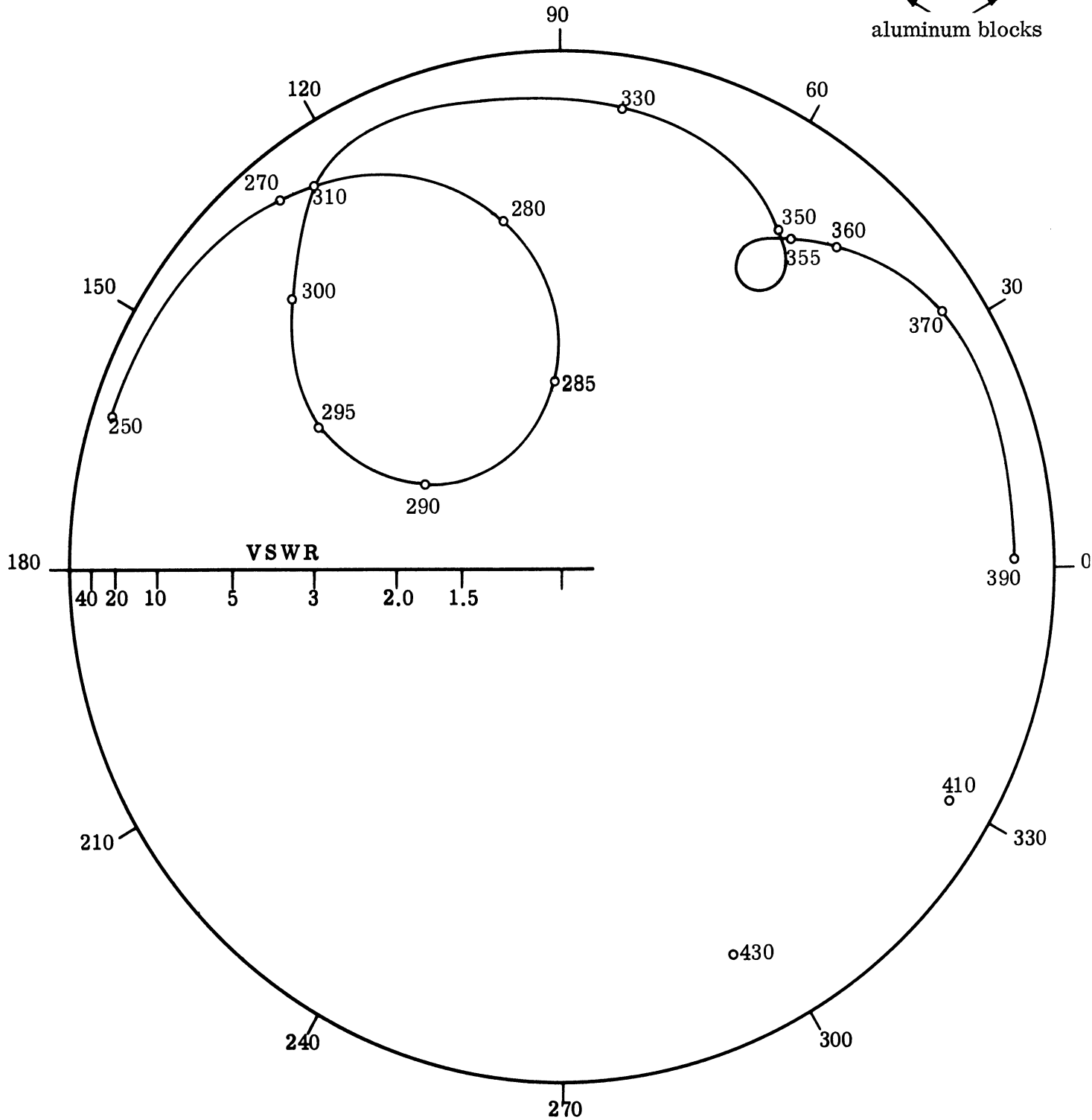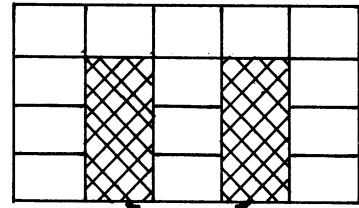
FIG. 5-6a: IMPEDANCE DIAGRAM OF SOLID FERRITE LOADED SLOT ANTENNA
WITH RIDGES (Frequency MHz).

steel blocks

90

120

60
250
260

150

270

30

280

180
VSWR

440

290

330
335
327
326
325
324

340

0

40 20 10   5   3   2.0   1.5

300

420

320

310

210

330

360

400

240

380

300

270
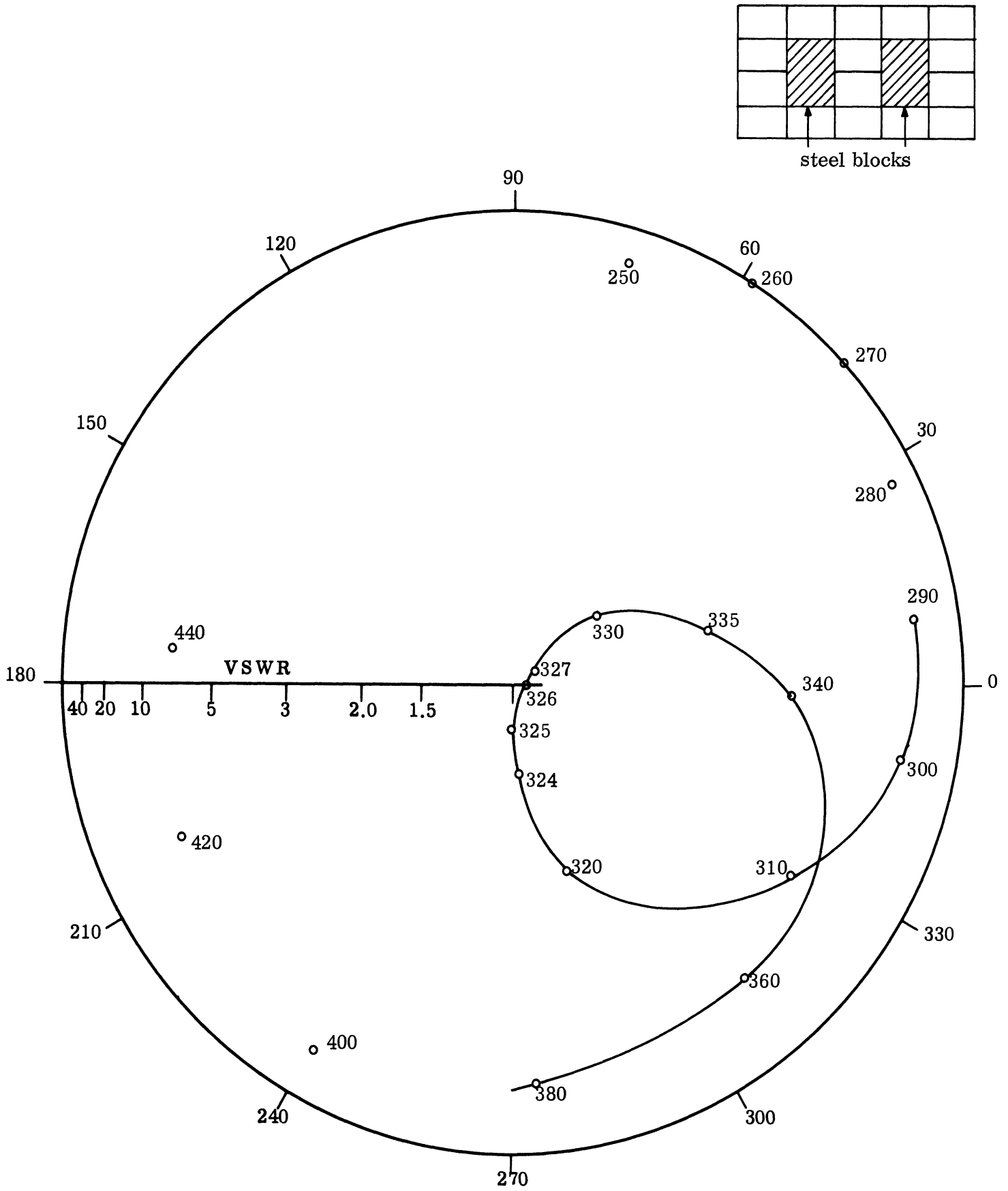
FIG. 5-6b: IMPEDANCE DIAGRAM OF SOLID FERRITE LOADED SLOT ANTENNA
WITH RIDGES (Frequency MHz).

105
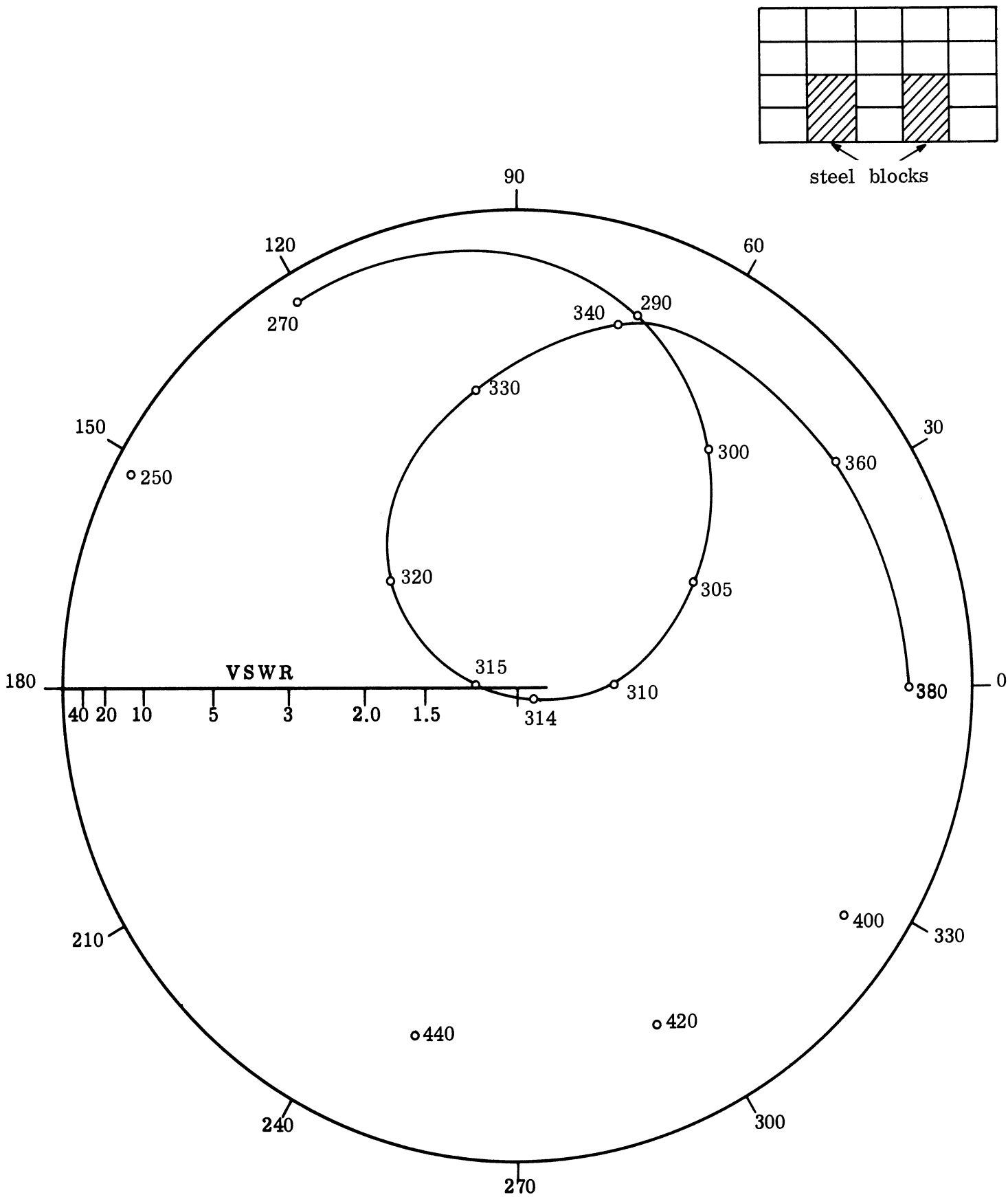
FIG. 5-6c: IMPEDANCE DIAGRAM OF SOLID FERRITE LOADED SLOT ANTENNA
WITH RIDGES (Frequency MHz).

Figure 5-6d shows an asymmetrical ridged arrangement used in the loaded slot antenna and the resulting impedance diagram. Again, an important lowering of the center frequency is noted. The resulting bandwidth of 27 MHz around 292 MHz may be useful. The higher frequency loop on the Smith Chart (around 360 MHz) is not considered valuable.

Other less successful experiments were attempted using ridged slot waveguide. Figures 5-6e, 5-6f and 5-6g show such loadings. Although the curves all appear single-looped and reasonably simple, they do not appear to have value either in lowering the center of operating frequency or increasing the bandwidth even when impedance transformations to the center of the Smith Chart are considered. Ridges extending down from the top and ridges covering all (or almost all) of the height of the slot were unsuccessful. Finally, various schemes of replacing ferrite blocks with balsa wood were attempted, the balsa wood acting essentially as free space or air. Such schemes invariably ended in raising, rather than lowering, the center of the operating frequency.

5.2.5 Conclusions and Summary

Table V-2 summarizes the results of the ridged slot antenna studies. Figures 5-5a, 5-5b, 5-6a, 5-6c and 5-6d showed configurations which were useful in lowering the operating frequency while maintaining a reasonable bandwidth. In all of these, it is noted that a single or double arm iris or ridge in the waveguide is used, extending to the bottom of the waveguide and partially to the top. Most irises or ridges are three blocks high (out of the four) and arranged in a central column. A decrease in center frequency of 60 MHz is not difficult to obtain. Ridges appear to have a wider bandwidth than irises.
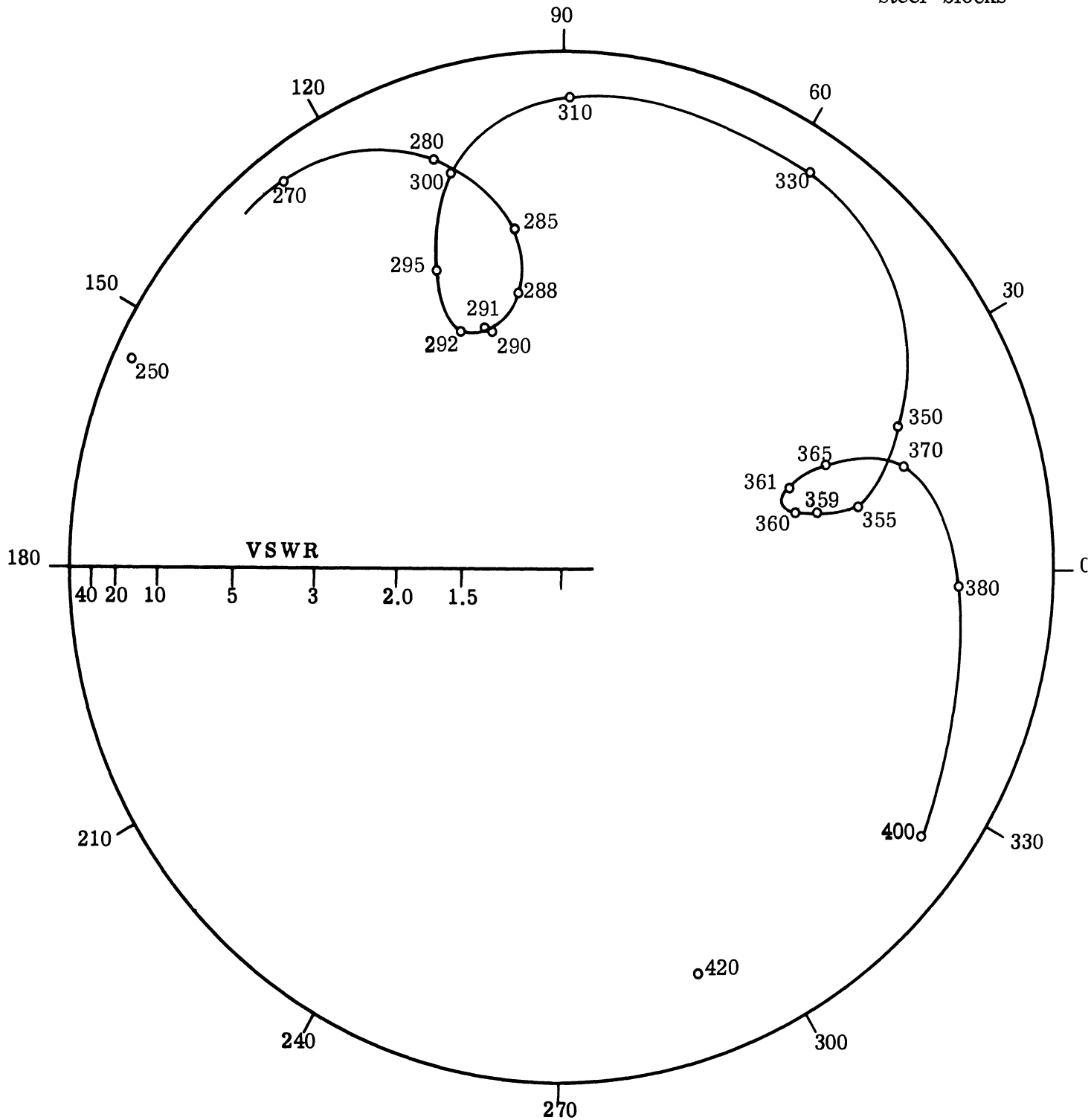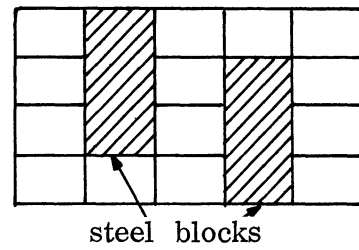
FIG. 5-6d: IMPEDANCE DIAGRAM OF SOLID-FERRITE LOADED SLOT ANTENNA WITH RIDGES (Frequency MHz).

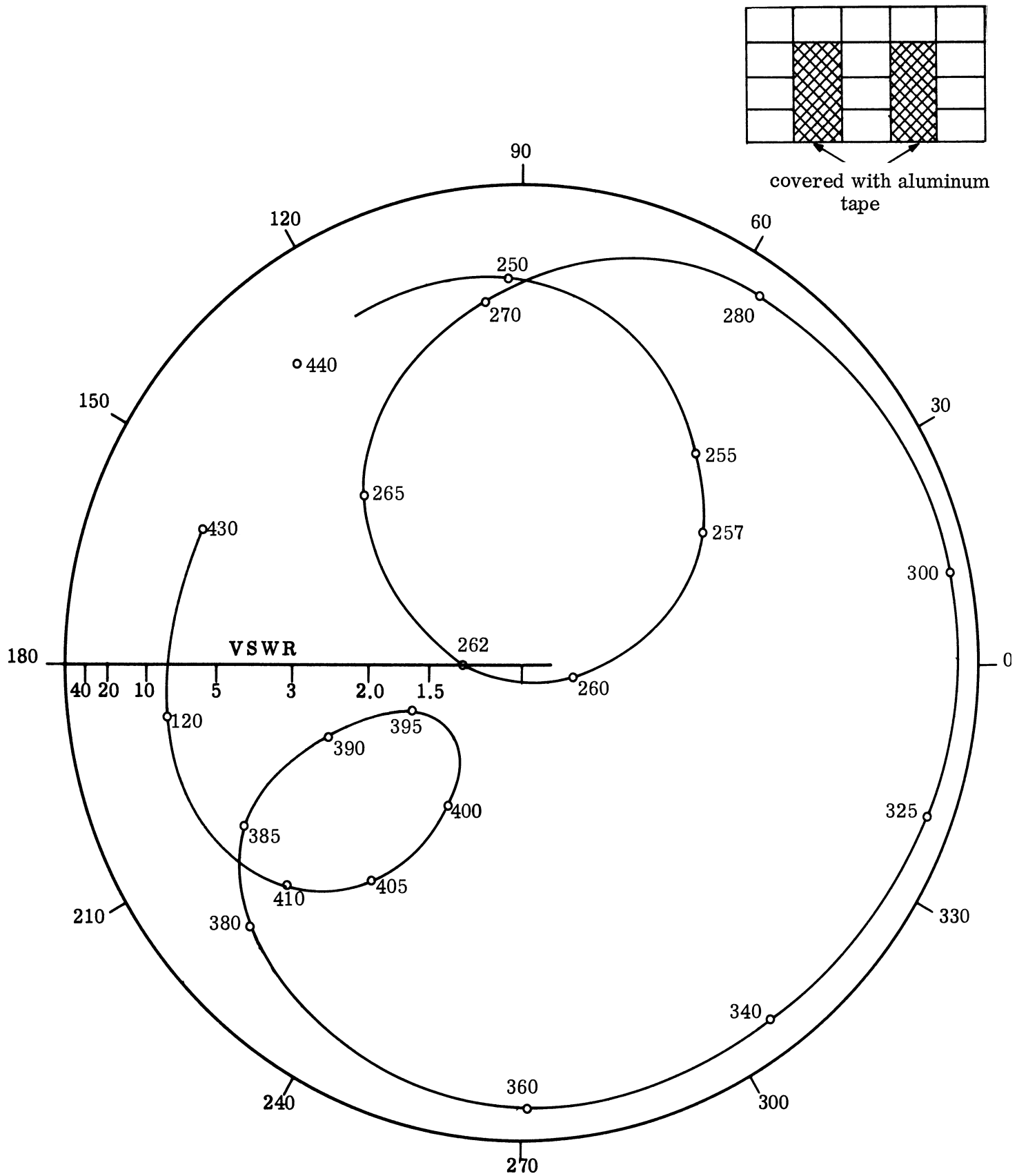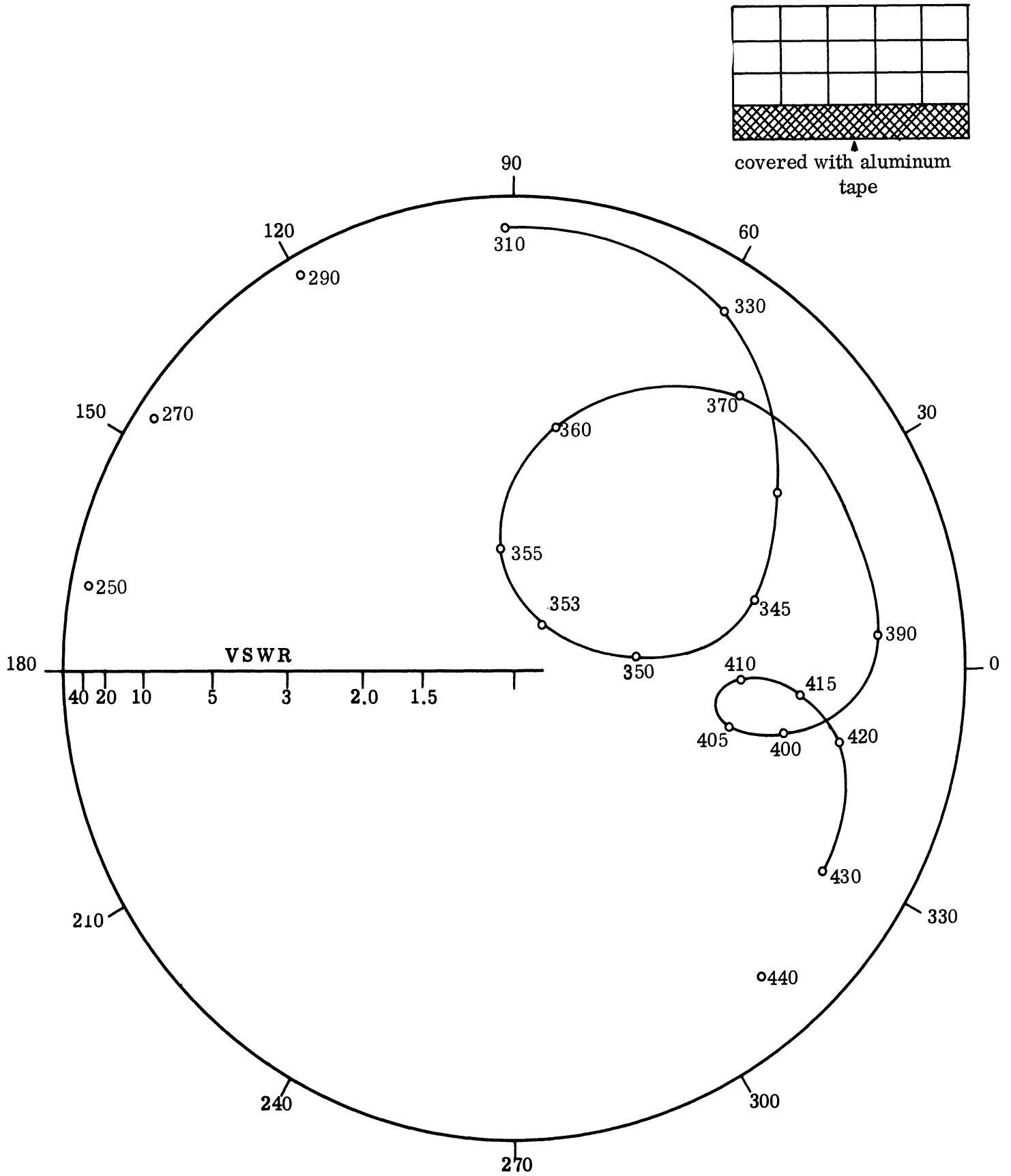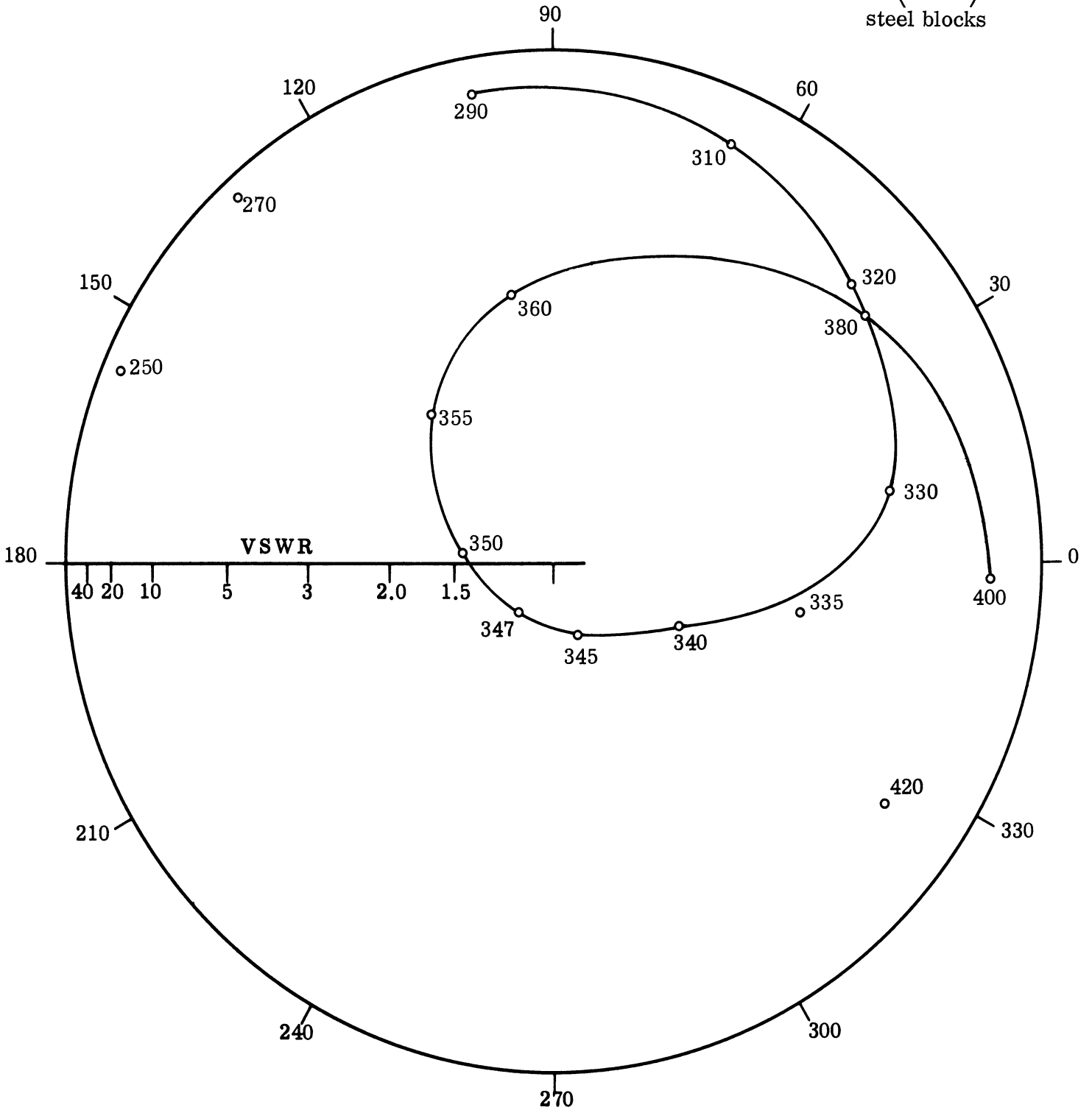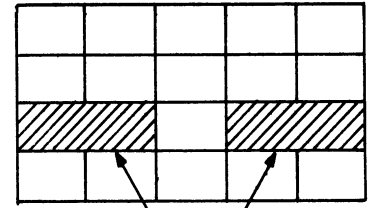FIG. 5-6e: IMPEDANCE DIAGRAM OF SOLID FERRITE LOADED SLOT ANTENNA WITH RIDGES (Frequency MHz)
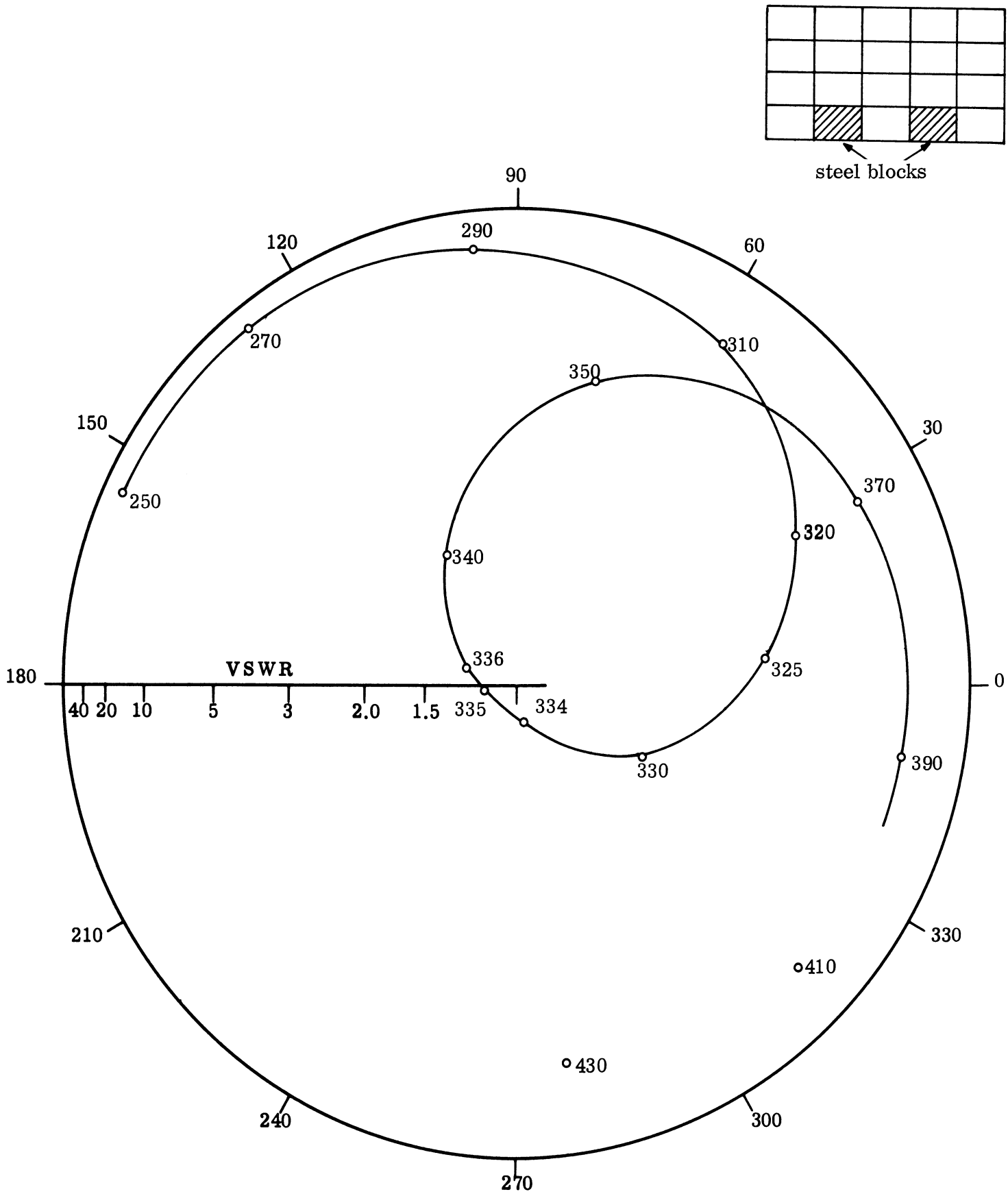
FIG. 5-6f: IMPEDANCE DIAGRAM OF SOLID FERRITE LOADED SLOT ANTENNA
WITH RIDGES (Frequency MHz).

steel block
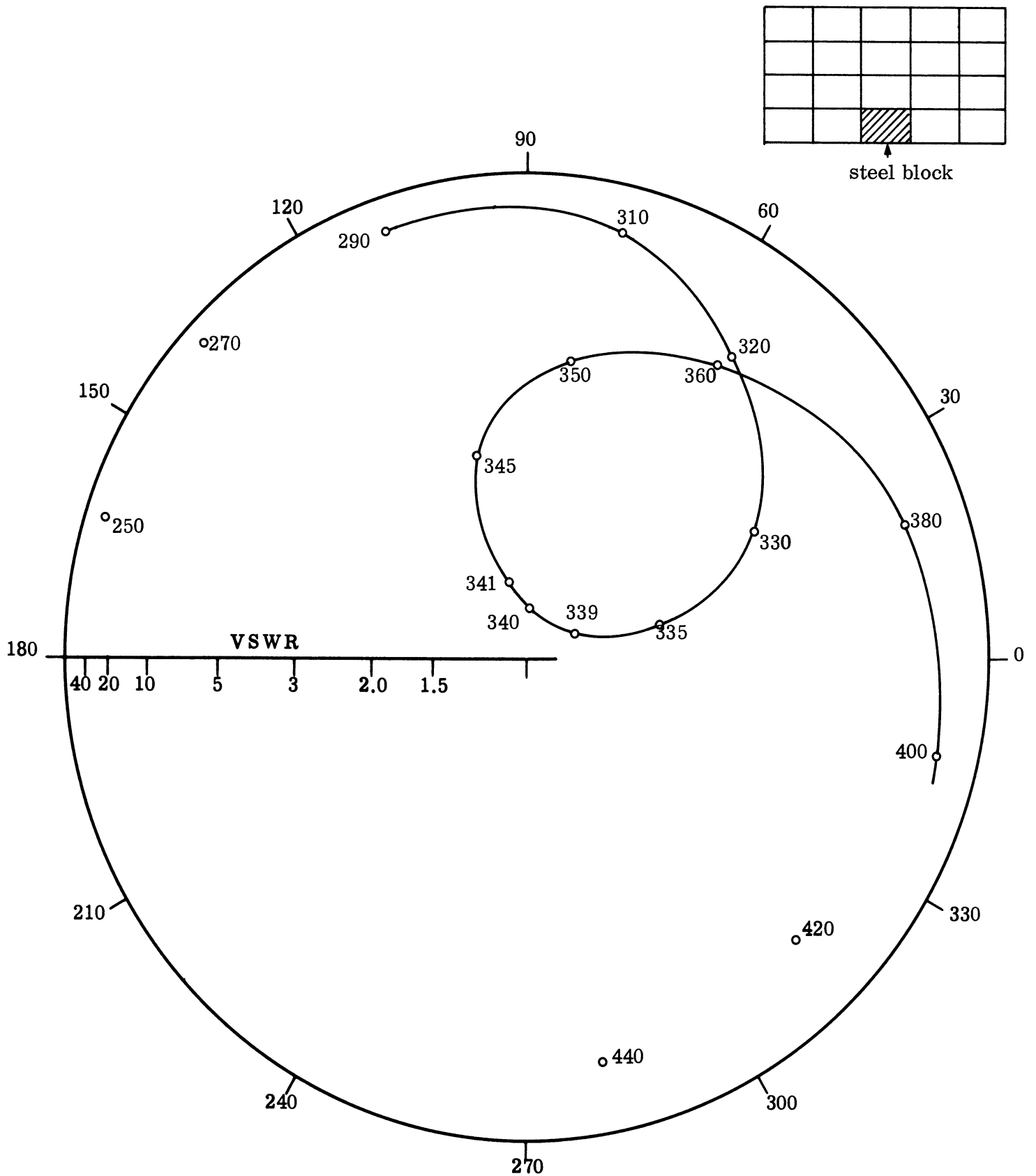
FIG. 5-6g: IMPEDANCE DIAGRAM OF SOLID FERRITE LOADED SLOT
ANTENNA WITH RIDGES (Frequency MHz).

TABLE V-2: SUMMARY OF RIDGE SLOT ANTENNAS

Figure No.	Center Frequency (MHz)	Bandwidth (MHz)	Remarks
5-4a	352	18	No tuner
5-4a	358	50	Optimum tuning
5-4b	344	23	Optimum tuning
5-5a	259	16^+	Optimum tuning
5-5b	261	20^+	Optimum tuning
5-5c	356	42	Optimum tuning
5-5d	273	13	Optimum tuning
5-6a	291	35^+	Optimum tuning
5-6b	330	50	Optimum tuning
5-6c	317	44^+	Optimum tuning
5-6d	292	27^+	Optimum tuning
5-6e	Not potentially useful		Optimum tuning
5-6f	Not potentially useful		Optimum tuning
5-6g	Not potentially useful		Optimum tuning

$^+$Indicates potentially useful results.

Although the impedance diagrams for various configurations of ridges and irises appear useful, the efficiency of the antenna as a radiator must yet be investigated. It is assumed that the antenna patterns will be the usual dipole patterns since the antennas are much smaller than 1λ.

In order to achieve the necessary impedance transformation to make the ridges or irises useful in transforming the impedance of the antenna, a better cavity should be designed for each ridge or iris configuration so that a real impedance is faced by the probe rather than the imaginary or partially imaginary impedances now seen. As mentioned, the probe was designed for a fully loaded cavity rather than the partially loaded cavities tested. In addition it may be necessary to specifically design the ridges or irises such that excessive energy concentrations are avoided, since energy concentrations lead to great losses in ferrite structures.

VI

CHARACTERISTICS OF FERRITE MATERIALS

Attention has been given to extending the use of ferrite loading to lower frequencies (down to 30 MHz). With this in mind, additional ferrite material was purchased (e.g. Q-3, from Indiana General). Some of the experiments in preliminary design are based upon forms of this material which have been readily available. This material appears to have reasonably good electrical and magnetic characteristics. Some of the designed experiments have been limited because of the availability of ferrite material in proper form. The Q-3 material has been obtained in three forms: 1) Stick (2.85" x 0.5" x 0.12"); 2) Cylindrical Rod (1.937" x 0.25"), and 3) Circular Toroids (0.5" OD x 0.28" ID x 0.25" thick).

Ultimately, it is expected that powdered type Q-3 ferrite will be obtained by using some of the solid forms mentioned above and pulverizing them through the use of a ball mill. Ferrite type Q-3 appears to have excellent characteristics below a frequency of 200 MHz. Available information on this ferrite, as obtained from advertising circulars, is somewhat controversial. The characteristics of manufacturer's publications are shown in Fig. 6-1 and will be discussed later. Measurements by this laboratory on the characteristics of the material as represented in Fig. 6-2 show some but not complete agreement with the published data. For measurement methods on Q-3 material see Sections 6.1 and 6.2.

In addition to Q-3, a considerable study has been made of other available ferrites. Table VI-1 gives names and manufacturer for several selected high-Q ferrites. The first ferrite, EAF-2, is the one presently used in this laboratory for ferrite-loaded antenna studies. Its properties have been thoroughly measured by this laboratory. All of the work involving experimental tests of antennas loaded with powdered ferrite have used this material.
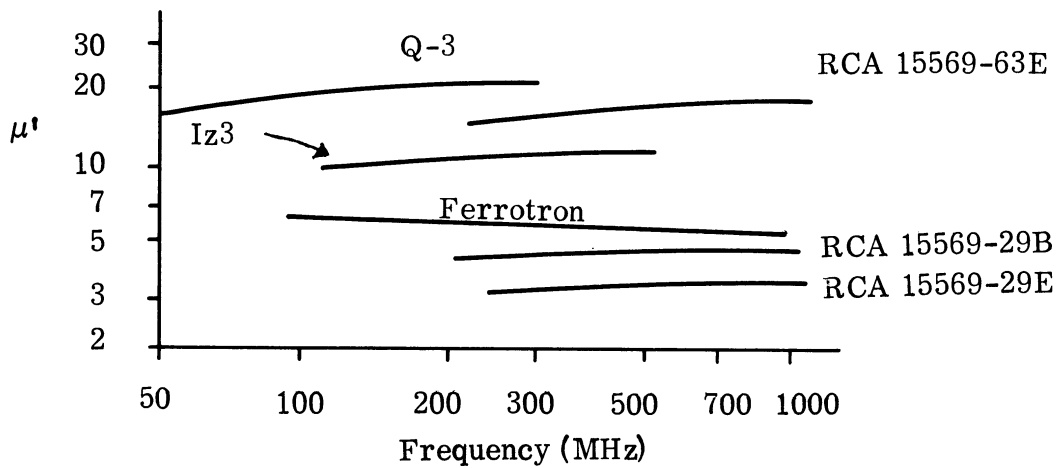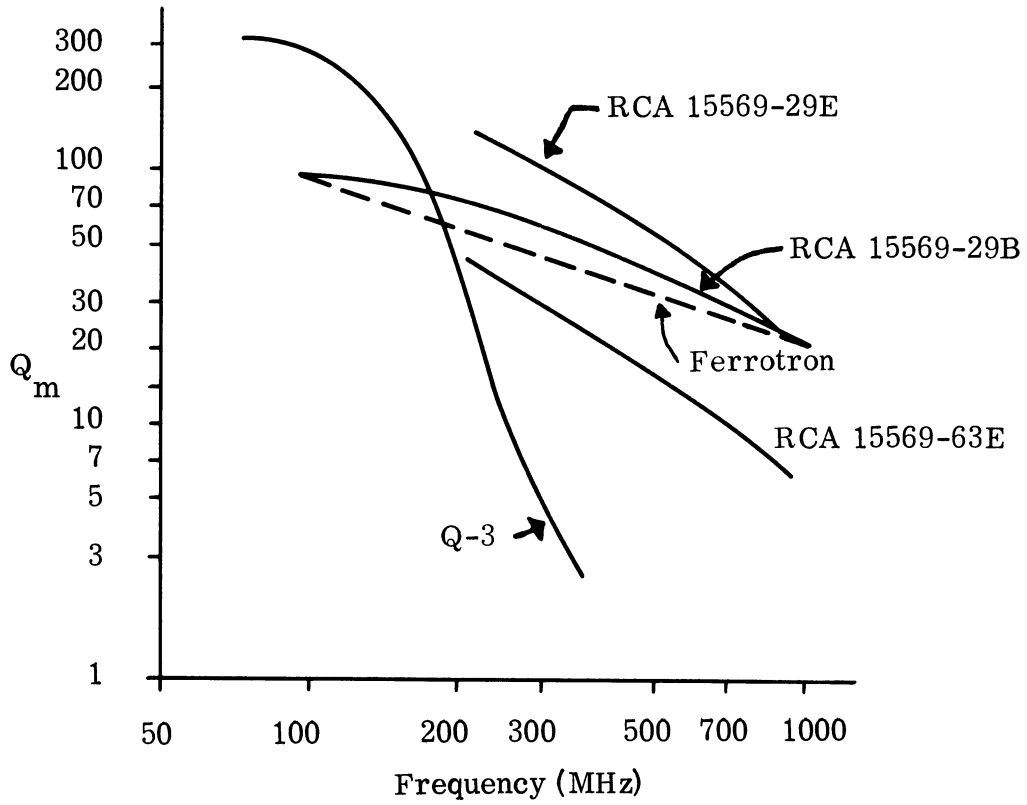
FIG. 6-1: FERRITE PROPERTIES, ADVERTISED VALUES
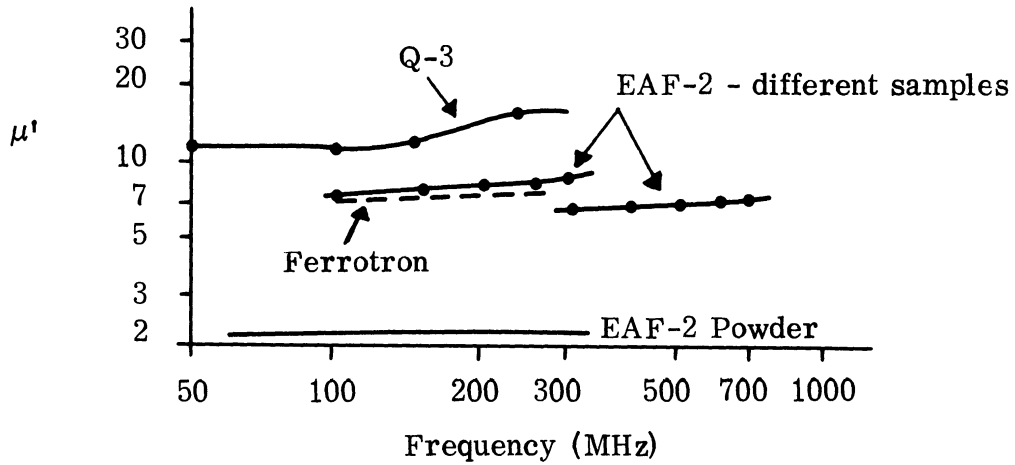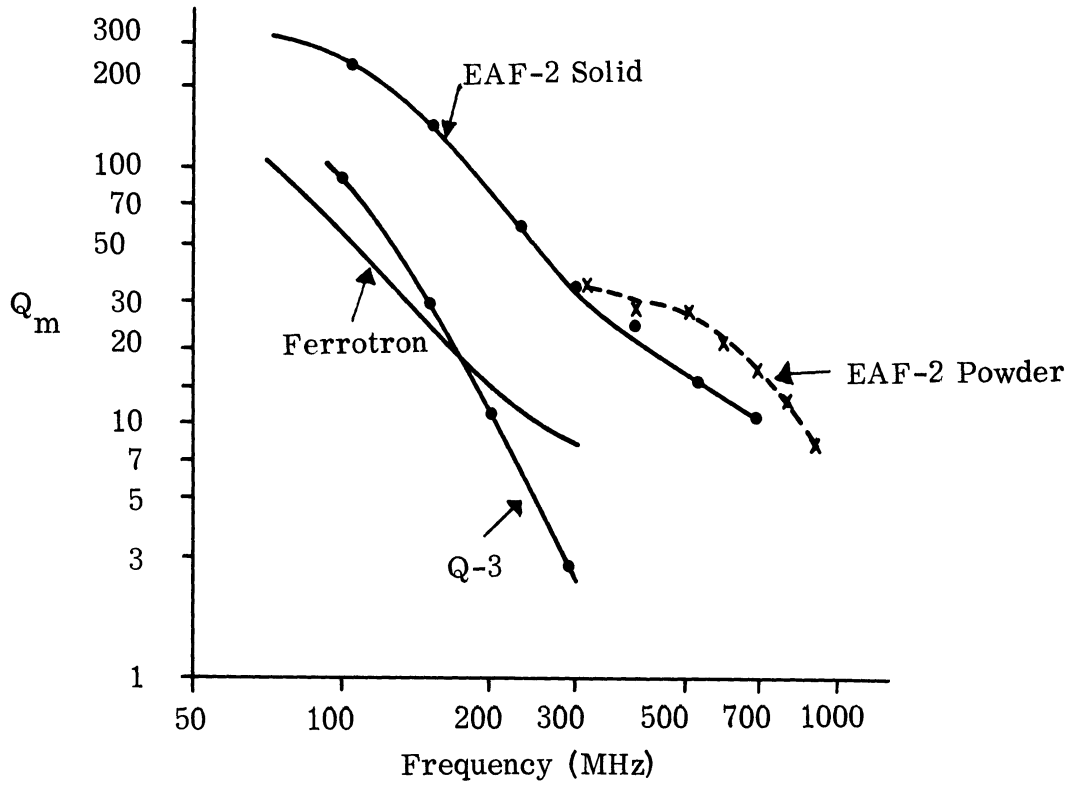
FIG. 6-2: FERRITE PROPERTIES AS MEASURED BY
THE UNIVERSITY OF MICHIGAN

Its formula is

$$\text{Ni}_{.9696}\text{Zn}_{.0404}\text{Co}_{.03}\text{Fe}_{1.84}\text{A}\ell_{.04}\text{O}_4 \cdot \tag{6.1}$$
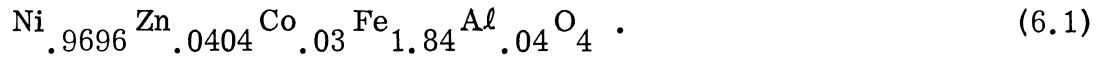
TABLE VI-1: SELECTED HIGH-Q FERRITES

Ferrite	Manufacturer	Remarks
EAF-2	Motorola	Production not repeatable. No longer available. Tested at U. of M.
Q-3	Indiana General	Several sizes on order. To be tested. Tested at U. of M.
Ferrotron	Polymer Corporation	Not a ferrite. Iron impregnated plastic. Excellent at high temperatures. Q_m and μ' measured at U. of M.
IZ3	Ferroxcube	Measured resonance in ϵ' at 100 MHz.
RCA 15569 Series	RCA	Tested for USAEC by RCA. RCA does not produce. Formula said to be reproductible. USAEC has indicated these materials are all magnetically oriented.
Eccosorb CR	Emerson and Cuming, Inc.	Recently tested at U. of M.

The EAF-2 material (designated in previous reports as type A) has been satisfactory for experiments on earlier contracts. It is the same material which was used in the detailed studies of the rectangular cavity-backed slot. The temperature dependence of this material has been reported (Lyon et al, 1964). Attempts to purchase more of this material have failed, due to the difficulty experienced in reproducing the high quality of the first batch.

The second ferrite, Q-3, has already been discussed.

The third ferrite, Ferrotron, has been recently tested by this laboratory (see Section 6.1). The tests did not substantiate its advertised high-Q properties at 300 MHz and above.

The fourth and fifth ferrites have not been tested by this laboratory except for brief dielectric tests on IZ3. The RCA materials (1963) are experimental and were developed for the US Army Signal Corps. Currently, RCA is not manufacturing this ferrite, although sufficient information is available for others to manufacture it. Figures 6-1 and 6-2 show the Q_m (magnetic Q) and μ' properties for the various ferrites investigated. From Fig. 6-2 it can be seen from the Q_m curves that the present EAF-2 ferrite from Motorola is better than any other available ferrite except for the RCA experimental ferrite shown in Fig. 6-1. Note that the RCA ferrites with very high Q at high frequencies also have very low μ properties. This is a common characteristic of ferrites - a very low loss factor usually is accompanied by a low permeability. Nevertheless, it does appear that several of the RCA ferrites are worth investigating for future application in antenna loading where the anisotropy associated with a favored orientation for magnetization can be advantageous or at least acceptable.

6.1 Derivation of Permeability Determination Equations

A resume of the method of obtaining both the real and imaginary components of relative permeability is given. See Fig. 6-3. First, a lossless calculation will be derived for thin samples. Later, a thick sample measurement for more accurate loss measurements will be given.

Let

$$Z_{s.c.} = jZ_f \tan\beta_f d \ . \qquad \text{(Considering a lossless transmission line.)}$$

$$\text{(6.2)}$$
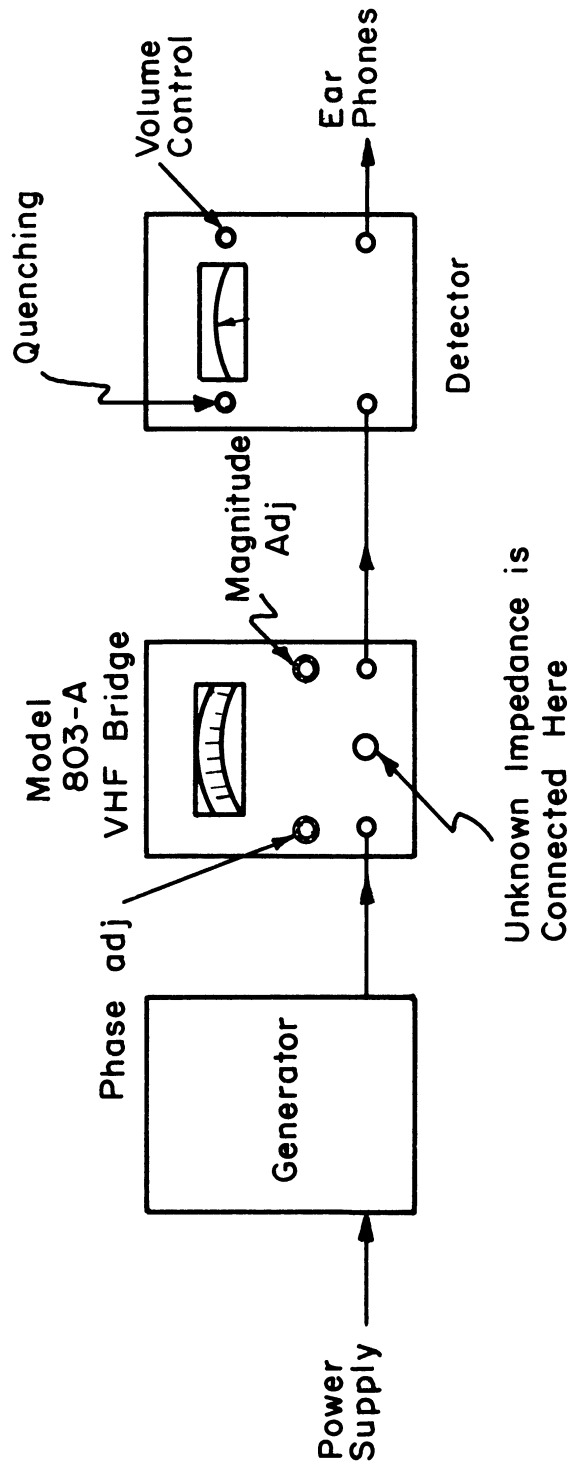
FIG. 6-3 : EXPERIMENTAL SETUP FOR μ_r AND ϵ_r MEASUREMENTS.

where

Z_f - characteristic impedance of ferrite medium

$$= \sqrt{\frac{\mu_r}{\epsilon_r}} \; Z_o \quad . \tag{6.3}$$

Z_o - characteristic impedance of the medium in the coaxial line.

β_f - propagation constant in ferrite

$$= \frac{2\pi}{\lambda_o} \sqrt{\mu_r \epsilon_r} \tag{6.4}$$

μ_r, ϵ_r - Relative permeability and permittivity.

The small thickness d validates the approximation $\tan \beta_f d. \simeq \beta_f d$ is within 6° with $\sqrt{\mu_r \epsilon_r} = 10$. This is reasonable for type Q-3 ferrite for μ_r and ϵ_r at 200 MHz.

$$Z_{sc} = j \sqrt{\frac{\mu_r}{\epsilon_r}} \cdot Z_o \cdot \tan \frac{2\pi}{\lambda_o} \sqrt{\mu_r \epsilon_r} \; d.$$

$$\tag{6.5}$$

$$\simeq j \sqrt{\frac{\mu_r}{\epsilon_r}} \; Z_o \cdot \frac{2\pi}{\lambda_o} \cdot \sqrt{\mu_r \epsilon_r} \; d.$$

$$\simeq j \mu_r Z_o \cdot \frac{2\pi}{\lambda_o} \; d$$

Then:

$$\mu_r \cong - \frac{jZ_{s.c.}\lambda_o}{Z_o \cdot 2\pi d} \tag{6.6}$$

Since Z_{sc} is almost purely imaginary,

$$\mu_r = \frac{|Z_{s.c.}|\lambda_o}{Z_o 2\pi d} \tag{6.7}$$

In order to measure losses, a much thicker sample was used. The following derivation does not use the $\tan\delta \approx \delta$ approximation, and thus is valid for much thicker samples.

Let

$$Z_{s.c.} = Z_f \tan\gamma_f d \tag{6.8}$$

$$Z_f = \sqrt{\frac{\mu}{\epsilon}} \quad Z_o = \frac{Z_{s.c.}}{\tanh\gamma_f d} \qquad (\mu \text{ and } \epsilon \text{ are relative values}) \tag{6.9}$$

Hence,

$$\mu = \frac{\left(Z_{s.c.}^2\right)\epsilon}{Z_o^2 \tanh^2\gamma_f d} \tag{6.10}$$

Let

$$\mu = \mu' - j\mu'' \tag{6.11}$$

and

$$Z_{s.c.} = Z_r' + jZ_r'' \tag{6.12}$$

Then assuming ϵ real,

$$\mu' - j\mu'' = \frac{(Z_r'^2 - Z_r''^2 + 2jZ_r'Z_r'')\,\epsilon}{Z_o^2 \tanh^2 \gamma_f d} \qquad (6.13)$$

Solving:

$$\mu' = \frac{(Z_r'^2 - Z_r''^2)\epsilon}{Z_o^2 \tanh^2 \gamma_f d} \qquad (6.14)$$

$$\mu'' = \frac{-2Z_r'Z_r''\,\epsilon}{Z_o^2 \tanh^2 \gamma_f d} \qquad (6.15)$$

Then:

$$\tan \delta = \frac{\mu''}{\mu'} = \frac{-2Z_r'Z_r''}{(Z_r'^2 - Z_r''^2)}$$

$$= \frac{2Z_r'Z_r''}{Z_r''^2 - Z_r'^2} \qquad (6.16)$$

Now:

$$Z_{s.c.} = Z_r' + jZ_r''$$

$$Z_r' = \left| Z_{s.c.} \right| \cos\theta \qquad (6.17)$$

$$Z_r'' = \left| Z_{s.c.} \right| \sin\theta \qquad (6.18)$$

Let

$$\phi = 90 - \theta$$

Then

$$Z'_r = \left| Z_{s.c.} \right| \sin\phi \tag{6.19}$$

$$Z''_r = \left| Z_{s.c.} \right| \cos\phi \tag{6.20}$$

Then

$$\tan\delta = \frac{2 \left| Z_{s.c.} \right|^2 \cos\phi \sin\phi}{\left| Z_{s.c.} \right|^2 (\cos^2\phi - \sin^2\phi)} \tag{6.21}$$

$$= \frac{\sin 2\phi}{\cos 2\phi}$$

$$= \tan 2\phi \tag{6.21}$$

Let:

$$Q_m = Q \text{ magnetic}$$

Then:

$$Q_m = \frac{1}{\tan\delta} = \cot 2\phi \tag{6.22}$$

6.2 Results of Permeability Measurements

Using the apparatus shown in Fig. 6-4, the procedure to obtain $Z_{s.c.}$ was as follows:
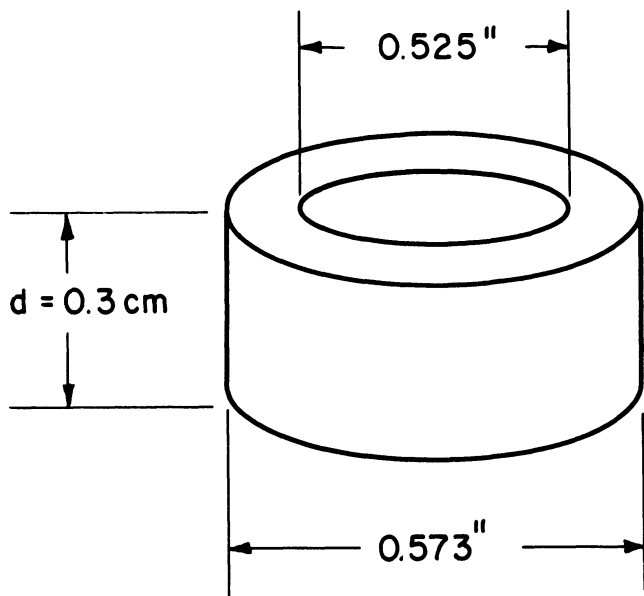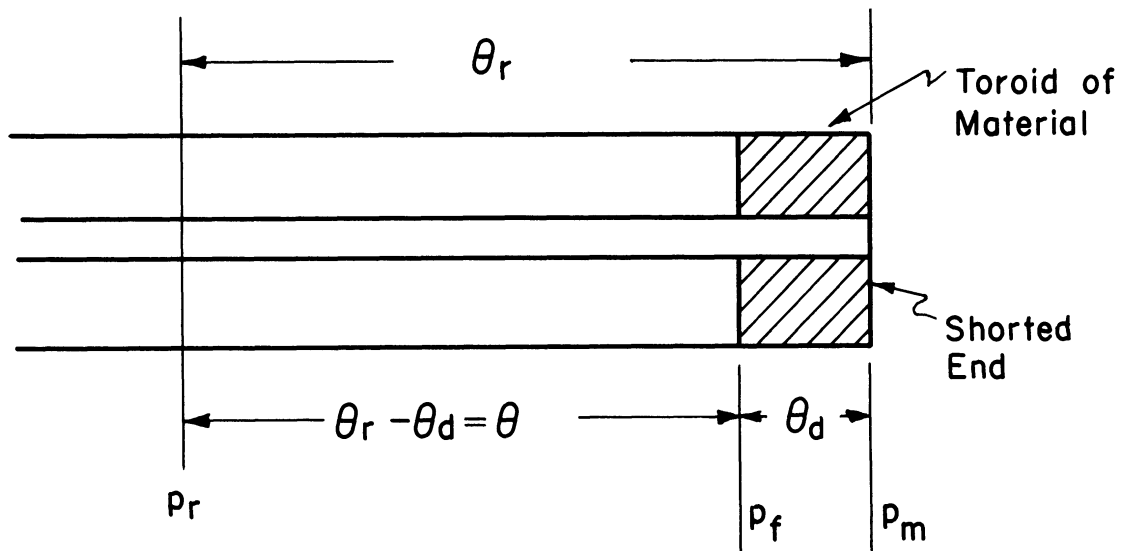
FIG. 6-4: GEOMETRY FOR TOROID MEASUREMENT TECHNIQUE.

1. The bridge is shorted and a null is obtained. The magnitude and phase readings corresponding to this null are the reference values for the short-circuit impedance without the ferrite specimen in the holder. This point is plotted on $Z - \theta$ chart (S_μ on Fig. 6-5). This point should have been at the short circuit point of the chart (Ohms, 90°).

However, since the bridge measures impedance not at the plane p_m, (See Fig. 6-3) but at p_r, the reference plane, this reading has to be translated by θ_r on the $Z - \theta$ chart to make it coincide with the true short circuit point of the chart.

2. The ferrite specimen is inserted in the holder of the coaxial cavity and a null is obtained as indicated by the detector. The readings on the VHF bridge corresponding to this null are plotted on $Z - \theta$ chart and this point is translated by $(\theta_r - \theta_d)$ in wavelengths to give $Z_{s.c.}$ at the plane p_f.

3. $Z_{s.c.}$ at the plane p_f represents the magnitude and phase of the impedance of the coaxial cavity with the specimen. The phase difference between reading in (1) and this reading indicates loss in the ferrite specimen corresponding to the loss tangent for the material. Actually the loss tangent equals the tangent of twice this difference angle (see derivation of formulas). A tabulation of the results based on data and simple calculations is given below in Table VI-2 for Q-3 ferrite and Table VI-3 for Emerson and Cuming, Inc., Eccosorb "CR". The "CR" (casting resin) material was a very recent measurement. Although it was designed to be a lossy microwave ferrite material, Table VI-3 shows that below 300 MHz, the μ is reasonably high and losses very low. Since the material has a high ϵ and can be easily cast, it will be further investigated as a useful loading ferrite.

The data obtained as outlined cannot give a small loss tangent very accurately, since it is difficult to obtain with precision the phase difference in step (3) from $Z - \theta$ chart. However, high losses can be measured accurately. The measured μ_r curve of Q-3 is somewhat lower than the published value; the measured loss curve

TABLE VI-2:

PERMEABILITY OF TYPE Q-3 FERRITE

f (MHz)	μ_r	Loss Tangent	Q-Magnetic
100	12.4	0.01746	57.290
125	12.3	0.02444	40.917
150	13.2	0.03492	28.636
175	13.2	0.05241	19.081
200	14.3	0.08749	11.43
225	16.0	0.1763	5.67
250	16.82	0.3244	3.07
300	16.4	very high	very low

The values of μ found above agree closely with published values.

Data taken by the same method on "Eccosorb C-R" material results in the information shown in Table VI-3.

TABLE VI-3:

PERMEABILITY OF ECCOSORB C-R

f (MHz)	Z short θ	Z	Z eccosorb θ	Z	Z eccosorb translated and corrected	μ_r	Q Magnetic
100	91.0^o	8.6	90.5	10	89.5	1.25	3.98	57
150	60	12.8	59.5	15.4	89.25	2.5	5.3	38
180	51	15.5	50.5	18.5	89.1	2.55	4.52	32
200	45.5	17.2	45	20.8	89	3.0	4.72	28.6
230	39.5	20.5	39	24.5	88.75	3.25	4.5	22.9
250	36.5	21.9	36.0	26.3	88.7	3.5	3.72	22
300	30.7	27.5	30.2	33.25	88.6	4.25	4.51	20.4
400	22.75	39.3	22.1	49.5	85	5.7	4.55	5.6

is much higher than advertised. The utmost care was taken in obtaining data. The final readings are the result of an average of three trials.

6.3 Permittivity Determination Method

Using Figs. 6-3 and 6-4 the method is similar to that described in Section 6.1 except the specimen is placed at a location in the coaxial cavity corresponding to a maximum of electric field. Thus

$$Z_{oc} = \frac{-jZ_f}{\tan\beta_f d} \qquad \text{(for a lossless line).}$$

$$= \frac{-jZ_o \lambda_o \sqrt{\mu_r/\epsilon_r}}{2\pi d \sqrt{\mu_r \epsilon_r}}$$

$$= \frac{-jZ_o \lambda_o}{2\pi \epsilon_r d} \tag{6.23}$$

Therefore,

$$\epsilon_r = \frac{-jZ_o \lambda_o}{2\pi Z_{oc} d} \tag{6.24}$$

And

$$\left| \epsilon_r \right| = \frac{Z_o \lambda_o}{2\pi \left| Z_{oc} \right| d} \tag{6.25}$$

The problem here is to create a perfect open circuit. This is done as follows:
1) A short is created and the impedance is measured. Use dotted lines on Fig. 6-5.

2) Open circuit impedance corresponding to (1) is found from the Z - θ chart.

3) The open circuit impedance obtained from (2) is adjusted on the bridge dial and a null is obtained corresponding to that by means of a short circuited adjustable line λ/4 length beyond the specimen.

4) The length of the short circuited stub is clamped. This is the exact λ/4 length which will create a perfect open circuit.

5) The ferrite piece is put then inside the holder and with the same length of stub as in (4) a null is obtained but the reading on the dial is not the Z_{oc} in the above formula.

6) Z-open in (2) is not actually open. It has to be ∞. So translate the value in (2) to ∞ points on Z - θ chart and note the angle of translation.

7) Translate impedance in (5) by the angle in (6) in the proper direction. (See the Z - θ chart Fig. 6-5 with construction done on it.)

8) The new point represents Z_{oc} used in the above formula. The results of data so obtained are in Table VI-4.

TABLE VI-4:

PERMITTIVITY OF TYPE Q-3 FERRITE

f (MHz)	short		open		measured/open with ferrite		actual open with ferrite		ϵ_r
	θ	(Z)	θ	(Z)	θ	(Z)	θ	(Z)	
100	90°	130	-90°	19	-90°	16.3	-90	1000	7.96
200	90°	16	-90°	155	-90°	116	-90	510	7.81
300	90°	14	-90°	180	-90°	115	-90	345	7.7

The ferrite is relativity lossless as far as the dielectric loss is concerned. Though a loss is detected at frequencies higher than 225 MHz, it is not accurately measurable without the help of very accurate instruments.

Note: Calculations of μ_r and ϵ_r for Q-3 ferrite are made at 200 MHz from Z $-\theta$ Chart

S_μ - Short circuit impedance for μ_r measurements

S_ϵ - S. C. impedance for ϵ_r measurements

S_{f_μ} - S. C. impedance with ferrite for μ_r measurements

0 - open circuit

hence - 0_{f_t} - Open circuit impedance with ferrite for ϵ_r measurements etc.

FIG. 6-5:   Z $-\theta$ CHART

VII

EFFICIENCY MEASUREMENTS

In this procedure, an arbitrary antenna is fed with constant power and the power received by the test antenna is compared to that of a standard dipole by means of a calibrated attenuator. The difference in attenuator settings is the relative gain of the standard antenna. Corrections are made for the VSWR of each antenna and for other non-antenna losses.

7.1 Efficiency Data on Ferrite Loaded Helix

Loading of a helix antenna with a low loss ferrite does not significantly alter the efficiency as a radiator at resonance. Table VII-1 gives the values of efficiency for various loadings of EAF-2 powdered ferrite. The resonance frequency of antenna No. 217 corresponds to 750 MHz with air and 550 MHz with a 3/8" loading of EAF-2 ferrite.

TABLE VII-1:

EFFICIENCY OF A HELIX ANTENNA (No. 217) WITH
SEVERAL FERRITE LOADINGS

Frequency (MHz)	Loading	Efficiency (per cent)
750	Air	60
550	3/8" Inside Layer EAF-2	61.2
550	1" Inside Layer EAF-2	41
550	Air	31.8
550	3/4" Outside Layer EAF-2	54.5

The efficiency of the outside loading of ferrite was measured at a frequency that was near resonance. Note that the reduction of efficiency is not statistically significant.

7.2 Measurement Procedures

The gain of the test antenna is obtained by adjusting a calibrated attenuator to produce equal receiver levels for both the test antenna and a standard half-wavelength dipole. Corrections to this relative gain figure are made for the mismatch of each antenna to its transmission line, losses that result in the baluns, and losses due to incompatible polarizations.

7.2.1 Measurements

The set up of the equipment as indicated in the Fig. 7-1 using a standard dipole as the receiving antenna. The power transmitted, attenuator setting and chart level are recorded (Part 1, Appendix C).

The dipole is then replaced with the test antenna, and the same power is fed to the transmitting antenna as before. The attenuator is adjusted to give the same chart level as determined in the preceding paragraph. The power transmitted, attenuator setting, and chart level are recorded (Part 2, Appendix C), for both E and H plane patterns of the test antenna. For circular polarization the antenna is rotated 90° on the axis of symmetry for additional E and H plane patterns.

The VSWR of the standard dipole at its connector (Part 1, Appendix C) and the test antenna are recorded (Part 2, Appendix C).

7.2.2 Calculations

If the test antenna is fed with an infinite balun, corrections must be made in both the gain calculation and the measured reflection factor. Attenuation data on cables may be obtained either by direct measurement, or by reference to standard tables. (e.g., Reference Data For Radio Engineers.)

If there is significant inefficiency in the standard dipole, the loss must be determined and a correction made in the measured reflection factor.

Since the impedance of the standard dipole and the test antenna are usually

```
┌──────────────┐                              ┌──────────────┐
│  Recv. Ant.  │                              │  Trans. Ant. │
│ (Std. Dipole)│ ◄──────────────────────────  │  (Arbitrary) │
│  (test Ant.) │                              │              │
└──────────────┘                              └──────────────┘
       │                                              ▲
       ▼                                              │
┌──────────────┐      ┌──────────┐            ┌──────────────┐
│              │      │  Power   │ ◄───────── │  Directional │
│  Attenuator  │      │  Meter   │            │   Coupler    │
└──────────────┘      └──────────┘            └──────────────┘
       │                                              ▲
       ▼                                              │
┌──────────────┐                              ┌──────────────┐
│   Receiver   │                              │    R. F.     │
│     or       │                              │  Generator   │
│    dipole    │                              │              │
└──────────────┘                              └──────────────┘
       │                                              ▲
       ▼                                              │
┌──────────────┐                              ┌──────────────┐
│ Rectangular  │                              │   1000 Hz    │
│   Plotter    │                              │    Osc.      │
└──────────────┘                              └──────────────┘
```
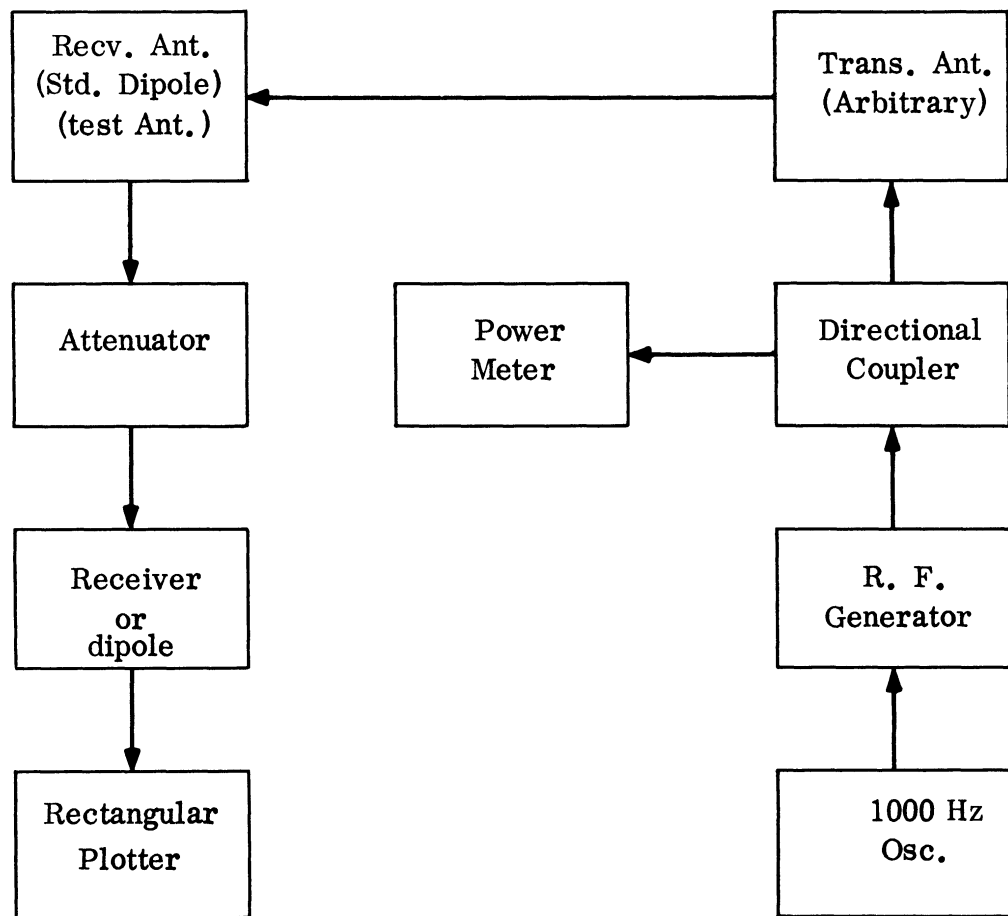
FIG. 7-1: EQUIPMENT SETUP FOR EFFICIENCY

different, the power fed to each antenna is usually different even though the incident powers are identical. The correction factor is the ratio of the dipole power transmission coefficient to that of the test. The power transmission coefficient is one minus the square of the voltage reflection factor.

In calculating the gain of the test antenna, the 2.15 db gain of a lossless half wave dipole (constant C in Appendix C) must be added. An extra 3.01 db must be added for a circularly polarized test antenna because half of the power in a linearly polarized wave is unavailable to a circularly polarized antenna.

At this point it is possible for the recorders of the data to make an estimate on the efficiency. The expression $d = \frac{32,600}{\phi\theta}$ is a fairly accurate formula for estimating the numerical directivity, d (Stegen, 1964). The values of ϕ and θ are the half power beamwidths of two orthogonal cuts. If there is rotational symmetry (as there usually is), ϕ and θ have the same value. Using this approximation, efficiency is $\frac{g}{d} \times 100$.

To calculate the directivity more precisely, a graphical integration of an antenna pattern must be made. If there is a high degree of rotational symmetry in the patterns, only one graphical integration need be performed. If there is significant asymmetry, graphical integrations must be performed on four or more cuts depending on the polarization and patterns. An average of the reciprocals of the directivities calculated for each pattern must be made; the reciprocal of the average is then the value of directivity to be used for calculating the efficiency.

To do the graphical integration, Table C-1 of Appendix C may conveniently be used, for either received voltage or power.

The directivity, d, is calculated by the formula:

$$d = \frac{229\ U_o}{(\text{width of square in}^o)\ (\text{total at bottom of Table C-1, Appendix C})} \qquad (7.1)$$

where U_o is the pattern maximum of the power. If the plot is of field strength, U_o^2 is used instead of U_o.

The formula is an approximation to the exact expression for directivity (Kraus, 1950).

$$d = \frac{4\pi U_o}{\int_0^{2\pi} \int_0^{\pi} U(\theta,\phi)\sin\theta\, d\theta\, d\phi} \qquad (7.2)$$

If there is independence of ϕ, as is often the case, the formula reduces to:

$$d = \frac{4U_o}{\int_0^{\pi} U(\theta)\sin\theta\, d\theta} = \frac{4U_o}{\int_0^{2\pi} U(\theta)\left|\sin\theta\right| d\theta} \qquad (7.3)$$

The integration may be a sum:

$$d \approx \frac{4U_o}{\sum_{i=1}^{n} U(\theta_i)\left|\sin\theta_i\right|\Delta_i\theta} \qquad (7.4)$$

If we express $\Delta_i\theta$ in degrees instead of radians:

$$d \approx \frac{4U_o}{\frac{2\pi}{360}\sum_{i=1}^{n} U(\theta)\left|\sin\theta_i\right|\Delta_i\theta} = \frac{229U_o}{\sum_{i=1}^{n} U(\theta_i)\left|\sin\theta_i\right|\Delta_i\theta}$$

$$= \frac{229 U_o}{\sum\limits_{i=1}^{n} |\sin\theta_i| \left(squares \big/ \Delta\theta_i\right) (\Delta\theta_i)}$$

$$= \frac{229 U_o}{\Delta\theta_i \sum\limits_{i=1}^{n} |\sin\theta_i| \left(squares \big/ \Delta\theta_i\right)} \tag{7.5}$$

since all of our $\Delta\theta_i$ are equal. This is the formula stated previously since $\sum\limits_{i=1}^{n}$ $|\sin\theta_i| \left(squares \big/ \Delta\theta_i\right)$ is the total at the bottom of Table C-1, Appendix C.

APPENDIX A
ENERGY TRANSFER BETWEEN A HELIX
AND A FERRITE ROD

Studies have been made of continuously excited (i. e. excited over a large portion of the antenna length) traveling wave antennas (Spitz, 1962; Walter, 1965; Weeks, 1957; Rumsey, 1953). Recently, this laboratory began studies of such antennas using ferrite materials. Specifically, a mathematical study of the energy transfer process from the exciter (in our case, a helix) to the ferrite rod (the intended radiating mechanism) has been made.

In a study of energy transfer into a ferrite rod one can start with the proposition that with two transmission lines coupled together, energy fed into one line will be transferred optimally to the second, under certain conditions. The voltage and current differential equations for each of the two transmission lines have been written. A consideration of the coefficients involved in these transmission lines indicates the dependence upon mutual coupling factors. When the second transmission line is to serve as a radiator, it is expected that the energy transferred to this line will be reradiated at the far end in the end fire direction

A. 1 Analysis

In order to cause a strong coupling between the feeding electric circuit and the receiving ferrite rod the phase velocity of the electric circuit in the axial direction must be adjusted to be approximately the same as the wave phase velocity in the ferrite rod.

The phase velocity along the axis of the helix is approximately:

$$v_p = c \sin \psi$$

where ψ is the pitch angle and c is the velocity of light. Treating the helix as a transmission line with distributed L and C, the ferrite slab may be considered to be another transmission line. The arrangement of lines is shown in Fig. A-1. Due to
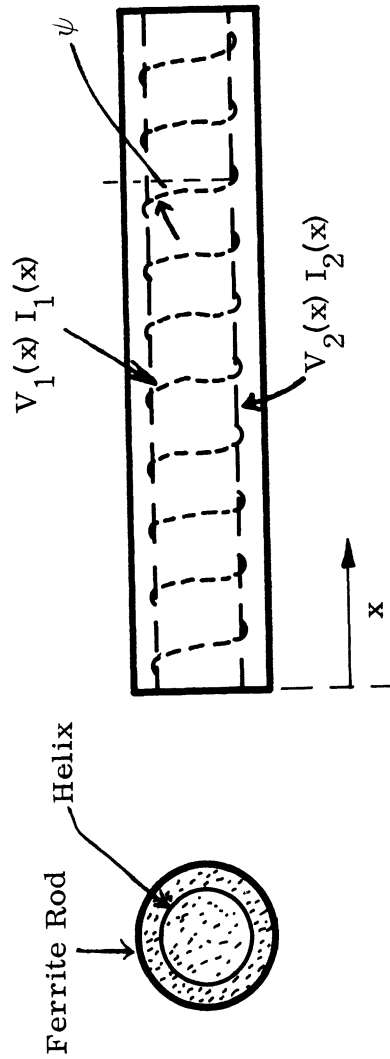
FIG. A-1: FERRITE ROD FED BY A HELIX

V_1, $I_1(x)$ are voltage and current along helix,

V_2, $I_2(x)$ are induced voltage and current along ferrite rod

the excitation of the helix, there is mutual energy coupling between the helix and the ferrite rod. The circuit equations are

Circuit No. 1: Helix

$$\frac{dV_1}{dx} = z_1 I_1 + z_{12} I_2 \tag{A.1}$$

$$\frac{dI_1}{dx} = y_1 V_1 + y_{12} V_2 \tag{A.2}$$

Circuit No. 2: Ferrite

$$\frac{dV_2}{dx} = z_2 I_2 + z_{21} I_1 \tag{A.3}$$

$$\frac{dI_2}{dx} = y_2 V_2 + y_{21} V_1 \qquad . \tag{A.4}$$

Let

$$Z_1 = \sqrt{z_1/y_1} \ , \qquad\qquad Z_2 = \sqrt{z_2/y_2} \qquad . \tag{A.5}$$

A.1, A.2 and A.3, A.4 can be rearranged into the form:

$$\frac{d}{dx}(V_1 \pm I_1 Z_1) = \mp \sqrt{z_1 y_1}\,(V_1 \pm I_1 Z_1) + z_{12} I_2 \pm y_{12} Z_1 V_2 \qquad . \tag{A.6}$$

$$\frac{d}{dx}(V_2 \pm I_2 Z_2) = \mp \sqrt{z_2 y_2}\,(V_2 \pm I_2 Z_2) + z_{21} I_1 \pm y_{21} Z_2 V_1 \qquad . \tag{A.7}$$

Define the following modes.

$$A_{1\pm} = \frac{V_1 \pm I_1 Z_1}{4\sqrt{Z_1}}, \qquad A_{2\pm} = \frac{V_2 \pm I_2 Z_2}{4\sqrt{Z_2}} . \qquad (A.8)$$

There are two modes (+ = forward, - = backward waves) propagating in each circuit. All modes mentioned are a subclassification within the modes existing on each line.

$$\begin{cases} V_1 = 2\sqrt{Z_1}(A_{1+} + A_{1-}) \\ \\ I_1 = \frac{2}{\sqrt{Z_1}}(A_{1+} - A_{1-}) \end{cases} \qquad \text{for Circuit No. 1} \qquad (A.9)$$

$$\begin{cases} V_2 = 2\sqrt{Z_2}(A_{2+} + A_{2-}) \\ \\ I_2 = \frac{2}{\sqrt{Z_2}}(A_{2+} - A_{2-}) \end{cases} \qquad \text{for Circuit No. 2} \qquad (A.10)$$

Substituting (A.8), (A.9) and (A.10) into (A.6) and (A.7) yields

$$\begin{cases} (\frac{d}{dx} \mp \sqrt{z_1 y_1})A_{1\pm} = \frac{z_{12}}{2\sqrt{Z_1 Z_2}}(A_{2+} - A_{2-}) \pm \frac{y_{12}\sqrt{Z_1 Z_2}}{2}(A_{2+} + A_{2-}) \qquad (A.11) \\ \\ (\frac{d}{dx} \mp \sqrt{z_2 y_2})A_{2\pm} = \frac{z_{21}}{2\sqrt{Z_1 Z_2}}(A_{1+} - A_{1-}) \pm \frac{y_{21}\sqrt{Z_1 Z_2}}{2}(A_{1+} + A_{1-}) . \qquad (A.12) \end{cases}$$

Next, equations (A.11) and (A.12) upon regrouping coefficients can be written,

$$(\frac{d}{dx} \mp \sqrt{z_1 y_1})A_{1\pm} = \left(\frac{z_{12}}{2\sqrt{Z_1 Z_2}} \pm \frac{y_{12}\sqrt{Z_1 Z_2}}{2}\right)A_{2+} - \left(\frac{z_{12}}{2\sqrt{Z_1 Z_2}} \mp \frac{y_{12}\sqrt{Z_1 Z_2}}{2}\right)A_{2-}$$

$$(A.13)$$

$$(\frac{d}{dx} \mp \sqrt{z_2 y_2})A_{2\pm} = \left(\frac{z_{21}}{2\sqrt{Z_1 Z_2}} \pm \frac{y_{21}\sqrt{Z_1 Z_2}}{2}\right)A_{1+} - \left(\frac{z_{21}}{2\sqrt{Z_1 Z_2}} \mp \frac{y_{21}\sqrt{Z_1 Z_2}}{2}\right)A_{1-} .$$

$$(A.14)$$

Note that A_{1+} means $A_{1+}(x)$. This simplified notation is used from here on. The above equations of specialized forms are the more general set of equations for the coupling of physical systems in terms of modes a_1, a_2, etc.

$$\frac{da_1}{dx} = c_{11}a_1 + c_{12}a_2 + c_{13}a_3 + \ldots \qquad (A.15)$$

$$\frac{da_2}{dx} = c_{21}a_1 + c_{22}a_2 + c_{23}a_3 + \ldots \qquad (A.16)$$

$$\frac{da_3}{dx} = c_{31}a_1 + c_{32}a_2 + c_{33}a_3 + \ldots \qquad (A.17)$$

Note that each of the above equations applies for each of the lines; the numerical subscript used in these is a mode designation.

Now:

A_{1+} = forward mode in Circuit No. 1

A_{2+} = forward mode in Circuit No. 2

A_{1-} = backward mode in Circuit No. 1

A_{2-} = backward mode in Circuit No. 2.

From equations (11) and (12) there are four possibilities of coupling among these four modes and these are

(1) coupling between A_{1+} and A_{2+}

(2) coupling between A_{1+} and A_{2-}

(3) coupling between A_{1-} and A_{2+}

(4) coupling between A_{1-} and A_{2-} .

The total or net power of the two lines at any plane located a distance x from the origin is given by

$$P(x) = \text{Re} \, \frac{V_1(x)I_1^*(x)}{2} + \text{Re} \, \frac{V_2(x)I_2^*(x)}{2} \quad . \tag{A.18}$$

Expressing P in terms of modes, this becomes

$$P(x) = 2\left[\left|A_{1+}(x)\right|^2 - \left|A_{1-}(x)\right|^2 + \left|A_{2+}(x)\right|^2 - \left|A_{2-}(x)\right|^2 \right] \tag{A.19}$$

Evaluating P at x = 0 yields

$$P(0) = 2\left[\left|A_{1+}(0)\right|^2 - \left|A_{1-}(0)\right|^2 \right] \quad . \tag{A.20}$$

Consider each of the four possibilities or cases of coupling in turn.

Coupling between two forward modes A_{1+} and A_{2+}

$$\left(\frac{d}{dx} - \sqrt{z_1 y_1}\right)A_{1+} = \left(\frac{z_{12}}{2\sqrt{Z_1 Z_2}} + \frac{y_{12}\sqrt{Z_1 Z_2}}{2}\right)A_{2+} - \left(\frac{z_{12}}{2\sqrt{Z_1 Z_2}} - \frac{y_{12}\sqrt{Z_1 Z_2}}{2}\right)A_{2-} \tag{A.21}$$

$$\left(\frac{d}{dx} - \sqrt{z_2 y_2}\right)A_{2+} = \left(\frac{z_{21}}{2\sqrt{Z_1 Z_2}} + \frac{y_{21}\sqrt{Z_1 Z_2}}{2}\right)A_{1+} - \left(\frac{z_{21}}{2\sqrt{Z_1 Z_2}} - \frac{y_{21}\sqrt{Z_1 Z_2}}{2}\right)A_{1-} \quad . \tag{A.22}$$

If the following inequality holds true for the greatest power transfer from Line No. 1 to Line 2,

$$\left| \frac{z_{12}}{2\sqrt{Z_1 Z_2}} + \frac{y_{12}\sqrt{Z_1 Z_2}}{2} \right| \gg \left| \frac{z_{12}}{2\sqrt{Z_1 Z_2}} - \frac{y_{12}\sqrt{Z_1 Z_2}}{2} \right|$$

Then equations (21) and (22) simplify as

$$\left(\frac{d}{dx} - \sqrt{z_1 y_1}\right)A_{1+} = \left(\frac{z_{12}}{2\sqrt{Z_1 Z_2}} + \frac{y_{12}\sqrt{Z_1 Z_2}}{2}\right)A_{2+} \tag{A.23}$$

$$\left(\frac{d}{dx} - \sqrt{z_2 y_2}\right)A_{2+} = \left(\frac{z_{21}}{2\sqrt{Z_1 Z_2}} + \frac{y_{21}\sqrt{Z_1 Z_2}}{2}\right)A_{1+} \quad . \tag{A.24}$$

Using the general forms for coupling there results,

$$\left(\frac{d}{dx} + jC_{11}\right)A_1 = C_{12}A_2 \quad \text{and} \quad \left(\frac{d}{dx} + jC_{22}\right)A_2 = C_{21}A_1 \quad .$$

The above equations are correct for either forward or backward waves. Assume A_{1+} and A_{2+} vary as $e^{\gamma x}$,

$$(\gamma + jC_{11})A_{1+} = C_{12}A_{2+} \tag{A.25}$$

$$(\gamma + jC_{22})A_{2+} = C_{21}A_{1+} \quad . \tag{A.26}$$

For a nontrivial solution, the determinant of the above equation must be zero, i.e.

$$\gamma, \gamma' = -j \frac{C_{11}+C_{22}}{2} \pm \sqrt{C_{12}C_{21} - \left(\frac{C_{11}-C_{22}}{2}\right)^2} . \tag{A.27}$$

Equations (25) and (26) are solved for a pair of values γ and γ' which apply only for coupling between A_{1+} and A_{2+} modes

$$A_{1+}(x) = Pe^{\gamma x} + Qe^{\gamma' x} \quad . \tag{A.28}$$

If the γ's are imaginary, the coupling is called passive ; if they are complex, the coupling is called active. Then the solution for each of the two lines must be

$$\begin{cases} A_{1+}(x) = Pe^{\gamma x} + Qe^{\gamma' x} & \tag{A.29} \\ \\ A_{2+}(x) = \frac{1}{C_{12}}\left[\frac{dA_{1+}(x)}{dx} + jC_{11}A_{1+}(x)\right] \quad . & \tag{A.30} \end{cases}$$

Initial conditions are:

$$A_{1+}(x) = A_{1+}(0) \tag{A.31}$$

$$A_{2+}(x) = 0 \qquad\qquad \text{at } x = 0 \quad . \tag{A.32}$$

The resulting values of the coefficients M and N are,

$$P = \frac{A_{1+}(0)\left[\gamma' + jC_{11}\right]}{j2\delta} \tag{A.33}$$

$$Q = - \frac{A_{1+}(0)\left[\gamma + jC_{11}\right]}{j2\delta} \tag{A.34}$$

where

$$\gamma' - \gamma = j\, 2\, \delta \qquad (A.35)$$

$$\delta = \sqrt{\left|C_{12} C_{21}\right| + \left(\frac{C_{11} - C_{22}}{2}\right)^2} \qquad (A.36)$$

$$A_{1+}(x) = \frac{A_{1+}(0)}{j\, 2\, \delta} \left[(\gamma' + jC_{11})e^{\gamma x} - (\gamma + jC_{11})e^{\gamma' x}\right] \qquad (A.37)$$

$$A_{2+}(x) = \frac{A_{1+}(0)\,(\gamma + jC_{11})\,(\gamma' + jC_{11})}{j\, 2\, \delta\, C_{12}} \left(e^{\gamma x} - e^{\gamma' x}\right) \qquad . \qquad (A.38)$$

Assume that γ's are pure imaginary quantities (lossless). Then

$$\gamma = -j\,(\beta + \delta), \qquad \gamma' = -j\,(\beta - \delta) \qquad (A.39)$$

where

$$\beta = \left(\frac{C_{11} + C_{22}}{2}\right) \qquad (A.40)$$

$$\delta = \sqrt{\left|C_{12} C_{21}\right| + \left(\frac{C_{11} - C_{22}}{2}\right)^2} \qquad (A.41)$$

P_{1+} = power in $A_{1+}(x)$ mode = $2\ A_{1+}(x)^2 = 2A_{1+}(x)A_{1+}^{*}(x)$.

$$P_{1+} = 2\left|A_{1+}(x)\right|^2 = 2\left|A_{1+}(0)\right|^2 \left[1 - \frac{1}{1 + \left(\frac{C_{11} - C_{22}}{2}\right)^2 \frac{1}{C_{12} C_{21}}} \sin^2 \delta x\right] \qquad (A.42)$$

Define F_{12} as the power transfer factor between modes A_{1+} and A_{2+}.

$$F_{12} = \frac{1}{1 + \left(\frac{C_{11} - C_{22}}{2}\right)^2 \frac{1}{C_{12} C_{21}}} \qquad . \qquad (A.43)$$

Then the powers in A_{1+} and A_{2+} are

$$P_{1+} = 2\left|A_{1+}(x)\right|^2 = 2\left|A_{1+}(0)\right|^2\left[1 - F_{12}\sin^2 \delta x\right] \tag{A.44}$$

$$P_{2+} = 2\left|A_{2+}(x)\right|^2 = 2\left|A_{1+}(0)\right|^2 - \left|A_{1+}(x)\right|^2 = \left|A_{1+}(0)\right|^2 F_{12}\sin^2 \delta x \ . \tag{A.45}$$

Figure A-2 shows the variation of power on the two lines for the forward mode. Note that power is first transferred from Line 1 to Line 2 beginning at $\delta x = 0$. Then from $\delta x = \pi/2$ to $\delta x = \pi$ power is coupled back to Line 1.
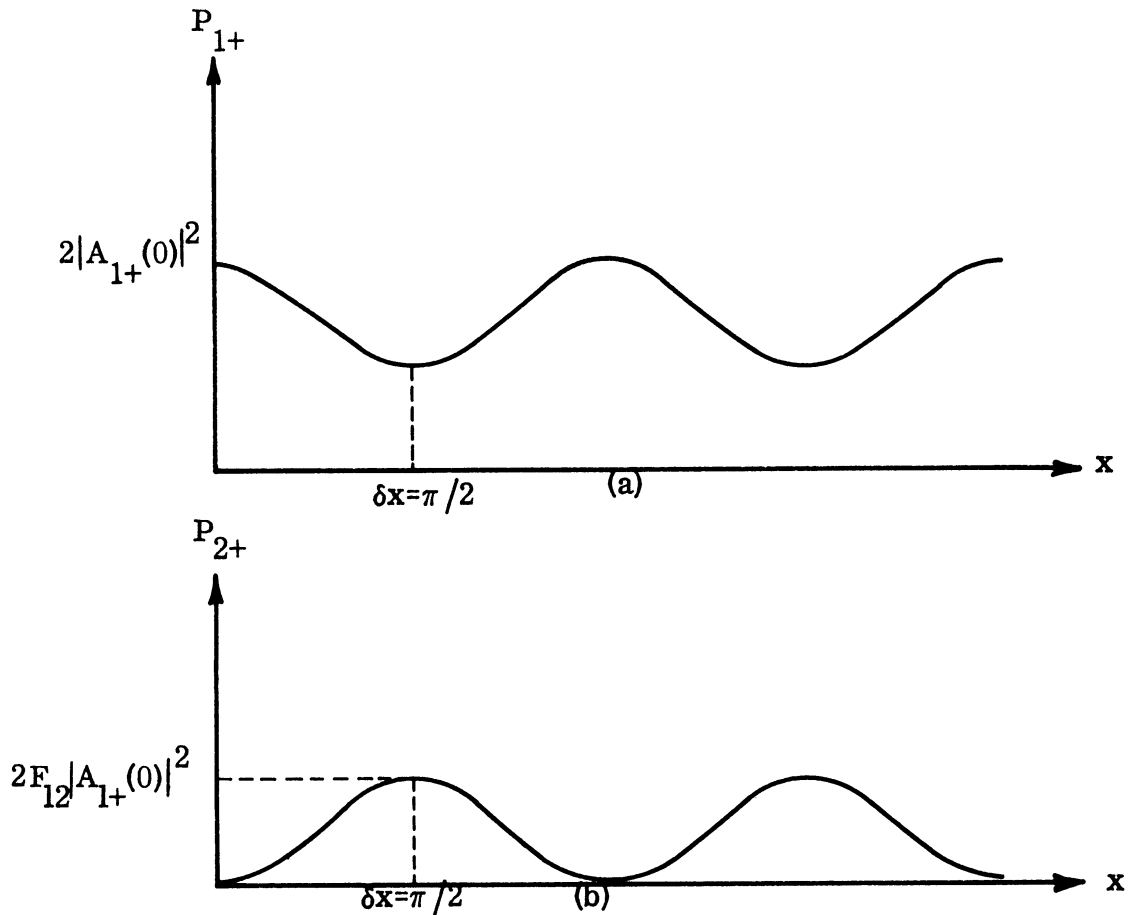
FIG. A-2: ENERGY TRANSFER BETWEEN TWO COUPLED LINES.

Comparing equations (15), (16), (23) and (24) yields

$$C_{11} = j\sqrt{z_1 y_1} \tag{A.46}$$

$$C_{12} = \frac{z_{12}}{2\sqrt{Z_1 Z_2}} + \frac{y_{12}\sqrt{Z_1 Z_2}}{2} \tag{A.47}$$

$$C_{22} = j\sqrt{z_2 y_2} \tag{A.48}$$

$$F_{12} = \cfrac{1}{1 - \left(\cfrac{\sqrt{z_1 y_1} - \sqrt{z_2 y_2}}{2}\right)^2 \cfrac{1}{\left(\cfrac{z_{12}}{2\sqrt{Z_1 Z_2}} + \cfrac{y_{12}\sqrt{Z_1 Z_2}}{2}\right)^2}} \tag{A.49}$$

if

$$z_1 = -j\omega L_1 \qquad z_2 = -j\omega L_2 \qquad Z_1 = \sqrt{L_1/C_1}$$

$$y_1 = -j\omega C_1 \qquad y_2 = -j\omega C_2$$

$$z_{12} = -j\omega M \qquad y_{12} = -j\omega N \qquad Z_2 = \sqrt{L_2/C_2}$$

where L, C, M and N are line parameters per unit length.

Then

$$F_{12} = \cfrac{1}{1 + \left(\cfrac{\omega\sqrt{L_1 C_1} - \omega\sqrt{L_2 C_2}}{2}\right)^2 \cfrac{1}{\left(\cfrac{j\omega M}{2\sqrt{\frac{L_1 L_2}{C_1 C_2}}} + \cfrac{j\omega N \sqrt{L_1 L_2/C_1 C_2}}{2}\right)^2}} \tag{A.50}$$

Optimum coupling, $F_{12} = 1$, occurs if $\omega\sqrt{L_1 C_1} = \omega\sqrt{L_2 C_2}$. This means total power transfer occurs.

$$P_{1+} = 2\left|A_{1+}(x)\right|^2 = 2\left|A_{1+}(0)\right|^2 \left[1 - \sin^2\left(\frac{\omega M}{2\sqrt{L_1 L_2 / C_1 C_2}} + \frac{\omega N\sqrt{L_1 L_2 / C_1 C_2}}{2}\right) x\right]$$

(A.51)

$$P_{2+} = 2\left|A_{2+}(x)\right|^2 = 2\left|A_{1+}(0)\right|^2 \sin^2\left(\frac{\omega M}{2\sqrt{L_1 L_2 / C_1 C_2}} + \frac{\omega N\sqrt{L_1 L_2 / C_1 C_2}}{2}\right) x .$$

(A.52)

There is very low coupling for Cases (2) and (3) involving, in each case, opposite modes. The coupling for Case (4) involving backward modes only on the two lines, is formulated in the same general manner as Case (1).

A.1 Experiments on Energy Transfer and Radiation

The experimental program will be used to confirm the energy transfer conditions prevailing for a ferrite radiator which is fed in a manner corresponding to one transmission line being coupled to another.

Certain definitive experiments were run using a spiral transmission line for Line No. 1, and various pitches and diameters of such a transmission were used. Line No. 2 was initially a flat ferrite slab; rods have also been used as described in Section 2. Measurements were used at various spacings of the transmission to the ferrite slab. Radiation from spiral transmission line was not wanted and therefore shielding was introduced so as to make measurements upon the radiation field of the ferrite slab alone. This meant that an objective was to study the ferrite slab as an end fire radiator, knowing that all energy so radiated had to be coupled at the second transmission line from Line No. 1. The results so far have been inconclusive. The coupling was a major problem in initial experiments with the slab.

APPENDIX B

LOADED HELIX AND CONICAL-HELIX ANTENNAS

B.1 Material Loaded Conical Helix

The problem discussed here is the reduction in size of a helix antenna with the addition of cylindrical loading material of arbitrary isotropic μ and ϵ. The radiation properties of a conical antenna are almost completely dependent on its active zone, the zone where the near fields are less tightly bound to the cone so that radiation of power can actually occur. This active zone may be described by a minimum of two parameters, the center of the active region and the width of the active region. Most of the theoretical work has been directed at finding the center of the active region of a conical antenna. A shift in this center has been assumed to mean a decrease in size or effective operating frequency of the antenna. Nevertheless, the width of the active zone in a conical antenna is quite large, and if the width of this active zone is not decreased in loading the antenna, then the size of this active zone imposes a limitation in the possible decrease in length of the conical antenna. Recent experimental evidence indicates that active zone width remains constant relative to a wavelength for various loadings (Section II).

Additional questions that appear to need answering include the contribution of the loading material (bound currents) to the radiation pattern. A volume integral of the bound currents requires a solution for the fields in the loading material. Also, the losses in the loading material are of great importance. These losses could be computed numerically or theoretically once the fields in the loading material have been computed.

A method suggested at the University of Illinois, and is used to some extent to analyze air loaded log conical problems, is to solve the helix problem first. Then, the conical helix is split up into many segments each of which is approximated as a

helix. The currents on the wires could then be solved point by point from the feed point by using attenuation, propagation velocities and impedances calculated from the helix solutions corresponding to each segment. The solution for attenuations and fields at each point would show clearly the whole shape of the active region of the antenna. This solution would be done numerically, since the helix solution itself requires a numerical solution in the fast wave or radiation region of operation.

B. 2 Loaded Helix Solution

The loaded helix problem is solvable if the loading material is assumed in concentric cylinder form, so that boundaries can be represented by a fixed radius. The propagation constant problem is then calculated by matching boundary values. There are two major models for the helix, the sheath helix and the tape helix.

B. 2. 1 Sheath Helix

The sheath helix model is well known in the literature (Pierce, 1950; Watkins, 1958). In addition, the sheath helix has been used to solve for the helix propagation with outside material loading (Tien, 1953; Suhl and Walker, 1954), in all cases for the $n = 0$ mode. Simple formulas were possible only for the "plane helix" approximation good for large helix diameters. In the bifilar helix case shown below, more general asympotic forms can be used that are good for any sized helix.

This helix model assumes an anisotropic conducting layer at the radius of the helix, i.e., conduction only parallel to the helix wires. No mention of the thickness of the wire is made. The sheath helix solution may be then specified in terms of the pitch angle and radius of the helix. The outstanding advantage of the sheath solution is that the spatial modes (the Fourier terms of the fields) describing the helix are not coupled; thus, the relative values of the inside and outside fields may be calculated for each mode independently of all others; in particular, the $n = -1$ mode that describes backfire radiation from a helix may be studied independently of all other modes. In addition, a hope of closed form solution exists because of

the existence of only one mode in any calculation.

The k-β diagram is a well known and important tool in the description of the propagation of any periodic structure. A typical k-β diagram, shown in Fig. B-1, is basically a plot of frequency on the vertical axis and phase shift per cell on the horizontal axis. The two 45° lines describe the propagation of backward and forward plane waves in free space. The line labeled C is the plot of the solution of β_{-1} versus k for a typical helix. It is known from coupled wave theory that waves having nearly the same propagation constant tend to couple their energy back and forth very efficiently. Thus, it is expected and well known that, when the helix characteristics of k versus β match those of a backward free space wave, the energy will be coupled efficiently from the helix to a radiating free space wave (the "active" region). Therefore, the region E and F shown in Fig. B-1 is called the radiation or fast wave region. In addition, it can be shown that the power in the n = -1 mode for backward waves is completely predominant over all other modes in this region. This justifies studying only the n = -1 mode for backward wave propagation with axial radiation. The calculations being performed are "free mode" solutions without mention of the relative amounts of different modes obtained from a more difficult "source" solution. The n = -1 mode is then assumed the predominant mode excited by whatever source is used.

B.3.1.a Full Core Loaded Sheath Helix. The TE and TM modes necessary to describe the sheath helix electric (e, E) and magnetic (h, H) fields are given for the nth mode by,

Inside		Outside	
$e_z = aI$	(B.1)	$E_z = AK$	(B.5)
$e_\phi = aC_1I + bC_2I'$	(B.2)	$E_\phi = AC_3K + BC_4K'$	(B.6)
$h_z = bI$	(B.3)	$H_z = BK$	(B.7)
$h_\phi = aC_5I' + bC_6I$	(B.4)	$H_\phi = AC_7K' + BC_8K$	(B.8)
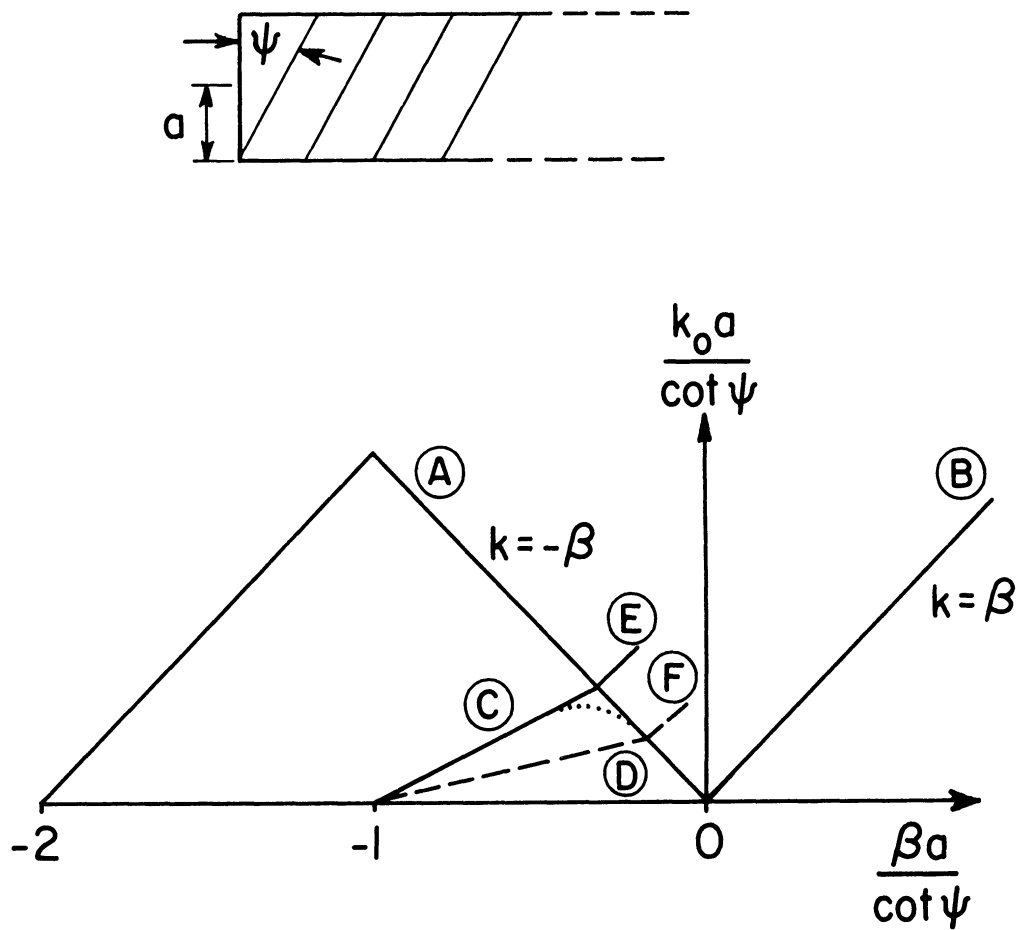
FIG. B-1: k - β DIAGRAM OF BIFILAR HELIX

where:

all constants and fields are understood to be for the nth mode (i.e. e_{zn}, a_n, $I_n(\gamma_n r)$) and have a $e^{j\omega t - j\beta z}$ factor omitted

IK $= I_n(\gamma_n r)$, $K_n(\gamma_n r)$, modified Bessel functions of the first and second kinds respectively;

the primes are derivatives with respect to argument.

$\beta = \beta_n$ is propagation constant along helix axis for the nth mode

$k = 2\pi f/c$ where f is frequency and c is the speed of light

$$\gamma = \sqrt{\beta^2 - k^2 \mu \epsilon} = \gamma_n \text{ for the } n^{th} \text{ mode}$$

$$\Gamma = \sqrt{\beta^2 - k^2} = \Gamma_n \text{ for the } n^{th} \text{ mode}$$

μ and ϵ are the relative permeability and dielectric constants, respectively, of the loading material.

$C_k(\gamma_n, \Gamma_n, \mu, \epsilon)$ are well known constants of the separation of variables method, (Watkins, 1958) given by:

$$C_1 = \frac{-n\beta}{\gamma^2 r} \qquad C_2 = \frac{-j\omega\mu\mu_o}{\gamma} \qquad C_3 = \frac{-n\beta}{\Gamma^2 r} \qquad C_4 = \frac{-j\omega\mu_o}{\Gamma_n}$$

(B.9)

$$C_5 = \frac{j\omega\epsilon\epsilon_o}{\gamma} \qquad C_6 = \frac{-n\beta}{\gamma^2 r} \qquad C_7 = \frac{j\omega\epsilon_o}{\Gamma_n} \qquad C_8 = \frac{-n\beta}{\Gamma^2 r}$$

where μ_o, ϵ_o are the MKS permeability and permittivity of free space; respectively, The boundary conditions   The standard

$$e_{11} = E_{11} = 0 \tag{B.10}$$

$$h_{11} = H_{11} \tag{B.11}$$

or, rewritten

$$E_z = e_z = 0 \tag{B.12}$$

$$E_\phi = e_z = 0 \tag{B.13}$$

$$e_3 + e_\phi \cot\psi = 0 \tag{B.14}$$

$$h_z + h_\phi \cot\psi - H_z - H_\phi \cot\psi = 0 \tag{B.15}$$

where

ψ = helix pitch angle

a = helix radius

$//,$ refer to parallel and perpendicular field components relative to the conductor direction

The fields are shown are understood to be at the point on $r = a$

These four boundary conditions give four homogeneous equations in five unknowns a, b, A, B, β for a given k, μ, ϵ for each mode independently. Upon eliminating a, b, A, B (or setting the determinant of the boundary condition equations equal to zero), an equation for β, the propagation constant of the nth mode, is obtained;

$$\frac{K_n'(\Gamma a)I_n'(\gamma a)}{K_n(\Gamma a)I_n(\gamma a)} = -\frac{1}{C} \frac{\left[\gamma^2 a^2 - n\beta a \cot\psi\right]^2}{k_o^2 \gamma^2 a^4 \cot^2\psi} \tag{B.16}$$

where

$$C = \frac{-\gamma \dfrac{K_n'(\quad a)}{K_n(\quad a)} - \epsilon \dfrac{I_n'(\gamma a)}{I_n(\gamma a)}}{\dfrac{1}{\mu}\dfrac{K_n'(\quad a)}{K_n(\gamma a)} - \dfrac{\gamma^3}{\Gamma^3}\dfrac{I_n'(\gamma a)}{I_n(\gamma a)}\left[\dfrac{\Gamma^2 a^2 - n\beta a \cot\psi}{\gamma^2 a^2 - n\gamma a \cot\psi}\right]} \tag{B.17}$$

Since $C \to 1$ as ϵ, $\mu \to 1$, Eq. (B.16) approaches the well known sheath determinantal equation in air. (Watkins, 1958). The material loading effects are entirely contained in the constants C, γ, and Γ.

For the simple slow wave case, where $\beta \gg k$, $\beta \cong \gamma \cong \Gamma$ (if μ, ϵ are not too large), the constant C becomes,

$$C^2 = \frac{\dfrac{K'_n}{K_n} \dfrac{I_n}{I'_n} - \epsilon}{\dfrac{1}{\mu} \dfrac{K'_n}{K_n} \dfrac{I_n}{I'_n} - 1} \tag{B.18}$$

where Bessel function arguments are understood.

By an investigation of the asymptotic forms for Bessel functions for large n,

$$\lim_{n \to \infty} \frac{K'_n I_n}{K_n I'_n} \to 1 \text{ for any argument} \tag{B.19}$$

Studies by many helix investigators such as Sensiper (1951), Watkins (1958), and this laboratory have shown the asymptotic products are fairly accurate for $n \geq 1$ for any argument, especially for large arguments. Using this approximation, and $\beta \cong \gamma \cong \Gamma$, the determinantal Eq. (1) becomes

$$\frac{K'_n I'_n}{K_n I_n} = - \frac{\left[\beta_n^2 a^2 - n\beta_n a \cot \psi \right]^2}{(C^2 k^2 a^2) \beta_n^2 a^2 \cot^2 \psi} \tag{B.20}$$

where

Bessel function arguments $(\beta_n a)$ are understood, and

$$C^2 \cong \frac{1 + \epsilon}{\dfrac{1}{\mu} + 1} \tag{B.21}$$

The constant C has been grouped with (ka), the frequency-size parameter, to show immediately that for a given βa, an increase in C causes a <u>decrease</u> in k a for the equation to be satisfied. Thus as μ or ϵ are increased, the frequency of radiation (or size) radiation is <u>decreased.</u> The slope of the k-β diagram, Fig. B-1, is thus reduced with loading to line D, by the multiplicative factor

$$\frac{1}{C} = \sqrt{\frac{1 + \dfrac{1}{\mu}}{1 + \epsilon}} \qquad\qquad (B.22)$$

which will be used as a nominal "reduction factor" throughout this report.

Equation (4) has been obtained from the sheath model and used by others (Suhl and Walker, 1954; Hair, 1964) for the effect of dielectric loading on sheath helices intended for traveling wave applications, For the n = 0 mode, it was necessary to assume the radius of the helix very large, called the "plane helix". The important difference in this case is that the n = -1 mode is of interest and, because of the bifilar winding, the n = 0 mode is not present. The "large n" asymptotic approximation can then be used for n $\geqslant$ 1, independent of the argument (helix size).

The solution so far, has not actually been for the radiation region (E and F in Fig. B-1), since slow waves were assumed, restricting the region of operation away from the k = -β line of radiation. Actually, in order to be valid, the restriction is imposed

$$\beta \gg k \sqrt{\mu\,\epsilon}$$

by the slow wave assumption that

$$\gamma \cong \Gamma \;.$$

Thus, for fairly high $\sqrt{\mu\epsilon}$, the equation breaks down practically everywhere. The reduction factor is thus only valid in the slow wave region for moderate $\sqrt{\mu\epsilon}$.

However, previously discussed, it has been shown by the University of Illinois (Klock, 1961; Dyson, 1965; Maclean, 1962) that the actual fast wave solution for helices in air may be approximated by extrapolating the slow wave solution by a straight line on the k-β diagram into the fast wave radiation region. In addition, the tape helix solution has been shown, for narrow tape helices in air, to approach the straight line k-β,

$$\frac{k_a}{\beta_a} = \sin\psi \qquad\qquad\qquad\qquad (B.23)$$

and for conical helices,

$$\frac{k_a}{\beta_a} = \sin\psi\cos\theta_o \qquad\qquad\qquad (B.24)$$

where θ_o is the half cone angle. These solutions are good approximations in both slow and fast wave regions of unloaded helices. Finally, sheath solutions phase velocity have always been close to tape solutions. Therefore the decrease in k-β slope, computed for the slow-wave, loaded, sheath helix, was applied to the narrow tape solution for the loaded helix and conical helix and extrapolated from the slow wave region into the radiation region. In addition, the ka corresponding to $k = -\beta$ was computed (Hong, 1965). Thus, the k-β diagrams for the loaded sheath helix (with some narrow tape approximations in addition) have slopes,

$$\text{Helix} \qquad \frac{ka}{\beta a} = \frac{\sin\psi}{C} \qquad\qquad\qquad (B.25)$$

$$\text{Cone} \qquad \frac{ka}{\beta a} = \frac{\sin\psi\cos\theta_o}{C} \qquad\qquad (B.26)$$

The line D in Fig. B-1 indicates a typical k-β diagram for a loaded helix.

If the intersection of the k-β line is assumed the point of backfire radiation, then the frequency--radius parameter for the helix in backfire radiation is; (Hong, 1965)

$$\text{Helix} \quad k_o a = \frac{\sqrt{\dfrac{1 + \dfrac{1}{\mu}}{1 + \epsilon}} \cos \psi}{1 + \sqrt{\dfrac{1 + \dfrac{1}{\mu}}{1 + \epsilon}} \sin \psi} \tag{B.27}$$

$$\begin{matrix}\text{Conical} \\ \text{Helix}\end{matrix} \quad k_o a = \frac{\sqrt{\dfrac{1 + \dfrac{1}{\mu}}{1 + \epsilon}} \cos \psi \cos \theta_o}{1 + \sqrt{\dfrac{1 + \dfrac{1}{\mu}}{1 + \epsilon}} \sin \psi \cos \theta_o} \tag{B.28}$$

which shows the size or frequency reduction, R, to be expected due to loading

$$R = \frac{ka\ (\text{loaded})}{ka\ (\text{unloaded})} = \frac{\sqrt{\dfrac{1 + \dfrac{1}{\mu}}{1 + \epsilon}}\, (1 + \sin \psi \cos \theta_o)}{1 + \sqrt{\dfrac{1 + \dfrac{1}{\mu}}{1 + \epsilon}}\, (\sin \psi \cos \theta_o)} \tag{B.29}$$

For the small $\sin \psi \cos \theta_o$ usually encountered

$$R \rightarrow \frac{\sqrt{1 + \dfrac{1}{\mu}}}{1 + \epsilon} = \frac{1}{C}$$

In conclusion, a determinantal equation for the full core loaded sheath helix has been solved for a slow wave approximation to the reduction factor caused by load-in. An extrapolation into the fast wave region gives an approximate helix antenna

reduction. Exact numerical calculations of Eq. (B-16) are in progress.

B.3.1.b Inside-Layer Loaded Sheath Helix. The inside-cylindrical-layer-loaded sheath helix problem is exactly the same as the full-core loaded sheath helix except that hybrid (combined TE and TM) modes must be used to describe the fields in the cylindrical loading at the helix-air boundary. These modes are expressed by matching the boundary fields at the interface of the air-core and the loading cylinder (r = a). The problem gets very complicated, so that at the outset, we assume

$$\gamma \cong \Gamma \cong \beta_n.$$

The fields at the helix-air interface (r = a) for the nth mode are,

Inside		Outside	
$e_z = a(I + C_9 K)$	(B.30)	$E_z = AK$	(B.34)
$e_\phi = aC_1(I + C_9 K) + bC_2(I' + C_{10} K')$	(B.31)	$E_\phi = AC_3 K + BC_4 K'$	(B.35)
$h_z = b(I + C_{10} K)$	(B.32)	$H_z = BK$	(B.36)
$H_\phi = aC_5(I' + C_9 K') + bC_6(I + C_{10} K)$	(B.33)	$H_\phi = AC_7 K' + BC_8 K$	(B.37)

where,

C_1 -- C_8 are defined in the earlier section,

$I, K = I_n(\Gamma_n a), K_n(\Gamma_n a)$ are modified Bessel Functions of order n corresponding to the nth mode.

The constants C_9 and C_{10} represent the solution for the hybrid modes in the loading cylinder,

$$C_9 = \frac{-I}{K}\left[1 - \frac{\epsilon\left(1 - \frac{K'I}{KI'}\right)}{\left(1 - \epsilon\frac{K'I}{KI'}\right)}\right] \quad \text{at } r = b \qquad (B.38)$$

$$C_{10} = \frac{-I}{K} \left[1 - \mu \frac{\left(1 - \frac{K'I}{KI'}\right)}{\left(1 - \mu \frac{K'I}{KI'}\right)} \right] \quad \text{at } r = b \qquad (B.39)$$

where it is stressed that here the Bessel function arguments ($\Gamma_n b$) in the last two equations use the radius of the inside air core, b, since the boundaries conditions for the hybrid modes are stated there.

Matching boundary conditions at the helix-air interface as before, and eliminating the four constants a, b, A, and B, one obtains a determinantal equation for β,

$$\frac{K'I'}{KI} = \frac{-\left[\beta^2 a^2 - n\beta a \cot \psi\right]}{(C_e^2 k^2 a^2)\beta^2 a^2 \cot^2} \qquad (B.40)$$

where the constant C_e for layer loading is

$$C_e^2 = \frac{K'I}{KI'} \left\{ \frac{1 - \epsilon\left(\left(\frac{I' + C_o K'}{I + C_9 K}\right)\frac{K}{K'}\right)}{\frac{1}{\mu}\frac{K'}{K}\left(\frac{I + C_{10} K}{I' + C_{10} K'}\right) - 1} \right\} \qquad (B.41)$$

The constant C_e is similar to C for the full core loading, with additional factors that carry the layer thickness.

Using the large order asymptotic approximations as discussed in the full core section for the n = -1 (backfire) mode, as well as large argument approximations; the constant C_e may be simplified to

$$C_e^2 \simeq \frac{1 + \epsilon C_{11}}{\frac{1}{\mu C_{12}} + 1} \qquad (B.42)$$

where

$$C_{11} = \frac{1 + \left(\frac{1-\epsilon}{1+\epsilon}\right) \exp\left[-2\beta(a-b)\right]}{1 - \left(\frac{1-\epsilon}{1+\epsilon}\right) \exp\left[-2\beta(a-b)\right]} \tag{B.43}$$

$$C_{12} = \frac{1 + \left(\frac{1-\mu}{1+\mu}\right) \exp\left[-2\beta(a-b)\right]}{1 - \left(\frac{1-\mu}{1+\mu}\right) \exp\left[-2\beta(a-b)\right]} \tag{B.44}$$

The asymptotic approximations employ the additional assumption in this case that (βa) and (βb) are fairly large (>5), which is true for the large β (>10) found in slow wave regions, if a and b are not small. The factors C_{11} and C_{12} determine the "effectiveness" of ϵ and μ, respectively; Fig. B-2 plots these functions which allow quick estimates of the effect of layer versus full core loading.

The constants C_{11} and C_{12} may be seen to approach $1/\epsilon$ or $1/\mu$, respectively, as thickness (b-a) approaches zero; this behavior is correct, since then $C_e \rightarrow 1$ and the determinantal equation approaches the classic sheath helix solution in air. For (b-a) large, C_{11} and C_{12} approach 1, which is correct since then C_e becomes the full-core loading factor. Notice that the β in the abscissa of Fig. B-2 is a function of the "effectiveness". Thus, this curve is not an explicit solution for the layer thickness. Nevertheless, the effect of thick layers (effectiveness = 1, where β is almost unchanged from the fully loaded case, may be quickly seen. For ϵ or μ <5, the effectiveness is over 90 per cent when $\beta(a-b)$ > 1.5. This may be related to layer thickness, since

$$\beta(a-b) \cong \frac{2\pi}{\lambda C \sin\psi} (a-b). \tag{B.45}$$
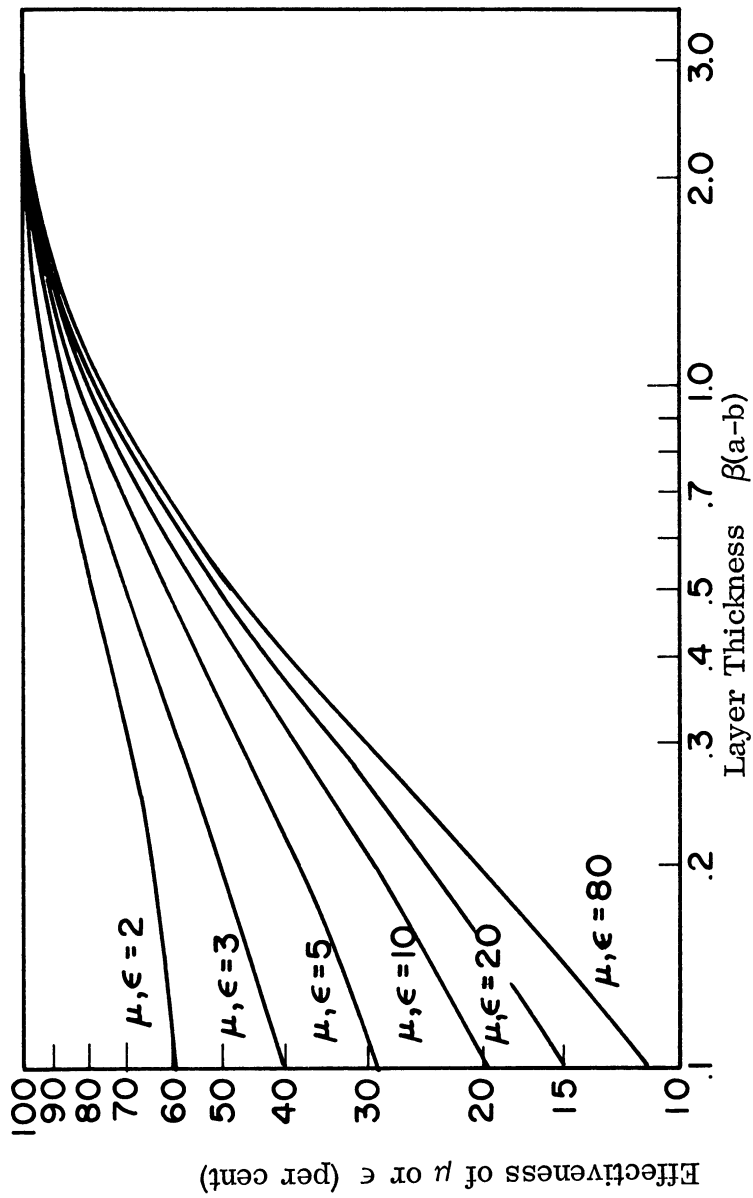
FIG. B-2: EFFECTIVENESS OF μ OR ϵ VERSUS LAYER THICKNESS

which gives,

$$a - b = .015\lambda$$

The thicknesses of loading tested were in the range $.006 - .02\lambda$ with $.02\lambda$ layers behaving approximately as full core.

The calculation for very thin layers would need a trial and error procedure (since β is changed drastically), or a regrouping of Eq. B.41 and more approximations. Further calculations of thickness effect are planned.

B.3.2 Tape-Helix Solution

The tape helix solution was originally done by Senseper (1951). The model consists of a very thin, narrow, conducting tape. In the case of the loaded tape helix, a cylinder of loading material is placed inside or outside or surrounding the tape. In this case, the solution is considerably more complex since all the spacial modes contribute to the propagation constant of any one mode. Nevertheless, several slow wave solutions have been performed for the loaded tape helix. One solution (Shestopalov, 1961) agrees with the full core sheath solution for the effect of ϵ in the slow wave region. It is necessary to distinguish between the slow wave and fast wave solutions since the slow wave solutions may be obtained relatively easily by using expressions and simplifications that heavily depend upon the fact that the phase velocity of the wave is much slower than that of free space, especially the assumption that β is real. These solutions are valid in the slow-wave region and of great use in the traveling wave tube problems they were usually solved for. Nevertheless, they are sometimes used to describe radiation characteristics of a helix in the fast wave region where the assumptions appear to have little or no validity. Work done by the University of Illinois (Dyson's, 1964; Klock, 1963) shows that, both experimentally and theoretically, the fast wave solutions for air-loaded helices tend to follow approximately a straight line into the fast wave region from

the slow wave region. These theoretical results are based on a numerical calcula-
tion allowing complex values of β, rather than the slow wave analytical solutions
assuming real β. The analytical solution for real values of β results in the trajec-
tory of the k-β solution that bends downward, as shown in Fig. B-1, the right hand
part of line C (dotted). The solution avoids the so called "forbidden" region by
assuming no radiation. Thus the solution for real β gives the incorrect solution in
the case of an open helix for both real and imaginary β. A present study is an
attempt to numerically solve for the propagation constant of loaded helix in the fast
wave region by digitally calculating the zeros of the characteristic equation with
complex β, including an attenuation constant, assumed due to radiation. This atten-
uation constant will give attenuation per cell for the various helix segments approx-
imating the conical antenna. It is hoped that by this attenuation constant, the width
of the active region may be estimated as well as the center of the active region.
The digital calculations are not yet completed. They will be included in a technical
report later this year.

APPENDIX C

EFFICIENCY FORMS

DATA AND WORK SHEET

Test Antenna No. _____   Date _____

Frequency (MHz) _____   By _____

Transmitting Antenna No. _____

Standard Antenna No. _____

Temperature _____

Part 1. (Standard Antenna)

   1. Power Transmitted _____

   2. Attenuator Setting _____

   3. Chart Level _____

   4. VSWR _____

Part 2. (Test Antenna)

   1. Power Transmitted _____

   2. Attenuator Setting _____

   3. Chart Level _____

   4. VSWR _____

Part 3. (Loss for Infinite Balun Feed)

Number of Feet of Coax _____

Attenuation in db/100 ft. _____

    Note: See pages 614, 615 of Reference Data for Radio

    Engineers, 4th Edition, International Telephone and Telegraph Company,

    (1956).

A = Attenuation in db =

a = Attenuation (numerical) = Antilog $\left(\dfrac{A}{10}\right)$ =

Γ_m = Reflection Factor (measured) = $\dfrac{S-1}{S+1}$ =

Γ_t = True Reflection factor = $a\Gamma_m$ =

Part 4. (Loss of lead cable to dipole)

    Please do calculations in the remainder of this page.

Part 5. (Calculation of Gain)

$$V = \text{VSWR Correction factor} = 10 \log \frac{1 - \Gamma^2_{\text{dipole}}}{1 - \Gamma^2_{\text{test}}} =$$

where Γ_{dipole} and Γ_{test} are the corrected reflection factors.

G = Gain of the test antenna in db =

$$C + A_{\text{test}} - A_{\text{dipole}} + V + L_{\text{test}} - L_{\text{dipole}}$$

where C = 2.15 db for a linearly polarized test antenna and 5.16 for a circularly polarized test antenna and L_{test} is the sum of the cable, balun, and hybrid losses between the connector and the tip of the test antenna, and L_{dipole} is the loss calculated for the dipole.

g = Gain (numerical) = Antilog $\left(\dfrac{G}{10} \right)$ =

Part 6. (Optional Check)

$$d \approx \frac{32,600}{\theta \phi} =$$

$$\eta \approx \frac{g}{d} \times 100 = \quad \text{per cent}$$

Part 7. (Calculating Directivity and Efficiency)

U_o = Height of pattern maximum expressed in number of squares =

$$d = \frac{229 \, U_o}{(\text{width of square in }^o) \, (\text{total at bottom of Table C-1})} =$$

η = Efficiency = $\dfrac{g}{d} \times 100 = \quad$ per cent

TABLE C-1: GRAPHICAL INTEGRATION

① Range (degrees)	② Number of Squares Under Curve (for E plot only)	③ Number of Squares Under Power Plot or Square of 4 for E Plot	④ Sine θ	⑤ Result
0 - 12			0.1045	
12 - 24			0.326	
24 - 36			0.500	
36 - 48			0.670	
48 - 60			0.810	
60 - 72			0.914	
72 - 84			0.979	
84 - 96			1.000	
96 - 108			0.979	
108 - 120			0.914	
120 - 132			0.810	
132 - 144			0.670	
144 - 156			0.500	
156 - 168			0.326	
168 - 180			0.1045	
180 - 168			0.1045	
168 - 156			0.326	
156 - 144			0.500	
144 - 132			0.670	
132 - 120			0.810	
120 - 108			0.914	
108 - 96			0.979	
96 - 84			1.000	
84 - 72			0.979	
72 - 60			0.914	
60 - 48			0.810	
48 - 36			0.670	
36 - 24			0.500	
24 - 12			0.326	
12 - 0			0.1045	
			⑥ Total	

ACKNOWLEDGEMENTS

The help of Terry B. Lewis and U. Edward Gilreath for their excellent laboratory measurements and many original ideas is gratefully acknowledged.

REFERENCES

Adams, A.T. (1964), "The Rectangular Cavity Slot Antenna with Homogeneous Isotropic Loading,""The University of Michigan Cooley Electronics Laboratory Report No. 05549-7-T.

Allen, J.L. (1964), "Array Antennas: New Applications for an Old Technique," IEEE Spectrum, 1, pp. 115-130.

Bevensee, R.M. (1964), Electromagnetic Slow Wave Systems, John Wiley and Sons, New York.

Bulgakov, B.M., V.P. Shestopalov, L.A. Shiskin and I.P. Yakimenko (1960), "Symmetrical Surface Waves in a Helix Waveguide with a Ferrite Medium," Radio. i. elek., 5, pp. 102-119.

Bulgakov, B.M., V.P. Shestopalov, L.A. Shiskin and I.P. Yakimenko, (1961), "The Irreversible Propagation of Waves in a Helix Waveguide Placed in a Ferrite Medium," Radio Eng. and Electronics, 4, pp. 118-134.

Chatterjee, J.L. (1953), "Radiation Field of a Conical Helix," J. Appl. Phys., 24, pp. 550-559.

Cheo, B.R. (August, 1965), "Radiating Slots on a Dielectric Filled Waveguide," New York University, Bronx, New York, Technical Report 400-118.

Dyson, J.D. (May, 1965), "The Characteristics and Design of the Conical Log-Spiral Antenna," University of Illinois Technical Report, AFAL-TR-65-124.

Hair, H.H. (December, 1964), "Development of Helical Phase Shifters," General Electric Company, Final Report prepared for MIT Lincoln Laboratories.

Hong, S. (2 September 1965), "Size Reduction of Bifilar Helical Antennas by Loading with Magnetic-Dielectric Material," The University of Michigan Radiation Laboratory, Memo 07260-504-M.

Jasik, H. (1961), Antenna Engineering Handbook, McGraw-Hill, New York, 9.

Jones, H.S., Jr. (1965), "Dielectric-Loaded Waveguide Slot Arrays," USAMC Harry Diamond Laboratories Technical Report TR-1269.

Kay, A.F. (May, 1956), "Mutual Coupling of Shunt Slots in the Broad Face of Rectangular Waveguide," Scientific Report No. 3, TRG, Inc., AD98799.

Knott, E.F., V.V. Liepa, T.B.A. Senior, "A Surface Field Measurement Facility," Proc. IEEE, 53, pp. 1105-1107.

Kornhauser, E.T. (1951), "Radiation Field of Helical Antennas with Sinusoidal Current," J. Appl. Phys., 22, pp. 887-891.

Kraus, J.D. (1950), Antennas, McGraw-Hill, New York.

Larson, R.W. and V.M. Powers (January, 1966), "Slots in Dielectrically Loaded Waveguide," Radio Science, 1, No. 1, pp. 31-35.

Louisell, W.H. (1960), Coupled Mode and Parametric Electronics, John Wiley and Sons, New York.

Lyon, J.A.M., et al (1965), "Study and Investigations of a UHF-VHF Antenna," The University of Michigan Radiation Laboratory Report 5549-1-F, AFAL-TR-65-64.

Lyon, J.A.M., et al (July, 1965), "Study and Investigation of UHF-VHF Antennas," Interim Engineering Report, U.S.A.F. Contract AF 33(615)-2100, The University of Michigan Radiation Laboratory Report No. 07140-1-T.

Oliner, A.A. (January, 1957), "The Impedance Properties of Narrow Radiating Slots in the Broadface of Rectangular Waveguide," Part I and II, Trans. IEEE, AP-5, pp. 4-20.

Patton, W.T. (1963), "The Backfire Bifilar Helical Antenna," The University of Illinois Technical Antenna Laboratory, Report No. 61, AD289084.

Pierce, J.R. (1950), Traveling Wave Tubes, D. vanNostrand, Inc., New York.

Radio Corporation of America (1963), "Hexagonal Magnetic Compounds, "RCA Report No. 8, AD420336.

Ramo, S. and J.R. Whinnery (1953), Fields and Waves in Modern Radio, John Wiley and Sons, New York, pp. 351, 370 and 371.

Ramsay, J.F. and B.V. Popovich (1963), "Series-Slotted Waveguide Array Antennas," IEEE International Conv. Record, Pt. 1, pp. 30-55.

Reference Data for Radio Engineers, (1956), 4th Ed., International Telephone and Telegraph Company, New York.

Rumsey, V.H. (1953), "Traveling Wave Slot Antennas," J.Appl. Phys., 24, pp. 1358-1365.

Shestopalov, V.P., A.A. Bulgakov and B.M. Bulgakov (1961), "Theoretical and Experimental Investigations of Helix-Dielectric Aerials," Radio. i. elek., 6, pp. 159-172.

Spitz, E. (1962), "A Class of New Type of Broadband Antennas," Electromagnetic Theory and Antennas, URSI Symposium, Copenhagen, (Ed. E.C. Jordan)

Stegen, Robert J. (July, 1964), "The Gain-Beam-Width Product of an Antenna," Correspondance, Trans. IEEE, AP-12, pp. 505-6.

Suhl, H. and Walker, L.R. (July, 1954), "Topics in Guided Wave Propagations Through Gyromagnetic Media," Bell Sys. Tech. J., 33, pp. 939-986.

Thourel, L. (1960), The Antenna, John Wiley and Sons, New York.

Tien, P.K. (1953), "Traveling Wave Tube Helix Impedance," Proc. IRE, 41, No. 11, pp. 1617-1623.

Walter, C.H. (1965), Traveling Wave Antennas, McGraw-Hill, New York.

Watkins, D.A. (1958), Topics in Electromagnetic Theory, John Wiley and Sons, New York.

Whiteside, H. (October, 1962), "Electromagnetic Field Probe," Harvard University Cruft Laboratory, Report No. TR-377.

Weeks, W.L. (1957), "Coupled Waveguide Excitation of Traveling Wave Slot Antennas," University of Illinois, Technical Report No. 27.

Yakimenko, I.P. and V.P. Shestopalov (1962), "An Experimental Investigation of a Helix Ferrite Waveguide," Radio Eng. and Electr. Phys., 7, pp. 1047-1054.

DOCUMENT CONTROL DATA - R&D

(Security classification of title, body of abstract and indexing annotation must be entered when the overall report is classified)

1. ORIGINATING ACTIVITY (Corporate author)	2a. REPORT SECURITY CLASSIFICATION
The University of Michigan Radiation Laboratory Department of Electrical Engineering	Unclassified
	2b. GROUP

3. REPORT TITLE

Study and Investigation of a UHF-VHF Antenna

4. DESCRIPTIVE NOTES *(Type of report and inclusive dates)*

Final Report - February 1965 through February 1966

5. AUTHOR(S) *(Last name, first name, initial)*

Lyon, John A. M., Alexopoulos, Nicholas G., Chen, Chao-Chun, Kazi, Abdul M. Rassweiler, George G., Smith, Dean L., and Wu, Pei-Rin

6. REPORT DATE	7a. TOTAL NO. OF PAGES	7b. NO. OF REFS
April 1966	170	39

8a. CONTRACT OR GRANT NO.	9a. ORIGINATOR'S REPORT NUMBER(S)
AF 33(615)-2102	7140-1-F
b. PROJECT NO. 6278	
c. Task 627801	9b. OTHER REPORT NO(S) *(Any other numbers that may be assigned this report)*
d.	AFAL-TR-66-101

10. AVAILABILITY/LIMITATION NOTICES Qualified requestors may obtain copies of this report from DDC. Distribution of this report restricted in accordance with US Export Act. DOD Dir. 203.4 AFR-400-10 and should not be disseminated to OTS.

11. SUPPLEMENTARY NOTES	12. SPONSORING MILITARY ACTIVITY
	Air Force Avionics Laboratory AVWE Research and Technology Division, AFSC Wright-Patterson AFB, Ohio 45433

13. ABSTRACT

This report indicates some of the advantages of using ferrite loading in a number of types of traveling wave antennas. Studies have been made on ferrite loaded helices and ferrite loaded log conical antennas. For a given frequency of operation it has been found possible to reduce the diameter of each of these types of antennas by a factor of approximately 55 - 70 per cent. Some variation in performance as a function of the amount of loading or thickness of the ferrite layer was observed. Near field probing techniques were used to show that ferrite loading changes the position of the active region on the log conical spiral. Likewise, near field probing shows that a particular region is active at a lower frequency when when ferrite loading is applied to a helix. The effects of ferrite loading on the log zigzag type are also indicated. Relatively high efficiencies have been obtained for the ferrite loading of helices and log conical spirals. The power limitation occasioned by the use of ferrite loading for the rectangular slot antenna has been examined. For rectangular slots loaded with powdered EAF-2 ferrite designed to operate at 300 MHz it is estimated that an average or cw power limit is less than 50 watts average.

DD FORM 1 JAN 64 1473

14. KEY WORDS	LINK A		LINK B		LINK C	
	ROLE	WT	ROLE	WT	ROLE	WT
Antennas UHF-VHF Ferrite Loading Techniques						

INSTRUCTIONS

1. ORIGINATING ACTIVITY: Enter the name and address of the contractor, subcontractor, grantee, Department of Defense activity or other organization (corporate author) issuing the report.

2a. REPORT SECURITY CLASSIFICATION: Enter the overall security classification of the report. Indicate whether "Restricted Data" is included. Marking is to be in accordance with appropriate security regulations.

2b. GROUP: Automatic downgrading is specified in DoD Directive 5200.10 and Armed Forces Industrial Manual. Enter the group number. Also, when applicable, show that optional markings have been used for Group 3 and Group 4 as authorized.

3. REPORT TITLE: Enter the complete report title in all capital letters. Titles in all cases should be unclassified. If a meaningful title cannot be selected without classification, show title classification in all capitals in parenthesis immediately following the title.

4. DESCRIPTIVE NOTES: If appropriate, enter the type of report, e.g., interim, progress, summary, annual, or final. Give the inclusive dates when a specific reporting period is covered.

5. AUTHOR(S): Enter the name(s) of author(s) as shown on or in the report. Enter last name, first name, middle initial. If military, show rank and branch of service. The name of the principal author is an absolute minimum requirement.

6. REPORT DATE: Enter the date of the report as day, month, year; or month, year. If more than one date appears on the report, use date of publication.

7a. TOTAL NUMBER OF PAGES: The total page count should follow normal pagination procedures, i.e., enter the number of pages containing information.

7b. NUMBER OF REFERENCES: Enter the total number of references cited in the report.

8a. CONTRACT OR GRANT NUMBER: If appropriate, enter the applicable number of the contract or grant under which the report was written.

8b, 8c, & 8d. PROJECT NUMBER: Enter the appropriate military department identification, such as project number, subproject number, system numbers, task number, etc.

9a. ORIGINATOR'S REPORT NUMBER(S): Enter the official report number by which the document will be identified and controlled by the originating activity. This number must be unique to this report.

9b. OTHER REPORT NUMBER(S): If the report has been assigned any other report numbers (either by the originator or by the sponsor), also enter this number(s).

10. AVAILABILITY/LIMITATION NOTICES: Enter any limitations on further dissemination of the report, other than those imposed by security classification, using standard statements such as:

(1) "Qualified requesters may obtain copies of this report from DDC."

(2) "Foreign announcement and dissemination of this report by DDC is not authorized."

(3) "U. S. Government agencies may obtain copies of this report directly from DDC. Other qualified DDC users shall request through

_____."

(4) "U. S. military agencies may obtain copies of this report directly from DDC. Other qualified users shall request through

_____."

(5) "All distribution of this report is controlled. Qualified DDC users shall request through

_____."

If the report has been furnished to the Office of Technical Services, Department of Commerce, for sale to the public, indicate this fact and enter the price, if known.

11. SUPPLEMENTARY NOTES: Use for additional explanatory notes.

12. SPONSORING MILITARY ACTIVITY: Enter the name of the departmental project office or laboratory sponsoring (paying for) the research and development. Include address.

13. ABSTRACT: Enter an abstract giving a brief and factual summary of the document indicative of the report, even though it may also appear elsewhere in the body of the technical report. If additional space is required, a continuation sheet shall be attached.

It is highly desirable that the abstract of classified reports be unclassified. Each paragraph of the abstract shall end with an indication of the military security classification of the information in the paragraph, represented as (TS), (S), (C), or (U).

There is no limitation on the length of the abstract. However, the suggested length is from 150 to 225 words.

14. KEY WORDS: Key words are technically meaningful terms or short phrases that characterize a report and may be used as index entries for cataloging the report. Key words must be selected so that no security classification is required. Identifiers, such as equipment model designation, trade name, military project code name, geographic location, may be used as key words but will be followed by an indication of technical context. The assignment of links, rules, and weights is optional.